VOL.107 NO.HY9. SEPT. 1981

JOURNAL OF THE HYDRAULICS DIVISION

PROCEEDINGS OF
THE AMERICAN SOCIETY
OF CIVIL ENGINEERS

VOL.107 NO.HY9. SEPT. 1981

JOURNAL OF THE HYDRAULICS DIVISION

PROCEEDINGS OF THE AMERICAN SOCIETY OF CIVIL ENGINEERS

ISSN 0044-796X

Melvin W. Anderson, Editor
University of South Florida

AMERICAN SOCIETY OF CIVIL ENGINEERS

CONTENTS

The Journal of the Hydraulics Division (ISSN 0044-796X) is published monthly by the American Society of Civil Engineers. Publications office is at 345 East 47th Street, New York, N.Y. 10017. Address all ASCE correspondence to the Editorial and General Offices at 345 East 47th Street, New York, N.Y. 10017. Allow six weeks for change of address to become effective. Subscription price to members is $16.50. Nonmember subscriptions available; prices obtainable on request. Second-class postage paid at New York, N.Y. and at additional mailing offices. HY.

POSTMASTER: Send address changes to American Society of Civil Engineers, 345 East 47th Street, New York, NY 10017.

DISCUSSION

Proc. Paper 16479

*Discussion period closed for this paper. Any other discussion received during this discussion period will be published in subsequent Journals.

16494 INTAKES AND OUTLETS FOR LOW-HEAD HYDROPOWER

KEY WORDS: **Axial flow turbines;** Draft tubes; Flow control; Head losses; **Hydroelectric power generation; Intakes; Low head;** Piers; **Standardization;** Turbines; Water flow

ABSTRACT: A state-of-the-art review on standardization in low-head hydroelectric development is presented. In addition, the current flow passage design practices are summarized. Several package units are available in the range from 100 hp to 6,700 hp (75 kW to 5,000 kW). These predesigned units reduce equipment costs through standardized manfacturing techniques. Several types of package units are considered. Manufacturer's standard flow passage dimensions are given for bulb and rim-generator turbines. These standard dimensions can be used for initial layout of a low-head hydroelectric development. Standard flow passage designs are feasible for similar sites; however, structural and geological considerations may cause design variations when site conditions vary. Simplified intake and draft tube designs may lead to less costly structures.

REFERENCE: Pugh, Clifford A. (Hydr. Engr., Dept. of the Interior, Water and Power Resources Service, Engrg. and Research Center, Denver, Colo.), "Intakes and Outlets for Low-Head Hydropower," *Journal of the Hydraulics Division,* ASCE, Vol. 107, No. HY9, **Proc. Paper 16494**, September, 1981, pp. 1029-1045

16490 LOOP EQUATIONS

KEY WORDS: **Algorithms; Computer programs;** Equations; Minicomputers; **Pipe flow;** Pumps; Regulators; Reservoirs; **Water distribution**

ABSTRACT: Unknown pipe characteristics may be helpful in the design and operation of water distribution networks. By using unknown pipe characteristics it becomes easier to select appropriate pipes, to choose boosters, and to regulate the flow through pumps using regulating valves. An algorithm is presented for automatically constructing and solving equations describing the behavior of water distribution networks when some pipe characteristics are unknown. It is based on loop equations and is therefore appropriate for implementation on minicomputers. Several applications and experiments are described.

REFERENCE: Gofman, Emanuel(aIBM Israel Scientific Center, The Technion City, Haifa, Israel), and Rodeh, Michael, "Loop Equations with Unknown Pipe Characteristics," *Journal of the Hydraulics Division,* ASCE, Vol. 107, No. HY9, **Proc. Paper 16490**, September, 1981, pp. 1047-1060

16492 PARAMETRIC STUDY OF FLOOD WAVE PROPAGATION

KEY WORDS: **Channels (waterways);** Finite difference method; **Floods; Flood waves;** Hydrographs; Open channel flow; Parametric hydrology; Unsteady flow; **Waves (water)**

ABSTRACT: A parametric study of the flood wave propagation problem is made, based on numerical solution of the nondimensionalized unsteady flow equations of open channels. The propagation of a sinusoidal flood wave in a prismatic channel is studied for uniform initial flow. The governing parameters (initial uniform flow Froude number, wave amplitude, wave duration, channel width parameter and side slope) are varied over a wide range. In all, 49 cases are studied. Effects of these governing parameters on the subsidence of stage and discharge and the speed of the wave peak are described in detail. The relative wave amplitude is found to vary linearly with F_0, the initial uniform flow froude number, for lower F_0 values. Wave duration has a very pronounced effect on subsidence with greater subsidence at lower wave duration values.

REFERENCE: Sridharan, K. (Asst. Prof., Civ. Engrg. Dept., Indian Inst. of Science, Bangalore, India 560012), and Kumar, M. S. Mohan, "Parametric Study of Flood Wave Propagation," *Journal of the Hydraulics Division,* ASCE, Vol. 107, No. HY9, **Proc. Paper 16492**, September, 1981, pp. 1061-1076

16506 DEMAND FORECASTING IN WATER SUPPLY NETWORKS

KEY WORDS: **Computerized scheduling;** Computer programs; **Consumer demand forecasting; Demand (economics);** Filtration; Optimization; Predictions; Time factors; **Water demand; Water supply;** Water supply forecasting

ABSTRACT: The problem of forecasting consumer water demands over a 24 hour period is formulated within the framework of an on-line computer based pump scheduling scheme for optimum operational control of a water supply network. Two well known forecasting techniques are considered and compared, in terms of accuracy and computational feasibility, using real data from a network in the United Kingdom.

REFERENCE: Perry, Patrick F. (Lect., Civ. Engrg. Dept., Imperial Coll., London SW7 2AZ, England), "Demand Forecasting in Water Supply Networks," *Journal of the Hydraulics Division,* ASCE, Vol. 107, No. HY9, **Proc. Paper 16506**, September, 1981, pp. 1077-1087

16505 SEDIMENT-CONTAMINANT TRANSPORT MODEL

KEY WORDS: **Contamination; Estuaries;** Finite element method; Hazardous materials; **James River; Models; Rivers; Sediment;** Sediment transport; **Water pollution**

ABSTRACT: The unsteady, two-dimensional model, FETRA, was developed to simulate both sediment and contaminant transport in rivers and esturies. The model consists of three submodels which, when used jointly accurately depict the interaction and migration of sediment, dissolved contaminants, and particulate contaminants. FETRA solves the migration (transport, deposition and resuspension) of cohesive and noncohesive sediments and particulate contaminants of three sediment-size fractions. FETRA was applied to the James River estuary to simulate the migration of river sediments and the pesticide, Kepone. Computed results produced by the model are very similar to field-measured data, meaning that FETRA is reasonably accurate.

REFERENCE: Onishi, Yasuo (Staff Engr., Pacific Northwest Lab., Battelle Memorial Institute for the Dept. of Energy, P.O. Box 999, Richland, Wash.), "Sediment-Contaminant Transport Model," *Journal of the Hydraulics Division,* ASCE, Vol. 107, No. HY9, **Proc. Paper 16505**, September, 1981, pp. 1089-1107

INTAKES AND OUTLETS FOR LOW-HEAD HYDROPOWER[a]

By Clifford A. Pugh,[1] A. M. ASCE

INTRODUCTION

The need for additional energy production in the United States has resulted in increased interest in the development of remaining hydropower resources. Much of the undeveloped capacity is in the low-head range (less than about 20 m).

The main obstacle to development of low-head sites has been economics. The cost per installed kW (kilowatt) is still higher than for fossil fuel plants in most cases. However, with the cost of fuels continuing to rise, the low-head hydropower alternative is becoming more favorable.

This paper outlines present design practices regarding flow passage design to determine if standardization or design changes are possible to reduce construction costs. In low-head plants, head losses could reduce the net effective head significantly. Therefore, it would be desirable to streamline the flow passages as much as possible. At the same time, economics dictate that the flow passage should be simple and small. With these conflicting interests in mind, the present design methods were examined to determine possible design changes to simplify present designs without introducing significant additional losses.

The design of penstock entrances for high-head dams is one example that illustrates the value of taking a close look at conventional design practices. It was conservatively estimated that $13,000,000 was saved in construction costs on the penstock entrances for the Third Powerplant at Grand Coulee, by reducing the size of the bellmouth entrances (18,19). Penstock entrances have historically been designed using the same criteria used in designing high-velocity conduits, whereas the velocity in the penstocks is much lower.

This state-of-the-art survey is based on information obtained in a literature search and on comments made by manufacturers and consultants in low-head hydroelectric development.

[a]Presented at the August 8–11, 1979, ASCE Hydraulics/Energy Divisions Conference, San Francisco, Calif.

[1]Hydr. Engr., Dept. of the Interior, Bureau of Reclamation, Engrg. and Research Center, Denver, Colo.

Note.—Discussion open until February 1, 1982. To extend the closing date one month, a written request must be filed with the Manager of Technical and Professional Publications, ASCE. Manuscript was submitted for review for possible publication on October 17, 1980. This paper is part of the Journal of the Hydraulics Division, Proceedings of the American Society of Civil Engineers, ©ASCE, Vol. 107, No. HY9, September, 1981. ISSN 0044-796X/81/0009-1029/$01.00.

In the head range between 10 ft and 148 ft (3 m and 45 m), turbines with propeller-type runners are typically used (12). If the runners are adjustable, the turbines are called "Kaplan turbines." These turbines are usually arranged with a vertical shaft, a spiral case, and an elbow-type draft tube (Fig. 1).

A large percentage of present low-head turbines are this type. However, at heads less than 66 ft (20 m), axial flow turbines have proved to be more economical. This paper is mainly concerned with the low-head range, less than 66 ft (20 m).

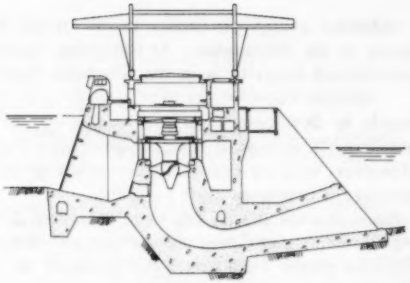

FIG. 1.—Vertical Kaplan Turbine

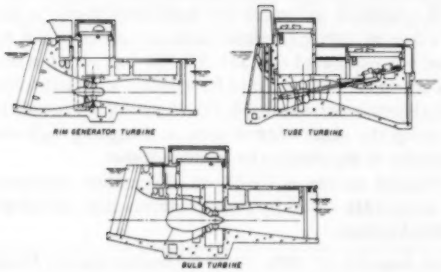

FIG. 2.—Axial Flow Turbines

Turbines in which the water is conducted to the distributor coaxially with the shaft are called "axial flow turbines" or sometimes "tubular turbines." To avoid confusion, the term "axial flow turbine" will be used in this paper. Axial flow turbines also use propeller-type runners. In some cases, adjustable (Kaplan) runners are used. The three primary types of axial flow units are shown in Fig. 2.

Package Units

A few package-type turbine and generator units are available in the low-head range. These predesigned units reduce equipment costs by eliminating the need for site-specific engineering and by using standardized manufacturing techniques. However, the standard flow passage shapes result in a loss in turbine efficiency. Butterfly valves (often used in the intake of package units) increase losses and cause an uneven flow distribution at the runner resulting in reduced operating efficiency. Standard-draft tube shapes also lead to a loss in efficiency due to sharp corners. Package units have either fixed runner blades or fixed wicket gate positions or both, resulting in less operational flexibility. The economics of each potential site should be evaluated to determine if the savings obtained with package units outweigh the losses. The following package units are presently available:

Tube Turbines

Allis-Chalmers Tube Turbine Units.—Ten standardized packaged designs are available. Single units have capacities to 6,700 hp (5,000 kW) at heads up to

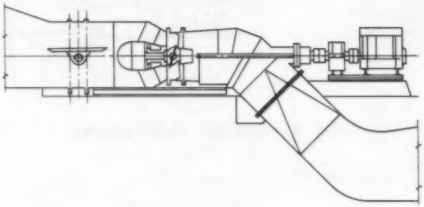

FIG. 3.—Standard Tube Turbine

49 ft (15 m). Flow is controlled with a butterfly valve in the intake. The wicket gates are fixed and the runners are either fixed or adjustable.

Karlstads Mekaniska Werkstad (KMW) Miniturbines.—These units are available for horizontal or vertical installation for flows from 35 ft^3/s–530 ft^3/s (1 m^3/s–15 m^3/s) and heads from 13 ft–82 ft (4 m–25 m). Outputs range from 134 hp–2,413 hp (100 kW–1,800 kW). The turbines have fixed guide vanes and fixed runner blades, although the position of the latter can be changed when the turbine is stationary. Flow is controlled with a butterfly valve. Fig. 3 shows a standard tube turbine.

Bulb Turbines

Fuji Package-type Bulb Turbine and Generator.—Available in 19 models covering a range of net heads from 16.4 ft–51 ft (5 m–18 m) and outputs from 402 hp–5,362 hp (300 kW–4,000 kW). The runner is of the fixed blade type and the flow is controlled with movable wicket gates. A sectional drawing of the standard bulb turbine and the generator is shown on Fig. 4.

Right Angle Drive Turbines

Neyrpic Standardized Right Angle Drive Unit.—Units vary in output from 100 kW–1,500 kW and cover a head range of 6 ft–60 ft (2 m–18 m) with discharges of 35 ft^3/s–750 ft^3/s (1 m^3/s–23 m^3/s). Flow is controlled with a downstream control gate at the end of the draft tube. Seven standard units are available with runner diameters from 18 to 71 inches (450 mm–1,800 mm). Fig. 5 shows a cross section through a right angle drive turbine.

Cross Flow Turbines

Ossberger "cross flow" turbine assemblies are available in a range of units which have the ability to cope with variations in head and discharge on small

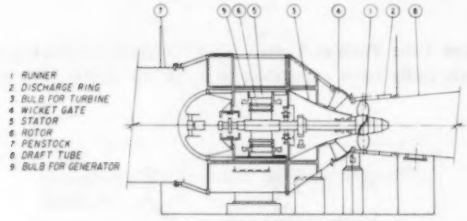

FIG. 4.—Standard Bulb Turbine

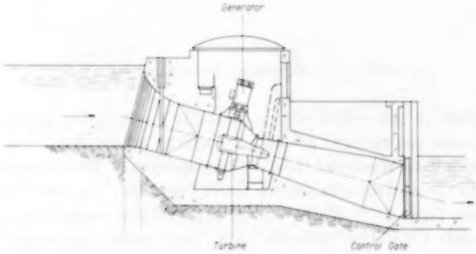

FIG. 5.—Right Angle Drive Turbine

dams. The cross flow turbine is a radial impulse-type turbine. The water is forced through a guide vane system and the blades of the cylindrical runners. The water then passes through the runners again to the outlet. Fig. 6 is a cross section through a cross flow turbine. The adjustable guide vane allows power generation from 16%–100% of design flow. Although the efficiency of this unit is not as high as for axial flow turbines, it may have widespread application to small sites where limited storage is available and flow and head vary widely.

Standard Dimensions

A few manufacturers provide drawings with standard flow passage dimensions. These dimensions were determined as a result of model tests and their operational experience over a period of years. Fig. 7 shows a cross section and plan of

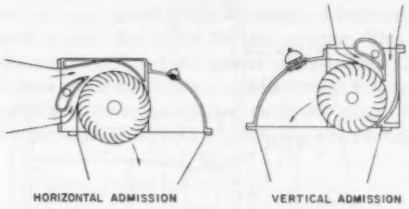

FIG. 6.—Cross-Flow Turbine

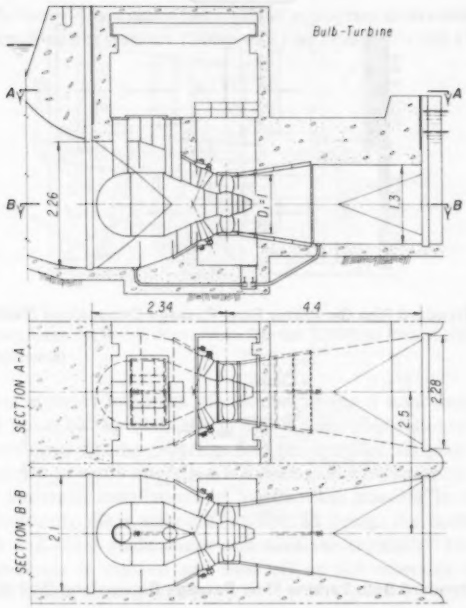

FIG. 7.—Standard Bulb Turbine Flow Passage Dimensions (Escher Wyss)

a bulb turbine according to Escher Wyss. The dimensions are given in terms of the runner diameter D-1. Fig. 8 shows Escher Wyss' standard dimensions for the "Straflo" rim-generator unit. Fig. 9 shows Fuji's standard flow passage dimensions in terms of runner diameter.

At this time there are no universally accepted flow passage shapes. Studies on optimization of flow passage shapes done by manufacturers are considered proprietary information. Therefore, the effect of simplifying intake and exit shapes on hydraulic losses is not well known. The shape of the flow passage is generally determined by the manufacturer and the standard design varies

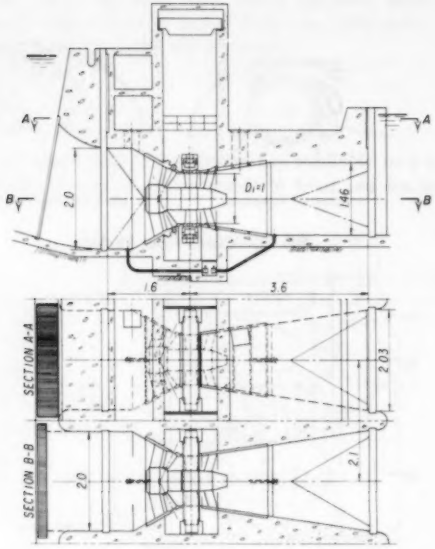

FIG. 8.—Standard Rim Generator Flow Passage Dimensions (Escher Wyss)

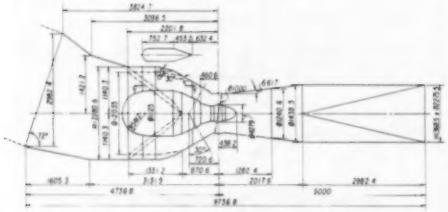

FIG. 9.—Standard Bulb-Turbine Flow Passage Dimensions (Fuji Electric Co.)

widely among manufacturers. The standard flow passage designs according to Fuji and Escher Wyss for bulb turbines illustrate the large variation in design among manufacturers (Fig. 7 versus Fig. 9). If data were available relating flow passage shape to hydraulic efficiency, a study could be done to evaluate the cost effectiveness of simplifying the intake shape to reduce the cost of the civil works.

Standard Designs for Line of Turbines

An alternative to standardization of flow passages in general would be to develop a standardized design for a series of powerplants to be installed at similar locations. A feasibility study was performed by Motor-Columbus Consulting Engineers to investigate harnessing of the Rhine River upstream of Lake Constance. The study investigated using 46 standard bulb units in 16 stations. Fig. 10 is a general layout developed for the project. This concept may be applicable to development of low-head power on American rivers with several possible low-head sites, such as the Ohio or Mississippi Rivers where numerous navigation dams without power generation currently exist. A standard design would reduce the costs associated with site-specific engineering for each powerplant.

Minipower Stations in Sweden

The Swedish Power Association has initiated a program to overhaul and replace discontinued small power stations 134 hp–2,011 hp (100 kW–1,500 kW) in Sweden (17).

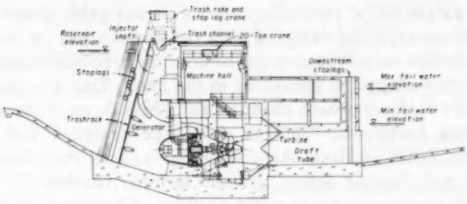

FIG. 10.—Powerplants on Rhine River from Domat (EMS) to Flasch (Motor Columbus Consulting Engineers)

The program includes hundreds of stations having a total installed capacity of about 3.15 hp $\times$ 10^5 hp (235 MW). A few simplified automated axial flow units were developed for the program. Sweden installed six pilot plants during the 1975–77 period to study operation and economics of the units selected.

In most of the small installations in Sweden it is possible to run the power stations intermittently. This makes it possible to design the turbine with fixed runner blades and fixed guide vanes and omit the regulator. The turbines are run as the reservoir is drained and shut off as the reservoir fills up again. The turbine efficiency is 90%–92%.

If the installations cannot be run intermittently, they can be run with regulation for constant water level upstream using units with movable runner blades. Turbine efficiency is 85%–91%.

The pilot stations indicated that it was difficult to bring the costs down enough to make the units economically profitable. However, the Swedish Government has made economic aid available (up to 35% of the cost) for the least profitable projects. Economic aid was considered to be justified since hydropower reduces

dependence on imported oil and is a renewable, environmentally acceptable form of energy that would otherwise be wasted.

Comment on Standardization

Most designers and consultants contacted feel that standardization of the inlet and outlet sections for low-head hydropower installations will not always be possible. The shape of the water passage is influenced by the structural support system requirements and the geology of the site. Even units designed by the same manufacturer vary from project to project.

Current Design Practices

This section summarizes material in technical literature, and comments made by manufacturers and designers concerning flow passage design. Many points covered in the references are described; however, the references should be referred to if more detail is required.

Forebay.—The design of the entrance channel in the forebay should provide a uniform flow distribution to avoid the tendency for vortices and to minimize trashrack losses. If the geometry of the approach channel is in question, a model study can be done to assure uniform approach flow conditions. Flow velocities and surges are of particular concern on navigable rivers. Run-of-river low-head dams are typically designed with the powerhouse on one side of the river and an overflow weir-type dam on the other side. In some cases an entrance channel to the powerhouse is excavated in the bank. This may cause problems of swirling flows in the approach channels and cross flows in the exit channel.

Intake—Vortex Formation.—Intakes should be designed with a sufficient submergence to avoid vortices. Air-entraining vortices may decrease turbine efficiency and pull floating debris into the turbine. Gordon (7) describes the development of design criteria to avoid vortices at low-head intakes based on a study of 29 existing hydroelectric intakes.

The intakes studied have the general configuration shown in Fig. 11. The factors which appear to affect the formation of a vortex are: (1) Geometry of the approach flow; (2) velocity at the intake; (3) the size of the intake, and (4) submergence. This article concentrates on the effects of velocity, intake size, and submergence on vortex formation. Gordon developed the following relationship by trial and error:

$$S = CVd^{0.5} \quad (1)$$

The effects of lateral approach flow were not evaluated in this study. However, Montreal Engineering Company of Canada uses a coefficient C of 0.3 for intakes with symmetrical flow and 0.4 for lateral approach flow (7) to determine minimum allowable submergence. These coefficients correspond to the lower and upper limits, respectively, of the shaded area on Fig. 11.

If the available submergence is not adequate, a model study can be done to study vortex formation. However, accurate prediction of vortex formation using a scale model is difficult. The effect of surface tension and air entrainment are important and are difficult to study in a Froude scale model. Durgin (6) describes a general method for investigating potential scale effects of free surface

vortices, so that a projection to prototype operating conditions can be made.

Zeigler (27) investigated the use of rafts placed under the water surface and other devices to prevent formation of air-entraining vortices at Grand Coulee Third Powerplant. The hydraulic model study included vortex tests on the effect of trashrack structures, upstream channel geometry, intake modifications, and submerged and floating rafts.

Bisaz (3) reports on the use of the flow "injector shaft." This device has the same effect as a raft. Because of an increase of surface current, vortices are suppressed. The injector was developed for bulb turbines on run-of-river plants to increase flow velocity on the surface to promote movement of floating debris toward the trashrack on the front of the powerhouse. The configuration of a typical flow injector is shown on Fig. 10.

Pier Design.—In typical run-of-river plants a flow separating pier divides the powerhouse and spillway. Piers also divide the intakes where there are multiple units. The size and shape of the pier should be carefully designed to avoid stagnant areas or flow disturbances which may cause excessive head losses or eddies. The HDC (Hydraulic Design Criteria) by the United States Army

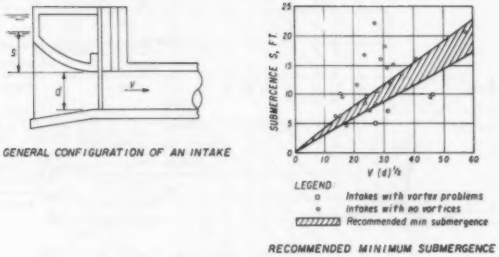

FIG. 11.—Submergence to Prevent Vortices

Corps of Engineers (22) contains design information useful in designing piers and intakes.

Rouve (20) outlines German practice in designing the size and shape of flow separating piers between a powerhouse and weir. The pier design procedure takes into account the location of the powerplant with respect to bends in the river, alinement with the weir, and the entrance channel to the powerplant cutting into the riverbank. Fig. 12 shows the general shape of the flow separating pier. The following are the limits on the length and width of the pier:

$$0.85B \leq L \leq 0.95B \quad \ldots\ldots (2)$$

$$0.28B \leq B_1 \leq 0.35B \quad \ldots\ldots (3)$$

$$0.72B \geq B_2 \geq 0.65B \quad \ldots\ldots (4)$$

the following formula defines the width of the pier (B):

$$B = CQ^{2/5} \quad \ldots\ldots (5)$$

The coefficient C varies between 0.7 and 1.4 depending on the factors mentioned

previously. Ref. 20 should be referred to for details of this design method.

The HDC sheets 111-5, 111-6, and 122-2 (22) describe pier effects for gated overflow spillways. Abutment effects are described in sheet 111-3/1 and 111-3/2. When spillways are operated with adjacent bays closed, the piers adjacent to the closed bays produce abutment-type effects. Although these pier design criteria are for spillways and not for submerged intakes they do show the relationship between pier shape and flow contractions. Fig. 13 shows five different pier nose shapes. Pier types 1 and 4 are the least desirable from the standpoint of negative pressures. However, negative pressures may not be a concern for low heads. Types 2, 3, and 3A were recommended for general use with high heads. Type 3A had the most desirable flow contraction characteristics.

Trashrack Design.—Trashracks are typically used to prevent large debris from entering the turbine. Orsborn (16) gives information on head losses through rectangular bar trashracks. The article evaluates previous work on trashrack and baffle losses and introduces additional data to supplement design information. Equations are developed to calculate the head loss as a function of the approach velocity and clear spacing between the rectangular bars. The head loss through

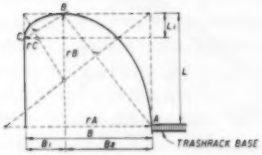

FIG. 12.—Flow Separating Pier between Powerhouse and Weir

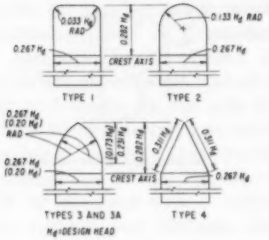

FIG. 13.—Pier Nose Shapes (Type 3A Dimensions in Parentheses)

the trashrack was found to be a minimum for bars with depth over thickness (d/t) ratios of about 3.0 for any solidarity (S) between 0.25 and 0.75, where solidarity is the ratio of the flow area blocked to the total flow area.

The possibility of flow induced trashrack vibrations should also be considered in the design. Trashracks spanning large intakes or subjected to high velocities are more likely to experience vibration problems. Vigander (24) describes trashrack vibration studies on the Raccoon Mountain Pumped-Storage Project. It was concluded from the tests that damping by either rubber pads or hydraulic baffle plates would effectively reduce flow induced vibrations on the Raccoon Mountain trashracks.

Intake Shape.—Intake shapes vary with the type of turbine used. Intakes are either circular or have a rectangular to circular transition. The face of the intake is either vertical or inclined. The hydraulic design of the intake is based largely on engineering judgment; the classical bellmouth criteria are used as a starting point. The entrance end of the bellmouth curve is then truncated to obtain a short intake profile which achieves required contraction in a length equal to approximately 1 runner diameter. General information on the effect

of intake shape on hydraulic losses is not available. Studies by Peterka (18) and Rhone (19) indicate, however, that the size of the intake could possibly be reduced without introducing excessive additional hydraulic losses, since flow separation and resulting energy losses are less of a problem at low velocities. The ideal bellmouth entrance design was developed for high-velocity conduits. Since the velocity for low-head turbines is much lower, it is possible that savings could be achieved in trashracks, bulkheads, entrance gates, and other areas by reducing the entrance size.

It might also be possible to simplify the framework by using flat surfaces to approximate curved surfaces. The cost effectiveness and practicality of these changes require further study to determine if reducing entrance sizes and simplifying intake shapes are worth pursuing in low-head powerplants.

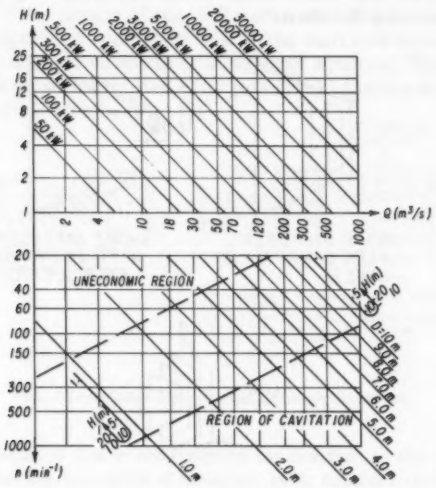

FIG. 14.—Runner Diameter Design Chart (1 m = 3.28 ft, 1 m^3/s = 35.3 ft^3/s, 1 kW = 0.746 Hp)

Fish Passage Allowances.—Intake velocities may be limited if fish passage facilities or screening devices are included in the design. This limitation may control the intake design. Optimum water velocities will depend on the type of fish and on the type of facilities used. Bell (2) gives fishway structure design criteria and other factors related to design of fish passage facilities.

Downstream passage of fish through low-head axial flow turbines may not be a serious problem since the openings between the wicket gates and the runners are generally large, the velocities are low, and the flow passages are straight. Bell (2) states that "turbines of modern design generally have a fish passage efficiency of 85 percent or higher."

Runner Diameter and Turbine Setting.—The turbine setting is determined by the allowable specific speed which is usually controlled by the cavitation potential.

From an economic standpoint, it is desirable to select the highest specific speed possible since this results in a smaller, lighter generator. The cavitation potential of an axial flow turbine is generally lower than a Kaplan unit. This allows the axial turbine to have a higher setting or a higher speed (12). Other factors such as smooth operating range and submergence also enter into the design. Heinemann (9) used data from 130-power stations to develop a design aid to determine runner diameter and the powerhouse size. The upper chart in Fig. 14 makes it possible to determine the capacity in kilowatts. In the lower diagram the runner diameter can be determined. The head, H, is marked on the lateral scales and a line is drawn connecting these points. The runner diameter can then be determined for a certain discharge (Q) or speed (n). The range of applicability is bounded by a region of uneconomic operation and the region of cavitation. The assumptions were checked by comparing existing projects with predictions using this chart.

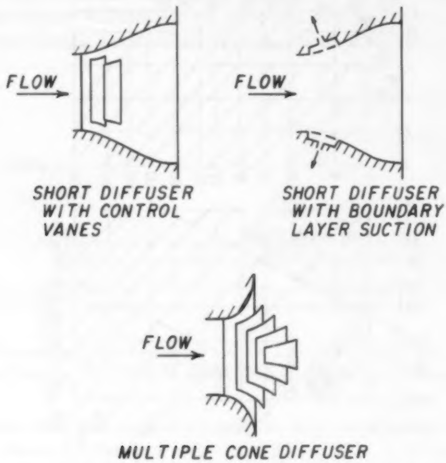

FIG. 15.—Possible Methods for Shortening Draft Tubes

Sutherland (21) also gives charts for finding the approximate runner diameter and rules of thumb enabling the approximate dimensions for an entire unit to be found. An empirical relation between diameter (D) and the ratio of power to head (in horsepower/head) is:

$$D = 0.24\,\frac{\mathrm{hp}}{H}^{0.4} \qquad (6)$$

in metric units. For power in terms of kilowatts of turbine output the formula is:

$$D = 0.272\,\frac{\mathrm{kW}}{H}^{0.4} \qquad (7)$$

Dadu (4) presents a method for developing a nomograph for determining the setting of a hydraulic turbine relative to the tailwater level. The turbine manufacturer must supply data concerning cavitation performance to develop the nomograph. This method is useful only for the installation under consideration.

Draft Tube.—The hydraulic design of the draft tube is customarily determined by the turbine manufacturer, since it is considered an integral part of the turbine in determining the turbine performance. However, there is potential for decreasing the length of draft tubes, thus decreasing the cost of the civil works. According to Kline (11), the most efficient conical draft tube would be about 10-runner diameters long with a total included angle divergence of about 7°. Economics usually limits the length of the draft tube to 4.5-runner diameters–5-runner diameters with the total angle of diversion of about 13°–15°. A study done on the feasibility of low-head hydroelectric generation in 1969 by Mercer (13) concluded that, "The section of the civil works structure where improvement would be most significant is the draft tube." The draft tube accounts for about 30% of the cost of the civil works in a low-head structure. There are several possible methods presented by Mercer for preventing boundary layer separation, thus shortening the draft tube (Fig. 15).

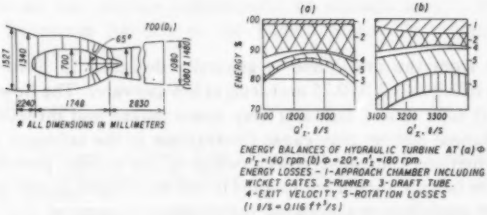

FIG. 16.—Model Bulb Turbine Energy Balances

The study concluded that a need existed for research in the design of draft tubes to apply modern principles of boundary layer control to reduce the length of draft tube diffusers. Research in this area has not been done on hydraulic turbines. The concept of boundary layer control has been bypassed in favor of simple conical diffuser designs because of the potential risks of complications involved with a new concept. Shortening the draft tube in this manner would probably require a successful demonstration project before it would be accepted. Oman (15) reports on research to shorten diffusers for wind turbines using boundary layer control. This research indicates that there is a promise of reducing the length of diffusers by an order of magnitude while maintaining efficiency.

Wirasinghe (25) deals with the question of whether addition of swirl to fluid, otherwise flowing axially, in a diffuser would improve its performance. Model studies indicated that the coefficient of performance of conical diffusers is improved by an addition of a swirl velocity component corresponding to a forced vortex. This paper concluded that the optimum swirl angle is about equal to the diffuser's total conical angle. Improvements are not likely to extend to diffusers with total conical angles greater than 30°.

Varlamov (23) reports on a study that investigated the interaction and losses

as flow moved through the various elements of the flow passage in a bulb turbine. Flow parameters were measured in various turbine operating modes, characterized by blade angles, $\theta = 0°$, 5°, and 20° and rotating speeds $N =$ 110 r/min, 140 r/min, and 180 r/min with various settings of the wicket gates. Based on these data, energy losses in individual sections of the flow passage are presented in a chart for several operating modes. Fig. 16 gives energy balances for two turbine operating modes. It should be noted that the selection of design data should be based on minimum total losses in the turbine as opposed to minimum losses in each section of the waterway. Fig. 16 shows the dimensions of the model.

Alestig (1), de Siervo (5), Isaev (10), Mikhailov (14), and Worster (26) provide additional information on draft tube design. Gubin (8) describes developments in design and construction of draft tubes in the Soviet Union and western countries. Several consultants indicate that the section of the draft tube immediately downstream from the runner is the most important. The design of this section is critical to the efficiency of the draft tube. Therefore, draft tube gates, and other obstructions should be at least 2-runner diameters downstream from the runner.

Tailrace

The outlet from the draft tube is generally designed to have a minimum submergence of 2.5 ft–3.3 ft (0.75 m–1.0 m) at low tailwater. The flow discharging from the draft tube at low tailwater may cause surges and turbulence and the rise of the channel bottom may cause fluctuations in the tailwater level. These tailwater fluctuations can cause power swings in the turbine performance. The channel and the tailrace should be designed to minimize these problems. However, tailrace design guidelines are sketchy, consultants recommend that a steep rise in the channel bottom be avoided, but the allowable rate of rise is not defined.

Conclusions

Complete standardization of flow passages for low-head hydropower developments is not feasible. Structural and geological considerations may cause design variation from site to site. Allowances for fish passage may control the design in some cases. Package units are presently available for small plants. These units have standard flow passages included. The low costs resulting from standardization are achieved at the expense of some loss in efficiency. However, the cost savings may be significant especially if several installations are considered as a group.

Standardized designs are feasible for similar site characteristics. Where geologic and structural considerations do not vary widely, the same design may be used for a series of installations, thus reducing the costs associated with site-specific engineering and design.

The hydraulic design of the draft tube is customarily determined by the manufacturer since it is considered an integral part of the turbine in determining turbine performance. Results of model tests done by manufacturers are not publicly available. However, modern techniques of boundary layer control may be useful in shortening draft tubes, thus considerably reducing construction

costs. The possibility of reducing draft tube lengths through boundary layer control has not been investigated in hydraulic turbines.

Intake shape is typically determined using design criteria for high velocity conduit entrances. It is possible that intake shapes may be reduced in size or simplified without a significant loss in efficiency. Velocities are generally low in turbine intakes and the resulting energy losses are also low. Simple flow passage shapes can be used in these low velocity areas without increasing energy losses.

Acknowledgments

The work upon which this paper was based was sponsored by the Department of Energy under agreement EG-77-A-36-1024 with the Water and Power Resources Service. The following companies provided some of the information used: Harza Engineering Company, International Engineering Company, Allis-Chalmers, Motor Columbus Consulting Engineers, Inc., F.W.E. Stapenhorst, Inc., Fuji Electric Company, Ltd., Escher Wyss, Ltd., Public Utility District No. 1 of Chelan County, Washington, Karlstads Mekaniska Werkstad, Swedish Power Association, and Hydro Energy Systems, Inc. (Neyrpic). Mention of these companies in no way implies endorsement or recommendation by the Water and Power Resources Service or the United States Government for these companies or their products.

Appendix I.—References

1. Alestig, R., "Influence of Draft Tube Dimensions on Kaplan Turbine Efficiencies," *Transactions, International Association for Hydraulic Research Symposium*, Part 1, Stockholm, Sweden, 1970.
2. Bell, M. C., "Fisheries Handbook of Engineering Requirements and Biological Criteria," *Fisheries—Engineering Research Programs*, Chapters 25 and 33, Corps of Engineers, North Pacific Division, Feb., 1973.
3. Bisaz, E., Taubmann, K. C., and Fischer, P., "Improvement in Transport of Floating Debris," *Water Power and Dam Construction*, Nov., 1976, pp. 41–45.
4. Dadu, V., and Bedros, N., "Determination of Low Head Turbine Installation Quota as Compared to the Downstream Level," Translated from the Rumanian: *Energetica* (Rumania), Vol. 25, No. 2, Feb., 1977, pp. 45–48. (Bureau of Reclamation Translation, May, 1978.)
5. de Siervo, F., and de Leva, F., "Modern Trends in Selecting and Designing Kaplan Turbines," *Water Power and Dam Construction*, Part 11, Jan., 1978, pp. 52–58.
6. Durgin, W. W., and Hecker, G. E., "The Modeling of Vortices at Intake Structures," *Joint Symposium on Design and Operation of Fluid Machinery*, ASME, ASCE, *Society of Civil Engineers*, Vol. 1, June, 1978, pp. 381–391.
7. Gordon, J. L., "Vortices at Intakes," *Water Power*, London, England, Apr., 1970, pp. 137–138.
8. Gubin, M. F., "Draft Tubes of Hydroelectric Stations," Energia Press, Moscow 1970, translated from Russian, Available from the United States Department of Commerce, National Technical Information Service, Springfield, Va.
9. Heinemann, E., Kraft, K. D., and Rouve, G., "Runner Diameter of Tubular Turbines," *Journal of the Power Division*, ASCE, Vol. 102, No. PO1, Proc. Paper 11833, Jan., 1976, pp. 53–61.
10. Isaev, I. M., "Influence of a Method of Air Admission on Pressure Surges in Draft Tube Models of Axial Hydro-Turbines," Translated from the Russian: *Gidromashinostroenie*, Trudy LPI, No. 215, Moscow and Leningrad, pp. 58–68, 1961, by D. L. King, No. 756, July, 1968.

11. Kline, S. J., Abbott, D. E., and Fox, R. W., "Optimum Design of Straight-Walled Diffusers," *Journal of Basic Engineering*, ASME, Sept., 1959, pp. 321–331.
12. "Low Head Power Generation with Bulb Turbines," *International Engineering Company, Inc.*
13. Mercer, A. G., "Study of Factors Affecting Feasibility of Low Head Hydroelectric Generation," *No. 14-06-D-6585, CER68-69AGM26*, Civil Engineering Department, Colorado State University, prepared for United States Department of the Interior, Bureau of Reclamation, March, 1969.
14. Mikhailov, I. E., Mityurev, E. L., Kazennov, V. V., Volshanik, V. V., and Bondarenko, B. V., "Effects of Slots and Apertures in Floors of the Diffusers of Draft Tubes on the Power Characteristics of Hydraulic Turbines with Adjustable Blades," In Russian, *Gidrotekh Stroit*, n 9, Sept., 1973, pp. 10–13.
15. Oman, R. A., Foreman, K. M., and Gilbert, B. L., *Investigation of Diffuser-Augmented Wind Turbines, Part II-Technical Report, Report RE-534*, Research Department, Grumman Aerospace Corporation, prepared for Wind Energy Conversion Branch, Division of Solar Energy, Jan., 1977.
16. Orsborn, J. F., "Rectangular-Bar Trashrack and Baffle Headlosses," *Journal of the Power Division*, ASCE, Vol. 94, No. PO2, Proc. Paper 6223, Nov., 1968, pp. 111–123.
17. Persson, Thorild, and Lasu, Sten, "Mini Powerstations in Sweden," Swedish Power Association, Sept. 1, 1978.
18. Peterka, A. J., and Lindholm, E. A., "A New Look at Penstock Entrance Designs," presented at the April 8–9, 1968, Western Water and Power Symposium, held at Los Angeles, Calif.
19. Rhone, T. J., "Hydraulic Model Studies for the Penstocks for Grand Coulee Third Powerplant," *Bureau of Reclamation Report No. REC-ERC-74-12*, Aug., 1974.
20. Rouve, Ing. Gerhard, "Der Krafthaustrennpfeiler. Stromungsverhaltnisse an gekrummten Wanden," *145 Arbeit Aus Dem Theodor-Rehbock-Flussbaulaboratorium*, Universitat Karlsruhe, Jan., 1958.
21. Sutherland, R. A., "Tubular Turbines," *Bulletin 309*, Washington State University College of Engineering Research Division, Technical Extension Service, 1968.
22. *Hydraulic Design Criteria*, Sheets 111-5, 111-6, 122-2, 111-3/1, 111-3/2, and 221-1, United States Army Corps of Engineers, prepared for Office, Chief of Engineers, by United States Army Engineer Waterways Experiment Station.
23. Varlamov, A. A., Liukonen, IU. N., and Ponarskii, L. I., "Study of the Operating Process of an Enclosed Hydraulic Turbine," Translation from Russian, *Energomashinostroenie*, No. 7, 1977, pp. 1-3, Bureau of Reclamation, May, 1978.
24. Vigander, S., and March, P., "Trashrack Vibration Studies, Raccoon Mountain Pumped-Storage Project," *Laboratory Report No. 1, Report No. 43-47*, Tennessee Valley Authority, Division of Water Control Planning Engineering Laboratory.
25. Wirasinghe, N. E. A., "Effect of Swirl on Conical Diffuser Performance," *Joint Symposium on Design and Operation of Fluid Machinery*, ASME, ASCE, Vol. 1, June, 1978, pp. 223–245.
26. Worster, R. C., "The Efficiency of Diffusers and Some Test Results on the Effect of Wall Roughness," *No. R.R. 554*, The British Hydromechanics Research Association, Mar., 1957.
27. Zeigler, E. R., "Hydraulic Model Vortex Study, Grand Coulee Third Powerplant," *REC-ERC-76-2*, United States Department of the Interior, Bureau of Reclamation, Feb., 1976.

Appendix II.—Notation

The following symbols are used in this paper:

B = pier width;
C = coefficient;
D = runner diameter;
d = intake diameter;
F = Froude number;

H = head;
Hd = design head;
L = pier length;
N = rotating speed;
n = specific speed;
Q = discharge;
r = pier radii;
R = Reynolds number;
S = submergence; and
V = flow velocity.

LOOP EQUATIONS WITH UNKNOWN PIPE CHARACTERISTICS

By Emanuel Gofman[1] and Michael Rodeh[2]

INTRODUCTION

Analyzing water distribution networks (WDNs) by computer programs has been carried out for more than a decade [see Shamir for a bibliography updated to June 1973 (5)]. The main theme has been to try to help the hydraulic engineer in solving those problems which are difficult to solve by hand. However, only a few computer programs have been developed to help in the daily operation of WDNs, such as irrigation systems. Moreover, the operation cost of WDNs is continually increasing due to the energy crisis. With these facts in mind, an easy-to-use interactive WDN analyzer seems to be called for.

To popularize the usage of such analyzers, programs should be developed which could be run simply and relatively inexpensively on minicomputers. One computer system developed along these lines in IBM (International Business Machines) Israel is the Water Distribution Network Analyzer (7) which is based upon the hydraulic network solver of Brailovsky and Rodeh (1) and extensions described herein.

Epp and Fowler (3) observed that loop equations tend to consume less computer memory (and probably less computer time) than node equations. Studies made in Israel indicate that the number of loops in irrigation water distribution networks almost never exceeds 30 (usually it is less than 15) while the number of pipes may be a few hundred, justifying Epp and Fowler's observation. Shamir and Howard (6) generalized the node equation formulation to deal with different types and combinations of unknowns. The unknowns may contain heads, water demands, and pipe characteristics. In (6) Shamir and Howard formulate several rules for the proper selection of unknowns.

In this paper a method is described for incorporating unknown pipe characteristics into loop oriented hydraulic network solvers. A pipe with unknown characteristics may have either a positive resistance (indicating that some regulating valve is to be partially closed) or a negative resistance (indicating that a proper

[1]IBM Israel Scientific Center, The Technion City, Haifa, Israel.
[2]IBM Research, 5600 Cottle Rd., San Jose, Calif. 95193. (On sabbatical from IBM Israel Scientific Center.)

Note.—Discussion open until February 1, 1982. To extend the closing date one month, a written request must be filed with the Manager of Technical and Professional Publications, ASCE. Manuscript was submitted for review for possible publication on December 3, 1980. This paper is part of the Journal of the Hydraulics Division, Proceedings of the American Society of Civil Engineers, ©ASCE, Vol. 107, No. HY9, September, 1981. ISSN 0044-796X/81/0009-1047/$01.00.

booster must be installed). We shall call these new objects—*head generators*. Notice that head generators differ from Jeppson and Davis' pressure reducing valves (4).

In Section 2 the concept of a head generators is explained and its effect on the loop equations is illustrated. In Section 3, Newton's method for solving loop equations with head generators is explained. The intuitive meaning of the constituents of the mathematical scheme is considered. Section 4 is devoted to an informal description of an algorithm for automatically constructing and solving the set of equations. In Section 5, some of the many possible applications of head generators are considered. In Section 6 a sufficient condition for the proper usage of head generators is given.

To those of the readers which are not interested in the details of the method of solving hydraulic problem with head generators we suggest reading Sections 2 and 5 only.

Mathematical Model

Let us consider a network with e edges (pipes) and n nodes, some of which are water sources. (Throughout this paper, only connected networks are considered.) In Fig. 1 we see a network with 8 edges and 7 nodes such that v_1 and v_4 are water sources. Let Q_i ($i = 1, 2, \ldots e$) denote the flow through the pipes and let D_j ($j = 1, 2, \ldots, n$) denote the water demands at the j-th node. Then the flow must obey two fundamental laws.

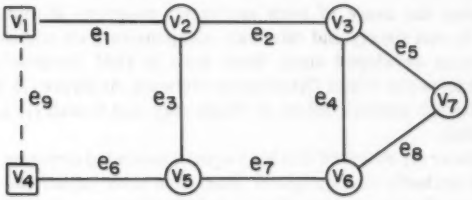

FIG. 1.—Example of Network

Conservation of Flow.—The flow entering into a node must be equal to the flow emanating from it (including the water demand). Formulating this law in terms of the Q_i's and D_j's yields n equations (one for each node). Since the network is considered to be a closed system, the amount of flow entering into or emanating from the network is zero. Therefore, one of the previously mentioned n equations depends on the others and thus, there are $n - 1$ independent equations of this type.

Conservation of Energy.—Each hydraulic element in the network has its impact on the head loss. Denoting the head loss by Δh the effect of such an element may be described as:

$$\Delta h = F(Q)$$

Denoting by Δh_i the head loss in the i-th pipe, the algebraic sum of the head

losses around every closed loop in the network must be equal to zero. If there exists more than one water source (such as in Fig. 1) then fictitious edges connecting one of them to all the others may be added to form fictitious loops. In Fig. 1, e_9 is fictitious. The head loss in a fictitious edge is simply the difference in the altitudes of the two endpoint nodes. A network may contain many distinct loops. For example, the network in Fig. 1 contains 3 real (nonfictitious) loops: (e_2, e_4, e_7, e_3), (e_4, e_5, e_8), and $(e_2, e_5, e_8, e_7, e_3)$ and three additional loops which contain the fictitious edge e_9. Energy should be conserved in each of them. However, it may be shown that not all of the energy equations are independent. In fact, a set of $e - n + 1$ loops may be chosen such that the corresponding equations are both independent and imply all the others. (If there are s sources then $s - 1$ additional loops must be added.)

The standard technique [e.g., see (2)] to construct such an independent set of loops is to find a spanning tree (a connected loop-less subnetwork which contains all the nodes) and then use the loops defined by the non-tree edges. For the network of Fig. 1, a possible spanning tree is the one drawn in Fig. 2. The node v_1 is the root (it is the only node into which no edge enters). Notice that the edges are directed from the root to the leaves. A nontree edge

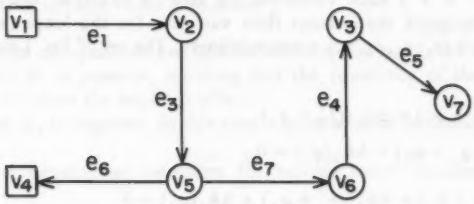

FIG. 2.—Spanning Tree for Network of Fig. 1

such as e_2 closes a loop, i.e. (e_3, e_7, e_4, e_2). The set of loops obtained using the procedure is called a *fundamental set of loops*.

Let us choose a direction for the nontree edges of the network in Fig. 1 as follows: e_2 is directed from v_3–v_2, e_8 is directed from v_7–v_6, and e_9 is directed from v_4–v_1. Then the following loop equations are obtained:

$$\Delta h_3(Q_3) + \Delta h_7(Q_7) + \Delta h_4(Q_4) + \Delta h_2(Q_2) = 0 \quad \ldots\ldots\ldots\ldots (1a)$$

$$\Delta h_4(Q_4) + \Delta h_5(Q_5) + \Delta h_8(Q_8) = 0 \quad \ldots\ldots\ldots\ldots\ldots\ldots (1b)$$

$$\Delta h_1(Q_1) + \Delta h_3(Q_3) + \Delta h_6(Q_6) + [z(v_4) - z(v_1)] = 0 \quad \ldots\ldots\ldots\ldots (1c)$$

$z(v_1)$ and $z(v_4)$ = the altitudes of v_1 and v_4, respectively. (Notice that in the foregoing equations, only + is used. For explanation see Section 4.)

To summarize, there are $(n - 1) + (e - n + 1) + (s - 1) = e + (s - 1)$ equations. The unknowns are the flows in the pipes, including the $s - 1$ fictitious pipes.

Every flow function, Q, is a superposition of two simpler flow functions – Q^T and Q^C, in which:

Q^T **is a Flow Function which may be Nonzero only on a Spanning Tree of**

the Network.—Q^T is responsible for conservation of flow and thus it may be thought of as carrying the water from a source to the nodes with nonzero water demand. Notice that once a spanning tree is chosen, the Q^T flow function is determined. Thus, for the spanning tree in Fig. 2, Q^T is given in the following description of the flow function Q^T for the spanning tree of Fig. 2:

Edge	value of flow, Q^T
e_1	$D_2 + D_5 + D_6 + D_3 + D_7$
e_3	$D_5 + D_6 + D_3 + D_7$
e_7	$D_6 + D_3 + D_7$
e_4	$D_3 + D_7$
e_5	D_7
other edges	0

Q^C **is Circular Flow Function.**—It may be described as a set of circular flows, one for each loop of the fundamental set of loops. This type of flow is responsible for the energy equations. The circular flow variables are denoted by $q_1, q_2, \ldots$ in which q_i is the circular flow in the i-th loop. As explained in the foregoing, there are $e - n + s$ such variables. To give an example, the variables q_1, q_2, q_3 will designate the circular flow variables for the loops (e_3, e_7, e_4, e_2), (e_4, e_5, e_8), and (e_1, e_3, e_6, e_9) correspondingly. The set of Eq. 1 may be written as:

$$\Delta h_3(Q_3^T + q_1 + q_3) + \Delta h_7(Q_7^T + q_1) + \Delta h_4(Q_4^T + q_1 + q_2) + \Delta h_2(q_1) = 0 \quad \ldots\ldots\ldots\ldots\ldots\ldots\ldots\ldots (2a)$$

$$\Delta h_4(Q_4^T + q_1 + q_2) + \Delta h_5(Q_5^T + q_2) + \Delta h_8(q_2) = 0 \quad \ldots\ldots\ldots\ldots (2b)$$

$$\Delta h_1(Q_1^T + q_3) + \Delta h_3(Q_3^T + q_1 + q_3) + \Delta h_6(Q_6^T + q_3) + [z(v_4) - z(v_1)] = 0 \quad \ldots\ldots\ldots\ldots\ldots\ldots\ldots\ldots\ldots\ldots (2c)$$

The computational advantage of decomposing the flow into Q^T and Q^C is that Q^T is easy to compute and must never be updated once the water demands are known, while Q^c depends only on $e - n + s$ variables, a number which in practice is much smaller than both e and n.

Till now the unknowns were the flows through the pipes. We wish to extend the model and allow the pipe characteristics to be unknown. The question may be posed as follows: given an edge, e_i, what should the *additional head loss* R_i in e_i be so that a certain hydraulic effect would be achieved? Notice that R_i is a new unknown and that Q_i—the flow through e_i—remains unknown. Thus, the head loss in e_i will be $R_i + \Delta h_i(Q_i)$. At the present we are interested in the ability to obtain a required pressure, P_j, in some node v_j. In general there may be several head generators, $R_1, \ldots, R_r$, on r of the edges and the requirements would be to achieve certain pressures in r nodes. In Section 5 we show how to use head generators to solve other types of problems.

It is obvious that the ordinary loop equations are not directly capable to model head generators. New variables as well as new equations are required. Let us consider an example first. Assume that a head generator is put on the

edge e_6 of Fig. 1, and that a pressure, P_1, is required at node v_7. A new variable R_1 is used to describe the effect of the head generator. The first two equations of (2) are not changed. The third equation is replaced by:

$$\Delta h_1(Q_1^T + q_3) + \Delta h_3(Q_3^T + q_1 + q_3) + \Delta h_6(Q_6^T + q_3) + R_1 + [z(v_4) - z(v_1)] = 0 \quad (2c')$$

To express the requirement for a fixed pressure in v_7 an additional equation must be introduced: using the spanning tree of Fig. 2 again, the path connecting the root to v_7 is $(e_1, e_3, e_7, e_4, e_5)$, and thus we get:

$$\Delta h_1(Q_1^T + q_3) + \Delta h_3(Q_3^T + q_1 + q_3) + \Delta h_7(Q_7^T + q_1) + \Delta h_4(Q_4^T + q_1 + q_2) + \Delta h_5(Q_5^T + q_2) + [z(v_7) + P_1 - z(v_1)] = 0 \quad (2d)$$

Notice that the new variable R_1 does not appear in the new Eq. 2*d* since the path from the root to v_7 does not include the edge on which a head generator is located.

Concerning the solvability of a system of loop equations in the presence of head generators, three cases may arise:

1. The system of equations has no solution or many solutions.
2. The term R_1 is positive, meaning that the resistance of the pipe should be increased to cause the required effect.
3. The term R_1 is negative. In this case a booster must be installed.

Let us now develop an algorithm for solving loops equations with head generators.

Newton's Method for Solving Loop Equations with Head Generators

Solving loop equations is usually done by Newton's method (3,5). To show how head generators come into the picture, let us consider first the case where there are no head generators at all. Let $\Delta\mathbf{q}$ be a vector of corrections to the circular flow (Δq_i is a correction to the circular flow q_i); $\mathbf{J}$—the Jacobian of the system of equations (to be explained later) and $\mathbf{h}$—a column vector whose i-th element is the total head loss in the i-th loop. Then, the system to be solved is:

$$\mathbf{J} \times \Delta\mathbf{q} = -\mathbf{h} \quad (3)$$

The content of the matrix $\mathbf{J}$ is: (1) $J_{i,i}$ is the derivative with respect to the flow of the head loss in the i-th loop; and (2) $J_{i,j}$ $(i \neq j)$ is the derivative with respect to the flow of the head loss in the edges common to the i-th and j-th loops. Notice that the matrix $\mathbf{J}$ is symmetric. Once $\mathbf{J}$ and $\mathbf{h}$ are available, the system (3) is solved, the $\Delta\mathbf{q}$ are used to update the circular flows and new $\mathbf{J}$ and $\mathbf{h}$ are computed. This is done again and again until the head loss $\mathbf{h}$ in all loops becomes negligible.

Now consider the case when head generators do exist. The system of equations to be solved is changed into:

$$\left[\begin{array}{c|c} \mathbf{A} & \mathbf{C}^{\mathbf{I}} \\ \hline \mathbf{B} & \mathbf{C}^{\mathbf{R}} \end{array}\right] \times \left[\begin{array}{c} \Delta\mathbf{q} \\ \hline \mathbf{R} \end{array}\right] = -\left[\begin{array}{c} \mathbf{h}^{\mathbf{I}} \\ \hline \mathbf{h}^{\mathbf{R}} \end{array}\right] \quad \ldots\ldots\ldots\ldots\ldots\ldots\ldots\ldots\ldots\ldots (4)$$

in which:

1. The variables are of two types: $\Delta\mathbf{q}$—as in (3), and $\mathbf{R}$—a vector of variables, one per each head generator.
2. The right hand side also comprises two parts: $\mathbf{h}^{\mathbf{I}}$ is identical to the $\mathbf{h}$ vector of (3) and $\mathbf{h}^{\mathbf{R}}$ is the difference between the actual pressure and the required in the nodes with fixed pressure.
3. The submatrix $\mathbf{A}$ is identical to the Jacobian of a standard network which does not contain any head generator.
4. The submatrix $\mathbf{B}$ has a column for every loop and a row for every node of fixed pressure. For the j-th loop and the i-th node with fixed pressure, $B_{i,j}$ is the derivative of the head loss in the edges common to the j-th loop and the path in the spanning tree connecting the root to the i-th node with fixed pressure.
5. The submatrices $\mathbf{C}^{\mathbf{I}}$ and $\mathbf{C}^{\mathbf{R}}$ are combinatorial: they contain only zeros and ones (the reason for the nonappearance of minus signs is given in Section 4). They have a column for every head generator. The rows of $\mathbf{C}^{\mathbf{I}}$ correspond to the loops: an entry of $\mathbf{C}^{\mathbf{I}}$ is equal to 1 if the j-th reduction valve is located on an edge which belongs to the corresponding loop. $\mathbf{C}^{\mathbf{R}}$ is similar to $\mathbf{C}^{\mathbf{I}}$ except that it involves paths to the nodes with fixed pressure rather than loops.

For our running example, using the notation $\Delta h_i'$ to denote the derivative of $\Delta h_i(Q)$ with respect to Q, the Jacobian is:

$$\begin{bmatrix} \Delta h_3' + \Delta h_7' + \Delta h_4' + \Delta h_2' & \Delta h_4' & \Delta h_3' & 0 \\ \Delta h_4' & \Delta h_4' + \Delta h_5' + \Delta h_8' & 0 & 0 \\ \Delta h_3' & 0 & \Delta h_1' + \Delta h_3' + \Delta h_6' & 1 \\ \Delta h_3' + \Delta h_7' + \Delta h_4' & \Delta h_4' + \Delta h_5' & \Delta h_1' + \Delta h_3' & 0 \end{bmatrix}$$

Notice that the Jacobian is not symmetric.

Now we describe an algorithm for constructing the set of equations, seen in Eq. 4.

An Algorithm for Constructing and Solving Loop Equations with Head Generators

Constructing Depth First Search Tree.—A depth first search tree is a spanning tree which is obtained by going as "deep" as possible: starting at the root, try to arrive at a new node; continue from there to a new node; continue going deeper and deeper until no new node can be reached; then backtrack and try to emanate again from the node visited before the one exhausted; if necessary, backtrack again. Thus, for the network in Fig. 1, the spanning tree of Fig. 2 is a depth first search tree: Start at v_1. Traverse e_1 and arrive at v_2. From there, to v_5 and v_4. From v_4 there is no way to arrive at a new edge since e_9 leads us back to v_1 which has been visited already (thus, e_9

is a nontree edge). Backtrack to v_5. Traverse e_7 towards v_6, then to v_3, then to v_7. The edge e_8 leads us back to v_6 and thus, e_8 is a nontree edge. Backtrack to v_3. The edge e_2 is again a nontree edge. Then backtrack to v_6, v_5, and v_1 and the algorithm terminates. Notice that the algorithm does not try to minimize path lengths. However, by Brailovsky and Rodeh's construction, there is no need to do so. For implementation details see (1).

Besides being very efficient, an important property of depth first search trees is that a nontree edge always connects a node with one of its ancestors in the tree. To show this property, the network of Fig. 1 is redrawn. Notice that the direction chosen for the tree edges is up, while that of the nontree edges is down (this is always possible).

Every nontree edge closes a loop. Traversing such a loop is done by following the nontree edge down and the tree edges up, until the upper node of the nontree edge is met. This explains why we never have to traverse an edge in a reverse direction. Even more interesting is the fact that the intersection

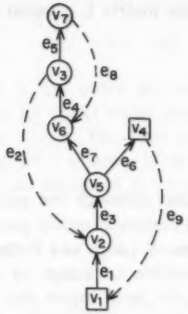

FIG. 3.—Network of Fig. 1 Redrawn

of every two such loops is a path in a tree connecting a node to one of its offsprings. Thus, traversing the intersection of every two loops is also done without using an edge in the reverse direction. Now it should become clear why only '+' signs and no '−' signs appear in Eqs. 1–2.

Head generators do not introduce any significant complication. If a head generator is located on an edge e_i then all loops passing through it must be found. In our case the head generator is located on e_6 and thus the only loop which passes through it is (e_1, e_3, e_6, e_9). Again, the choice of edge directions ensure that only 0 and 1 (and never -1) will appear in the submatrices $\mathbf{C}^{\mathrm{I}}$ and $\mathbf{C}^{\mathrm{R}}$ of (4).

Representing Loops, Paths and Intersections.—To take advantage of the above properties of depth first search trees, the loops, paths and their intersections may be represented explicitly:

1. A loop—by the nontree edge defining it.
2. A path—by its uppermost node.

3. The intersection of two loops—by their uppermost and lowermost nodes in common.

4. The intersection of a loop and a path—by their uppermost common node (the lowermost node is simply the lowermost node of the loop).

Notice that the intersection of two paths is not used and thus need not be represented.

Noticing that the submatrices $\mathbf{C}^{\mathbf{I}}$ and $\mathbf{C}^{\mathbf{R}}$ are static (they do not depend on the current valves of the variables), the following matrix $\mathbf{L}$ may be precomputed (computed once, independent of the water demands):

$$\mathbf{L} = \left[\begin{array}{c|c} \mathbf{L}^{\mathbf{II}} & C^{I} \\ \hline \mathbf{L}^{\mathbf{IP}} & C^{P} \end{array}\right]$$

in which $\mathbf{L}^{\mathbf{II}}$ contains the uppermost and lowermost nodes common to the i-th; and j-th loop positions (i, j) and (j, i), respectively (in which $i > j$); $\mathbf{L}^{\mathbf{IP}}$ contains the uppermost nodes common to loops and paths.

For out running example, the matrix $\mathbf{L}$ is equal to:

$$\begin{bmatrix} 0 & v_6 & v_5 & 0 \\ v_3 & 0 & 0 & 0 \\ v_2 & 0 & 0 & 1 \\ v_3 & v_7 & v_5 & 0 \end{bmatrix}$$

The crucial point here is that although the matrix construction may appear to be hard, it is very efficient computationally [see (1)].

Computing Head Losses Around Loops and Paths.—Traversing the tree edges starting at the root, it is possible to assign to each node, v, the sum $s(v)$ of the head losses (including the head losses due to the existence of the head generators, along the path leading to it. Referring to Fig. 3 the following values of $s(v)$ for every node, v, are obtained:

node	corresponding value of s
v_1	0
v_2	Δh_1
v_3	$\Delta h_1 + \Delta h_3 + \Delta h_7 + \Delta h_4$
v_4	$\Delta h_1 + \Delta h_3 + \Delta h_6 + R_1$
v_5	$\Delta h_1 + \Delta h_3$
v_6	$\Delta h_1 + \Delta h_3 + \Delta h_7$
v_7	$\Delta h_1 + \Delta h_3 + \Delta h_7 + \Delta h_4 + \Delta h_5$

The foregoing data may be computed by a single traversal of each edge. Now computing the head loss along a loop defined by an edge e_i connecting v_j to v_k is simply $s(v_j) - s(v_k) + \Delta h_i$. For a path connecting the root to a node v_j the sum of the headloss is even easier; it is equal to $s(v_j)$.

Computing Derivative of Head Losses Along Loops and Intersections.—This operation is identical to that of computing head losses along paths, except that the endpoints are found in the matrix $\mathbf{L}$, and that derivatives rather than the

head losses themselves are involved (thus, the head generators do not appear).

Solving Equations and Updating Circular Flow.—In Section 4.2–4.3 a method for constructing the system (4) of equations has been proposed. If the head losses along loops are negligible and the head at the nodes with fixed pressure is close to that required then the computation is completed. Otherwise the corrections $\Delta \mathbf{q}$ must be distributed along the edges of the corresponding circuits. The nice properties of the depth-first search trees may be used again. For every nontree edge, the only entry of the vector of corrections which contributes to that edge is the one which corresponds to the loop defined by the edge. Thus, referring to Fig. 3, the correction of e_2, e_8, and e_9 is Δq_1, Δq_2, and Δq_3, respectively.

As for the tree edges, proceed as follows: Assign a value $d(v)$ (initially zero) to every node; add Δq_i to the tail and $-\Delta q_i$ to the head of every nontree edge with correction Δq_i. For the network in Fig. 3 the values $d(v)$'s are given by the values of $d(v)$ for every node, v:

node	v_1	v_2	v_3	v_4	v_5	v_6	v_7
the corresponding value of d	$-\Delta q_3$	$-\Delta q_1$	Δq_1	Δq_3	0	$-\Delta q_2$	Δq_2

Now scan the tree edges in a top down manner, scanning an edge only if all the edges emanating from its upper node have been scanned already, and accumulate the values of the $d(v)$'s. The final correction of the circular flow in an edge is equal to the final $d(v)$ where v is its uppernode. For the preceding example we get the accumulated values of d, for all nodes:

node	v_1	v_2	v_3	v_4	v_5	v_6	v_7
the corresponding accumulated value of d	0	Δq_3	$\Delta q_1 + \Delta q_3$	Δq_3	$\Delta q_1 + \Delta q_3$	Δq_1	Δq_2

Thus, the corrections of the circular flow in the edges are the correction to the circular flows through the edges:

edge	e_1	e_2	e_3	e_4	e_5	e_6	e_7	e_8	e_9
correction of flow	Δq_3	Δq_1	$\Delta q_1 + \Delta q_3$	$\Delta q_1 + \Delta q_2$	Δq_2	Δq_3	Δq_1	Δq_2	Δq_3

Again, this method for updating the flow through the edges is computationally appealing since it is very efficient. Specific algorithmic details appear in (1).

Applications

In this section we consider several practical applications of head generators. One of the simplest cases is when the given network contains a well and a reservoir. The target is to fill the reservoir as fast as possible while still keeping the pressure at the valves sufficiently high. To this effect a regulating valve is available, by which the flow into the reservoir may be controlled. Referring

to Fig. 1 assume that the altitudes and water demands at the nodes are as follows:

node	v_1	v_2	v_3	v_4	v_5	v_6	v_7
altitude (in meters)	100	70	32	50	30	32	35
water demand	source	—	—	reservoir	—	—	150 m^3/h

Also assume that the regulating valve is on pipe e_6, the required pressure at v_7 is 30 m and the pipe parameters are:

pipe	e_1	e_2	e_3	e_4	e_5	e_6	e_7	e_8
length (in meters)	100	100	100	100	150	100	100	100
diameter (in millimeters)	150	100	150	100	100	150	100	100
Hazen-Williams coefficient	110	110	110	110	110	110	110	100

To model this setup a head generator is introduced on e_6 and the following results are obtained: (1) The flow in e_1 is 220.3 m^3/h and in e_6 it is −70.3, namely, water is indeed entering into the reservoir; and (2) the regulation valve should create a head loss of 34.1 m. (These results were obtained using the experimental system developed in the IBM Israel Scientific Center.)

Now assume that a discharge of 180 m^3/h rather than 150 m^3/h is required in v_7. In such a case the source, v_1, cannot supply all the demand in the required pressure. To obtain a pressure of 30 m at v_7 a booster must be installed on e_6. It must yield a head of 47.1 m in a discharge of 58 m^3/h. This time v_1 will supply only 122 m^3/h.

As a third example, assume that a pump with the following characteristics is installed on e_6:

discharge	50	60	70	80	90
head	65	62	57	50	40
efficiency, as a percentage	65	68	65	61	55

For a water demand of 180 m^3/h source v_1 supplies 99.1 m^3/h; the reservoir v_4 supplies 80.9 m^3/h; the pump works with 60.2% efficiency creating a pressure of 49.2 m consuming 18.3 kW; the pressure at v_7 is 31.2 m. If a head generator is introduced on e_6 to lower the pressure at v_7 to 30 m the results are: v_1 supplies 122 m^3/h; v_4 supplies 58 m^3/h; the pump works with 67.6% efficiency creating a pressure of 62.7 m consuming only 14.9 kW. The regulating valve must cause a head loss of 15.6 m. It should be mentioned that the energy consumption per cubic meter is increased from 0.226 kW–0.256 kW but the total amount of water passing through the pump is lower. To summarize this case, a method to save energy by a regulating valve has been demonstrated.

To conclude this section we must point out that the solutions to (4) must be inspected with care. Consider our network again, and assume that pipe e_6 is closed and the water demand at v_7 is 90 m^3/h. Then the pressure at v_7 will be 54.1 m. In order to lower the pressure to 30 m one may consider installing

a regulating valve on e_8. This will yield the required pressure for a somewhat unexpected price: a booster, creating a head of 30.6 m for a discharge of 11.9 m^3/h from v_7–v_6 must be installed. In this way the flow through e_5 is increased, the head losses increase also and the pressure at v_7 is decreased. We doubt whether such a solution is reasonable.

As for the efficiency of the proposed algorithm, all the solutions quoted above require at most 5 iterations (some took only 4) to achieve a maximal head loss imbalance around loops of less than 0.01 m.

On Solvability of System of Equations in Presence of Head Generators

It is well known that in the absence of head generators the system of equations (3), virtually always, has a unique solution. When head generators are introduced the corresponding set of Eqs. 4 may have no solution or many solutions. The network of Fig. 4, in which v_2 and v_5 are nodes with fixed pressure, v_1 is the water source and e_2 and e_5 are edges with head generators, is in general not solvable: the two head generators have an effect of one and thus, there is no way to create the required pressure on both v_2 and v_5 (except for specific pressure requirements). This type of unsolvability of (4) is due to the topological

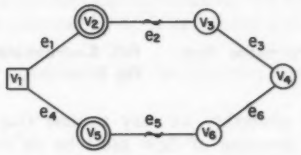

FIG. 4.—Two Head Generators with Effect of One

structure of the network. In order to prevent improper allocation of head generator and nodes with fixed pressure in the network, a sufficient condition is developed.

First, notice that we may assume that the network contains only one water source. Otherwise choose one of the several water sources as a reference node, connect it to the others by edges with negligible resistance on which head generators are located, and consider these water sources as nodes with zero pressure. An obvious necessary condition for solvability of (4) for arbitrary pipe characteristics is that the number of head generators equals the number of nodes with fixed pressure (not counting the reference node, although the pressure there is known).

A sufficient condition for the existence of pipe characteristics for which (4) has a unique solution is the existence of a connected subnetwork G' of the given network G such that:

1. All head generators, nodes with fixed pressure and the unique water source belong to G'.
2. G' is loopless.
3. For every two nodes with fixed pressure (or a node with fixed pressure and the water source) the unique path in G' connecting them contains at least one head generator.

The proof that these conditions are indeed sufficient is given in Appendix I. Notice that the network of Fig. 4 does not satisfy the aforementioned sufficient conditions. If the water source were v_4 rather than v_1 then the required pressures in v_2 and v_5 could be achieved.

A network which topologically seems all right may be problematic with respect to certain data. Consider, e.g., the network of Fig. 5. Assume that v_1 is a water source, v_4 is a node with a required pressure P, all the edges are identical and e_5 contains a head generator. If the problem has a solution with a nonzero flow through the pipe e_5, then the reverse flow is an alternative solution, as can easily be seen by symmetry. Therefore, two solutions are possible.

If the altitudes of all the nodes are zero and $P > 0$ then the problem has no solution of all. The reason is that the head generator must have a nonzero

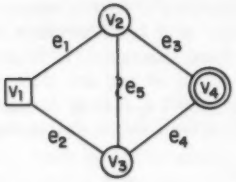

FIG. 5.—Example of Symmetric Network

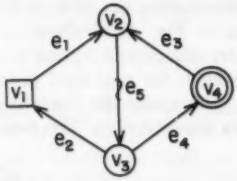

FIG. 6.—Possible Flow in Network of Fig. 5

effect. Without loss of generality we may assume that the flow through e_5 goes from v_2–v_3. The direction of flow must be as in Fig. 6. Assuming a water demand D_4 at v_4 and denoting the flow through pipes by Q_i we get:

$$\Delta h(Q_1) + \Delta h(Q_2) = \Delta h(Q_3) + \Delta h(Q_4).$$

But $Q_2 = Q_1 - D_4$ and $Q_3 = Q_4 - D$

and thus $\Delta h(Q_1) + \Delta h(Q_1 - D_4) = \Delta h(Q_4) + \Delta h(Q_4 - D_4)$.

Since Δh is a monotonic function this implies that $Q_1 = Q_4$; therefore $Q_2 < Q_4$ and the head loss in e_2 is smaller than in e_4, and a positive pressure at v_4 cannot be achieved.

Conclusions

Quite extensive experimentation with head generators has been conducted in Israel during 1978–80. It was found that the method is very useful for both designing and operating water distribution networks. The computer time needed to construct and solve the system of equations is negligible. In fact, even large networks with about 300 pipes and 25 loops, water sources and head generators can be solved efficiently on a portable computer such as the IBM/5110. It is believed that this would have been impossible if node equations were involved, due to storage limitations. An easy-to-use interface was inevitable if these ideas were to be widely used. The system developed in Israel contains such an interface, and indeed, many hydraulic engineers, students and even farm managers have used the system with only minor guidance.

Acknowledgment

We wish to acknowledge fruitful conversations with Dov Ramm and great help in carrying out experiments given to us by J. Heller of the Israel Ministry of Agriculture, and Z. Shavit of the Israel Water Workers Association.

Appendix I.—Proof of Sufficient Condition of Section 6

G' is a loopless subgraph of the given network, G, which contains all head generators, nodes with fixed pressure and the reference node. G' may be augmented by nodes and edges to form a spanning tree, T, rooted at the reference node. The head generators may be renumbered according to their distance from the root such that R_1 is the closest to the root, R_2 is next to closest, etc. If two head generators have equal distances from the root, the order between them is arbitrary.

For every node with fixed pressure we associate the head generator closest to it on the way to the root. Condition (3) implies that this association is biunique. Otherwise two nodes with fixed pressure would be associated with the same head generator, which implies that the path connecting them in the tree does not contain any head generator. Let us renumber the nodes with fixed pressure such that the i-th node (denoted by u_i) is associated with the i-th head generator (denoted by R_i).

Referring to Eqs. 4 constructed for the spanning tree, T, the matrix $\mathbf{C^R}$ has the form:

$$C_{ij}^R = \begin{cases} 0 & \text{if } i<j \\ 0, 1, -1 & \text{if } i>j \\ 1, -1 & \text{if } i=j \end{cases}$$

Thus, the matrix $\mathbf{C^R}$ is nonsingular. It has an additional interesting property: if $C_{ij}^R \neq 0$ then the first j entries of the i-th row are all equal to the first j entries of the j-th row. Thus, if k is the maximal column number such that $C_{ik}^R \neq 0$ and $k < i$, then by subtracting the k-th row from the i-th row, the i-th row will contain a nonzero element only in position C_{ii}^R.

Now consider some initial flow Q^T which is zero in all the nontree edges. Perturb Q^T by adding a circular flow of 1 m^3/h around each of the loops, to obtain a flow Q. Choose pipe parameters such that the resistance of each nontree edge is very high while those of all the tree edges are very low. The matrix $\mathbf{A}$ of (4) will have big elements along the diagonal and small elements elsewhere. The elements of the matrix $\mathbf{B}$ will also be small. Thus, by subtracting rows to transform $\mathbf{C^R}$ into a unit matrix, the elements of $\mathbf{B}$ remain small. Then the rows of $\mathbf{C^R}$ may be used to transform $\mathbf{C^I}$ into a matrix of zeros only, leaving the diagonal of $\mathbf{A}$ large. This shows that the Jacobian of (4) may be made nonsingular, and therefore, that (4) is solvable.

Appendix II.—References

1. Brailovsky, M., and Rodeh, M., "An Improved Hydraulic Network Solver," TR065-IBM Israel Scientific Center, June, 1978.

2. Bryant, P. R., "Graph Theory Applied to Electrical Networks," *Graph Theory and Theoretical Physics*, F. Harary, ed., Academic Press, New York, N.Y., 1967.
3. Epp, R., and Fowler, A. G., "Efficient Code for Steady-State flows in Networks," *Journal of the Hydraulics Division*, ASCE, Vol. 96, No. HY1, Proc. Paper 7002, Jan., 1970, pp. 43–56.
4. Jeppson, W. R., and Davis, A. L., "Pressure Reducing Valves in Pipe Network Analyses," *Journal of the Hydraulics Division*, ASCE, Vol. 102, No. HY7, Proc. Paper 12252, July, 1976, pp. 987–1001.
5. Shamir, U., "Water Distribution Systems Analysis," *RC-4389*, IBM Thomas J. Watson Research Center, Yorktown Heights, N.Y., Jan., 1973.
6. Shamir, U., and Howard, D. D. C., "Engineering Analysis of Water-Distribution Systems," *Journal American Water Works Association*, Vol. 69, No. 9, Sept., 1977.
7. "Water Distribution Network Analyzer," *5788-ZWA*, IBM Israel, May, 1980.

Appendix III.—Notation

The following symbols are used in this paper:

$\mathbf{A}, \mathbf{B}, \mathbf{C}^{\mathrm{I}}, \mathbf{C}^{\mathrm{R}}$ = submatrices of Jacobian of system of equations when head generators are present;
$D_1, D_2, \ldots$ = water demand at v_1, v_2, ...;
$d(v)$ = an auxiliary vector to compute correction to flow;
e = number of edges in network;
$e_1, e_2, \ldots$ = edges (pipes);
$\mathbf{h}$ = vector of head losses around loops;
$\mathbf{J}$ = Jacobian of standard problem (with no head generators);
$\mathbf{L}$ = matrix representing intersections of loops and paths;
$\mathbf{L}^{\mathrm{II}}, \mathbf{L}^{\mathrm{IP}}$ = submatrices of $\mathbf{L}$;
n = number of nodes in network;
$Q_1, Q_2, \ldots$ = flow through pipes e_1, e_2, ...;
q_i = variable expressing circular flow around i-th loop;
Q^C = vector of circular flow;
Q^T = vector of flows which is nonzero only on spanning tree;
R_i = i-th head generator;
s = number of sources;
$s(v)$ = sum of head losses on path from root to v;
$v_1 v_2, \ldots$ = nodes;
$z(v_i)$ = altitude of v_i;
$\Delta h_i'$ = derivative of head loss in e_i;
$\Delta\mathbf{h}$ = vector of head losses; and
$\Delta\mathbf{q}$ = vector of corrections to circular flow.

PARAMETRIC STUDY OF FLOOD WAVE PROPAGATION

By K. Sridharan[1] and M. S. Mohan Kumar[2]

INTRODUCTION

The one-dimensional, gradually varied, unsteady flow equations, commonly referred to as Saint-Venant equations, form the basis of study of flood wave motion in open channels. Recent studies in this area were generally concerned with finding new methods for solution of these equations. A number of numerical schemes have been proposed based on finite difference methods. These schemes can be broadly classified into the characteristic methods in which the integration is done along with characteristics (2,3,7,9,11) and direct methods in which the basic equations are directly expressed in finite difference form (1,5,7,13). The direct methods can again be classified into explicit (5,7,10,12) and implicit finite difference methods (1,7,10,13). The explicit methods which advance the solution by simple explicit algebraic expressions suffer from the disadvantage of restricted stability. In the implicit method, unconditional stability is obtained at the cost of algebraic complexity.

Most of the earlier studies on numerical solution of flood wave problem either deal with the task of developing new numerical schemes, improving old schemes or applying these methods to specific field problems. There have been comparative studies of different numerical schemes by Liggett and Woolhiser (7), Price (10), and Strelkoff (13). A generalized parametric study on the flood wave problem is relatively scarce. Mozayeny and Song (9) studied the subsidence of a sinusoidal wave in a long rectangular channel of 1-ft (0.305-m) width with an initial uniform flow depth of 0.3 ft (0.0915 m). A sinusoidal wave of 30 sec duration was taken as the inflow hydrograph. Using the characteristic method on a rectangular grid, they studied the effect of wave amplitude, Manning's n and bed slope on subsidence of the wave. While these studies give an indication of the nature of damping of a flood wave in a prismatic channel, the studies are of a very restricted nature and the wave amplitude range considered, namely 0.002 ft (0.610 mm) to 0.02 ft (6.1 mm) forms a very small fraction of the initial flow depth of 0.3 ft (0.0915 m). A qualitative study of subsidence in prismatic channels for such small amplitude waves was also made by Henderson

[1]Asst. Prof., Civ. Engrg. Dept., Indian Inst. of Science, Bangalore, India 560012.
[2]Research Scholar, Civ. Engrg. Dept., Indian Inst. of Science, Bangalore, India 560012.

Note.—Discussion open until February 1, 1982. To extend the closing date one month, a written request must be filed with the Manager of Technical and Professional Publications, ASCE. Manuscript was submitted for review for possible publication on December 4, 1980. This paper is part of the Journal of the Hydraulics Division, Proceedings of the American Society of Civil Engineers, ©ASCE, Vol. 107, No. HY9, September, 1981. ISSN 0044-796X/81/0009-1061/$01.00.

(4) and it was concluded that there could be significant subsidence in prismatic channels.

In order to obtain a generalized picture of the damping of a flood wave in a prismatic channel, it would be better to convert the problem into a nondimensional form and make a parametric study to investigate the effects of flow parameters, wave parameters and channel shape parameters. The utility of such a nondimensional approach for steady varied flow, has already been demonstrated by Lakshmana Rao and Sridharan (6). A nondimensional parametric study for unsteady flows was made by Sakkas and Strelkoff (11) for the dam break problem.

The present paper presents a parametric study of flood wave propagation problem based on numerical solution of the nondimensionalized unsteady flow equations. The propagation of a sinusoidal flood wave in a prismatic channel is studied for uniform initial flow. The governing parameters, namely the initial uniform flow Froude number, the wave parameters and the channel shape parameters are varied over a wide range.

Formulation of Problem

The one dimensional equation of continuity and motion for unsteady channel flows are written as

$$vw\frac{\partial y}{\partial x} + a\frac{\partial v}{\partial x} + w\frac{\partial y}{\partial t} = 0 \quad \ldots\ldots\ldots\ldots\ldots\ldots\ldots\ldots\ldots\ldots (1)$$

$$g\frac{\partial y}{\partial x} + v\frac{\partial v}{\partial x} + \frac{\partial v}{\partial t} = gS_o\left(1 - \frac{S_f}{S_o}\right) \quad \ldots\ldots\ldots\ldots\ldots\ldots\ldots\ldots\ldots\ldots (2)$$

in which x = distance along the channel; t = time; y = depth of flow; v = velocity of flow: a = cross-sectional area of flow; w = top width of flow; S_o = bed slope; S_f = friction slope; and g = gravitational acceleration. If the initial flow is taken to be uniform, from Manning's formula, assuming $n = n_o$

$$\frac{S_f}{S_o} = \left(\frac{v}{v_o}\right)^2\left(\frac{r}{r_o}\right)^{-4/3} \quad \ldots\ldots\ldots\ldots\ldots\ldots\ldots\ldots\ldots\ldots (3)$$

in which r = hydraulic radius and subscript o refers to initial uniform flow conditions. Eqs. 1 and 2 are nondimensionalized to enable a generalized parametric study, as follows. The depth y is nondimensionalized with respect to y_o, initial uniform flow depth; all cross-sectional dimensions are nondimensionalized with respect to y_o; the longitudinal distance along the channel x is nondimensionalized with respect to $l_o = y_o/S_o$; the velocity v is nondimensionalized with respect to v_o, initial uniform flow velocity; time t is nondimensionalized with respect to $t_o = l_o/v_o$. With this nondimensionalization, Eqs. 1 and 2 become,

$$V\frac{\partial Y}{\partial X} + \phi_1(Y)\frac{\partial V}{\partial X} + \frac{\partial Y}{\partial T} = 0 \quad \ldots\ldots\ldots\ldots\ldots\ldots\ldots\ldots\ldots\ldots (4)$$

$$\frac{\partial Y}{\partial X} + \frac{F_o^2 d_o}{y_o}V\frac{\partial V}{\partial X} + \frac{F_o^2 d_o}{y_o}\frac{\partial V}{\partial T} = 1 - V^2\phi_2(Y) \quad \ldots\ldots\ldots\ldots\ldots\ldots\ldots (5)$$

in which capital letters denote the nondimensional quantities with the corresponding small letters denoting the dimensional quantities; d_o is the hydraulic mean depth corresponding to a depth y_o given by

$$d_o = \frac{a_o}{w_o} \quad \ldots\ldots\ldots\ldots\ldots\ldots\ldots\ldots\ldots\ldots\ldots\ldots\ldots\ldots\ldots\ldots\ldots\ldots\ldots\ldots (6)$$

F_o is the uniform flow Froude number given by

$$\mathsf{F}_o = \frac{v_o}{\sqrt{g d_o}} \quad \ldots\ldots\ldots\ldots\ldots\ldots\ldots\ldots\ldots\ldots\ldots\ldots\ldots\ldots\ldots\ldots\ldots\ldots\ldots\ldots (7)$$

ϕ_1 and ϕ_2 are functions of Y given by

$$\phi_1(Y) = \frac{A}{W} \quad \ldots\ldots\ldots\ldots\ldots\ldots\ldots\ldots\ldots\ldots\ldots\ldots\ldots\ldots\ldots\ldots\ldots\ldots\ldots\ldots (8)$$

$$\phi_2(Y) = \left(\frac{r}{r_o}\right)^{-4/3} \quad \ldots\ldots\ldots\ldots\ldots\ldots\ldots\ldots\ldots\ldots\ldots\ldots\ldots\ldots\ldots\ldots\ldots\ldots\ldots\ldots (9)$$

For rectangular and trapezoidal channel shapes considered in this study, d_o/y_o, ϕ_1 and ϕ_2 are functions of B_t and Z in which $B_t = y_o/b$ is the inverse of the nondimensional bed width with b = channel bed width and Z is the side slope of the channel ($Z = 0$ for rectangular channels).

The present studies are concerned with the propagation of a sinusoidal flood wave along a prismatic channel in which the initial flow is uniform. At the left boundary, $X = 0$, a sinusoidal inflow hydrograph starting at $T = 0$ is considered. The sinusoidal wave introduced at $x = 0$ is of the form

$$y = y_o + \frac{y_w}{2}\left[1 - \cos\left(\frac{2\pi t}{t_w}\right)\right]; \quad 0 \le t \le t_w y = y_o; \quad t > t_w \ldots\ldots (10)$$

in which y_w = wave amplitude; and t_w = duration over which the wave exists at $x = 0$. Nondimensionalization of Eq. 10 leads to

$$Y = 1 + \frac{Y_w}{2}\left[1 - \cos\left(\frac{2\pi T}{T_w}\right)\right]; \quad 0 \le T \le T_w\, Y = 1; \quad T > T_w \ldots\ldots (11)$$

$$\text{in which} \quad Y_w = \frac{y_w}{y_o}; \quad T_w = \frac{t_w}{t_o} \quad \ldots\ldots\ldots\ldots\ldots\ldots\ldots\ldots\ldots\ldots (12)$$

The initial characteristic along which $Y = 1$; and $V = 1$ may be treated as the right boundary of the solution region.

Cases Studied and Methodology

The parameters governing the problem defined by Eqs. 4, 5, and 11 are the initial flow Froude number F_o, nondimensional wave amplitude Y_w, nondimensional wave duration T_w and the channel shape parameters. For rectangular and trapezoidal channels, the shape parameters are B_t and Z. These parameters are varied over a wide range systematically and their effects on subsidence of the wave is studied. The initial uniform flow number, F_o is varied over

the range of 0.1–0.7; Y_w is varied 15 fold from 0.1–1.5; T_w is varied six fold from 0.5–3.0; B_t is varied from 0–1 corresponding to very wide channels to very narrow channels; Z is varied from 0–3. As the study is concerned with subsidence of flood waves, the wave parameter values for different cases are chosen such that shock formation does not occur.

An irregular characteristic grid method has been used to get the solution. Liggett and Woolhiser (7) has compared this method with other numerical methods and claim this method to be the most accurate one. A disadvantage of this method is the need to interpolate the results for depth and velocity at fixed sections or fixed time as the solution is obtained at grid points governed by the characteristics. In the present computations, interpolation was done continuously as the computations progress. Two cases studied by Mozayeny and Song (9) were solved using the characteristic grid method after nondimensionalization of the relevant data. The results from the characteristic grid method and those obtained by Mozayeny and Song (9) using characteristic method as a rectangular grid compared well. The subsidence indicated by Mozayeny and Song was slightly larger with respect to the results from the characteristic grid method.

Computations were made on the DEC 1090 digital computer for 49 cases in all and for each case, computations were made for over 50,000 grid points in the XT plane. Effects of F_o, Y_w, T_w, B_t, and Z on the modification of stage hydrographs, discharge hydrographs, instantaneous wave profiles, stage and discharge subsidence rates and the speed of the wave peak were studied in detail. The results are presented in a summarized form here laying stress on stage and discharge subsidence rates.

Analysis of Results

Stage and Discharge Hydrographs.—Typical results of the modification of stage and discharge hydrographs are presented in Figs. 1 and 2 respectively, for a wide channel ($B_t = 0$) with $F_o = 0.3$, $Y_w = 0.5$ and $T_w = 3.0$. The nondimensional discharge is defined by

$$Q = \frac{q}{q_o} \quad \text{. . . . . (13)}$$

in which q = discharge at any location and time and q_o initial uniform flow discharge. It is seen from Figs. 1 and 2 that there is a significant subsidence of the wave with distance, which was observed in varying degrees for all the cases. The rate of rise of the hydrograph is found to be greater than the rate of recession as typical of a flood wave. The tail end of the discharge hydrograph at $X = 0$ dips below 1.0, a trend observed by Mozayeny and Song (9) also. This is because in the recession stage of a flood, the same stage yields lower discharge due to the nature of water surface profile along the channel.

Effect of Froude Number on Subsidence.—Subsidence of stage is studied in terms of the relative wave amplitude Y_w^* defined by

$$Y_w^*(X) = \frac{Y_{max}(X) - 1}{Y_w} \quad \text{. . . . . (14)}$$

Thus, the relative wave amplitude gives the local wave amplitude normalized

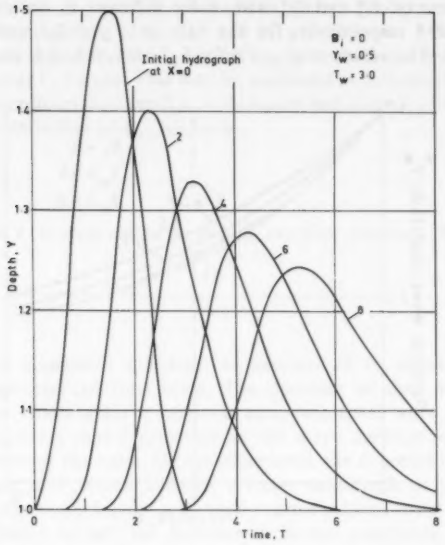

FIG. 1.—Modification of Stage Hydrograph with Distance, $F_o = 0.3$

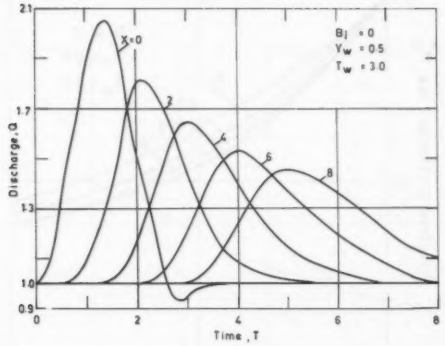

FIG. 2.—Modification of Discharge Hydrograph with Distance, $F_o = 0.3$

with respect to the initial wave amplitude at $X = 0$. Subsidence of discharge is considered in terms of an analogous quantity, the relative discharge rise Q_w^* defined by

$$Q_w^*(X) = \frac{Q_{max}(X) - 1}{Q_{max}(0) - 1} \quad \ldots \ldots \ldots \ldots \ldots \ldots \ldots \ldots \ldots \ldots \ldots \ldots \quad (15)$$

The variations of Y_w^* and Q_w^* with X for different F_o values are presented in Figs. 3 and 4 respectively, for the case of $Y_w = 0.5$ and $T_w = 3.0$ for wide channels. The values of $Q_{max}(0)$ for $F_o = 0.1$, 0.3, 0.5, and 0.7 are 2.050,

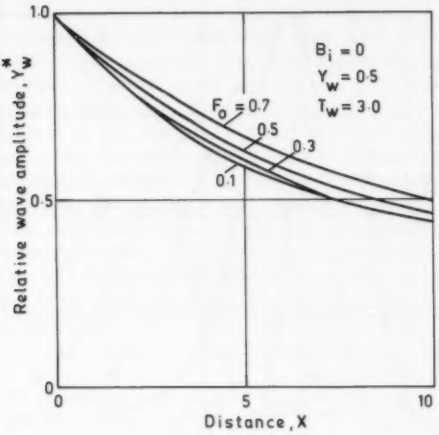

FIG. 3.—Subsidence of Relative Wave Amplitude—Effect of Froude Number

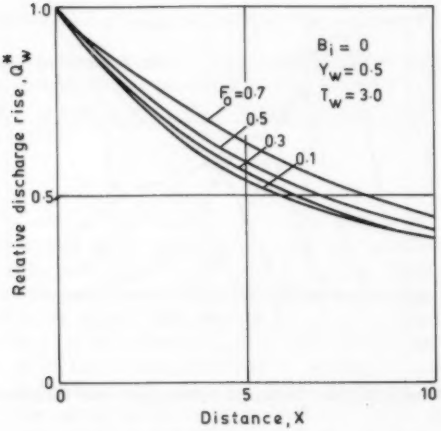

FIG. 4.—Subsidence of Relative Discharge Rise—Effect of Froude Number

2.055, 2.057, and 2.058, respectively. Computations showed that for $Y_w = 0.5$ and $F_o > 0.8$, local supercritical flow might occur during the time of peak of the wave. Thus, computations were restricted to $F_o < 0.8$. The significant

damping of the wave in prismatic channels is clearly brought out by Figs. 3 and 4. The wave amplitude at $X = 5$ and 10 are 59% and 44% respectively of the initial wave amplitude for F_o on the rate of subsidence with subsidence being more at lower F_o values. This may be explained as follows. If we consider a specified initial uniform flow depth y_o and channel bed slope S_o, from Manning's formula and the definition of F_o, we have

$$n \propto \frac{1}{\mathsf{F}_o}; \quad v_o \propto \mathsf{F}_o \quad \text{(16)}$$

The length scale l_o is constant as y_o and S_o are kept constant. The time scale t_o, varies as

$$t_o = \frac{l_o}{v_o} \propto \frac{1}{\mathsf{F}_o} \quad \text{(17)}$$

Thus, under the conditions specified, an increase of F_o denotes a decrease of channel roughness and time scale. The decrease of time scale implies a flood of shorter duration for a constant nondimensional wave duration, T_w. Computations indicate that a reduction in the wave duration would result in a larger subsidence of the wave. On the other hand, the decrease of n associated with the increase of F_o would indicate a lesser subsidence of the wave. The fact that the subsidence is lesser for higher F_o values indicate the greater influence of the second factor, namely the decrease in channel roughness. Computations for different combinations of Y_w and T_w consistently confirm this observation.

Mozayeny and Song (9) reported an exponential decay for the wave amplitude with distance. The present results show that subsidence in the initial reaches

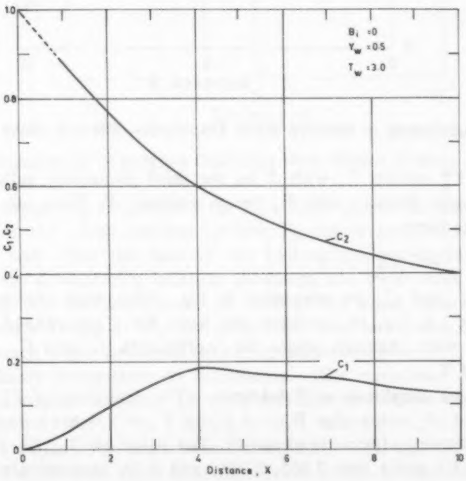

FIG. 5.—Variation of C_1 and C_2 with X

is given by an exponential relationship such as

$$Y_w^* = e^{-KX} \quad \ldots \quad (18)$$

However, as the wave form is modified with distance, a constant exponent does not describe the subsidence rate for the entire reach. The results show that corresponding to a greater subsidence and therefore greater change in the wave form, the limiting X up to which K remains constant is less for lower F_o values. For the results given in Fig. 3, K value for the initial reach is found to vary with F_o, from 0.104 up to $X = 5$ for $F_o = 0.1$ to 0.075 up to $X = 8$ for $F_o = 0.7$. The channel reach considered by Mozayeny and Song corresponds to X less than 0.35 and thus a constant K was obtained for the entire length.

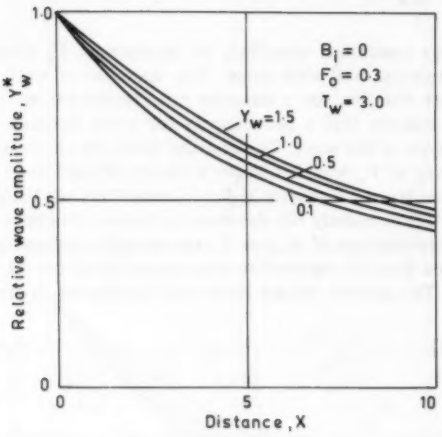

FIG. 6.—Subsidence of Relative Wave Amplitude—Effect of Wave Amplitude

A plot of Y_w^* against F_o with X as the third parameter indicated that Y_w^* varied practically linearly with F_o for a constant X. Thus, an equation was obtained in the form

$$Y_w^* = C_1(X)F_o + C_2(X) \quad \ldots \quad (19)$$

Results for C_1 and C_2 are presented in Fig. 5 for wide channels for $Y_w = 0.5$ and $T_w = 3.0$. Eq. 19 can form the basis for a generalized prediction of subsidence in wide channels where the coefficients, C_1 and C_2, are functions of X, T_w, and Y_w.

Effect of Wave Amplitude on Subsidence.—The variations of Y_w^* and Q_w^* with X for different Y_w values for $F_o = 0.3$ and $T_w = 3.0$ are presented in Figs. 6 and 7 respectively, for wide channels. The value of $Q_{max}(0)$ for $Y_w = 0.1$, 0.5, 1.0, and 1.5 are 1.186, 2.055, 3.354, and 5.05, respectively. It is clearly seen from Figs. 6 and 7 that wave amplitude has some effect on the relative subsidence rate confirming the nonlinearity of the phenomenon. Subsidence

is relatively lesser for higher wave amplitudes, but this nonlinearity effect is clearly lesser in results of relative discharge rise. In fact beyond a particular X value, the Q_w^* values are practically identical for different Y_w values. The wave amplitude at $X = 10$ is 48% and 42% of the initial wave amplitude at $X = 0$ for $Y_w = 1.5$ and 0.1, respectively. The corresponding discharge rise at $X = 10$ is 39% of the original discharge rise at $X = 0$ for both $Y_w = 1.5$ and 0.1.

Effect of Wave Duration on Subsidence.—The variations of Y_w^* and Q_w^* with X for different T_w values for $F_o = 0.3$ and $Y_w = 0.5$ are presented in Figs. 8 and 9 respectively, for wide channels. The values of $Q_{max}(0)$ for $T_w = 0.5$, 1.0, 2.0, and 3.0 are 2.486, 2.274, 2.116, and 2.055, respectively. It is seen that wave period has a pronounced effect on the subsidence rate. The wave amplitude subsides to 13% of the original amplitude at $X = 5$ for $T_w = 0.5$

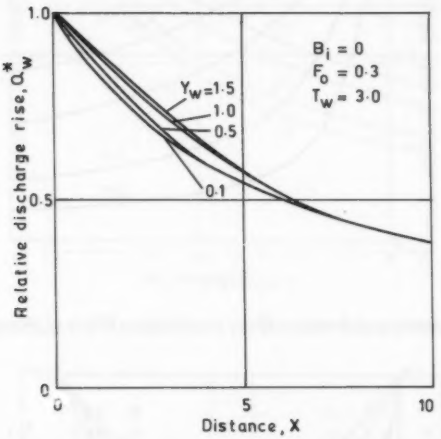

FIG. 7.—Subsidence of Relative Discharge Rise—Effect of Wave Amplitude

while the corresponding value is 60% for $T_w = 3.0$ (Fig. 8). The rate of subsidence is very large in the initial reaches for low T_w values and the subsidence rate comes down only after the base of the hydrograph has spread significantly at a sufficiently downstream location increasing the local wave duration. The results in Figs. 6–9 indicate that as the bulk of the wave form reduces, either through reduction of Y_w or T_w, the subsidence rate increases. But a variation in T_w has a much larger influence than a variation in Y_w.

Effect of Shape Parameters on Subsidence.—The variations of Y_w^* and Q_w^* with X in rectangular channels ($Z = 0$) for different values of B_i are shown in Figs. 10 and 11 for $F_o = 0.3$, $Y_w = 0.5$, and $T_w = 3.0$. The values of $Q_{max}(0)$ for $B_i = 0$, 0.1, 0.5, and 1.0 are 2.055, 1.969, 1.826, and 1.767, respectively. These results show that there is a significant effect of the width parameter on the rate of subsidence. From Manning's formula and the definition of Froude number (Eq. 7), for rectangular channels, (in metric units)

$$n = \frac{y_o^{1/6}}{\sqrt{g}\,F_o} \frac{S_o^{1/2}}{(1+2B_i)^{2/3}} \quad \ldots\ldots\ldots\ldots\ldots\ldots\ldots\ldots\ldots\ldots\ldots\ldots \quad (20)$$

If the depth and the length scales are taken as constants, y_o and S_o are constants. Thus, for a constant F_o, Manning's n decreases as B_i increases. Therefore, when computations are made for a constant F_o value, a change in B_i also implies a change in n value as governed by Eq. 20. Thus the results for narrower

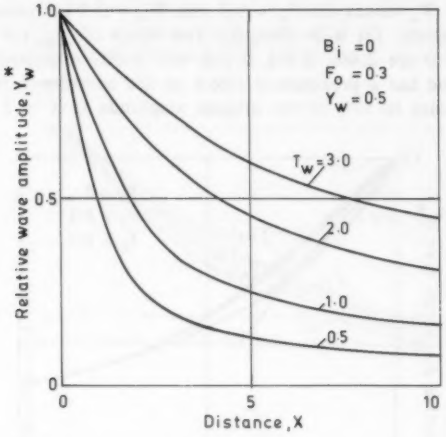

FIG. 8.—Subsidence of Relative Wave Amplitude—Effect of Wave Duration

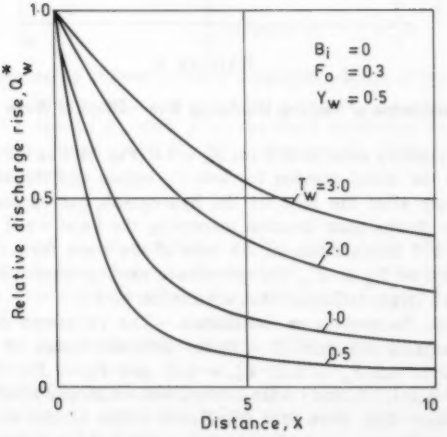

FIG. 9.—Subsidence of Relative Discharge Rise—Effect of Wave Duration

channels (larger B_i) corresponds to studies with a smaller n value than for wide channels. In spite of this, a greater subsidence rate is observed for narrower channels (Figs. 10 and 11) indicating a very significant effect of the width parameter on the rate of subsidence. The side walls have a pronounced effect on the subsidence in narrow channels.

The effect of channel side slope Z on subsidence is shown in Fig. 12(a)–12(c) in which Y_w^* variation is given for $Z = 0$, 1, 2, and 3 for constant B_i values.

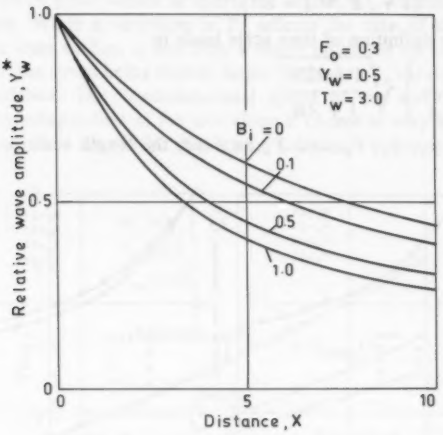

FIG. 10.—Subsidence of Relative Wave Amplitude—Effect of Width Parameter

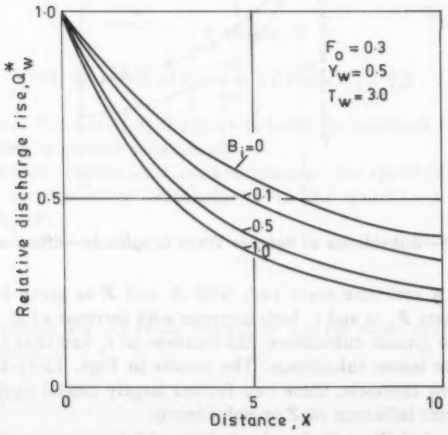

FIG. 11.—Subsidence of Relative Discharge Rise—Effect of Width Parameter

Similar results were observed for discharge subsidence also. Effect of side slope Z as subsidence is pronounced in narrow channels [Fig. 12(*c*)], while, it is insignificant in the case of relatively wide channels [Fig. 12(*a*)]. For $B_i = 1$, the rectangular channel has clearly a greater subsidence while there is again only a small influence of Z in the range $1 \leq Z \leq 3$.

For trapezoidal channels, the equation corresponding to Eq. 20 is

$$n = \frac{\sqrt{S_o}\, y_o^{1/6}}{\sqrt{g}\, \mathrm{F}_o} \frac{(1 + ZB_i)^{1/6} \sqrt{1 + 2ZB_i}}{(1 + 2B_i \sqrt{1 + Z^2})^{2/3}} \quad \ldots \ldots \ldots \ldots \ldots \ldots \ldots \quad (21)$$

In addition, the definition of time scale leads to

$$t_o = \left[\frac{\sqrt{y_o}}{S_o \mathrm{F}_o \sqrt{g}} \right] \sqrt{\frac{1 + 2ZB_i}{1 + ZB_i}} \quad \ldots \ldots \ldots \ldots \ldots \ldots \ldots \quad (22)$$

If we consider y_o, S_o, F_o, and Y_w as fixed, the length scale is constant while

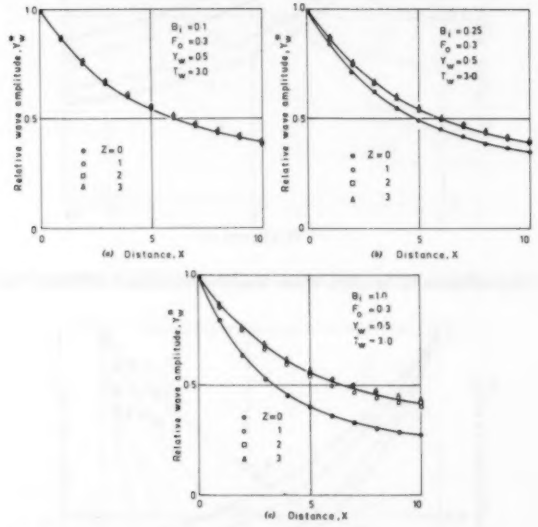

FIG. 12.(*a,b,c*)—Subsidence of Relative Wave Amplitude—Effect of Side Slope

the Manning's n and time scale vary with B_i and Z as given by Eqs. 21 and 22. For a constant B_i, n and t_o both increase with increase of Z. While increase of n will lead to greater subsidence, the increase of t_o and thus t_w (for constant T_w) will lead to lesser subsidence. The results in Figs. 12(*a*)–12(*c*) show that except in narrow channels, these two factors largely cancel each other leading to an insignificant influence of Z on subsidence.

Speed of Travel of Wave Peak.—In studying the propagation of a flood wave, two principal questions arise, namely, the magnitude of the wave peak at a

particular location and the time at which the peak arrives at the location. The path of the wave peak in the XT plane was studied for all the computational cases and only a summary of the results are indicated here. Computational results show that the nondimensional speed of the wave peak does not vary significantly with F_o. However, the actual speed of the wave increases as F_o increases as the velocity scale is directly proportional to F_o. This greater speed of the wave peak corresponds to the lesser subsidence at higher F_o values. Initial wave amplitude Y_w has a fairly significant influence on the speed of travel of the wave peak which is more for higher Y_w values corresponding to larger depths. While a variation in T_w affects the rate of subsidence very significantly as seen earlier, it has only a small influence on the speed of the wave peak, with the speed being slightly larger for higher T_w values corresponding to lesser subsidence. The nondimensional speed of the wave peak is found to be practically independent of the side slope Z except in very narrow channels in which the speed is slower in rectangular channels corresponding to larger

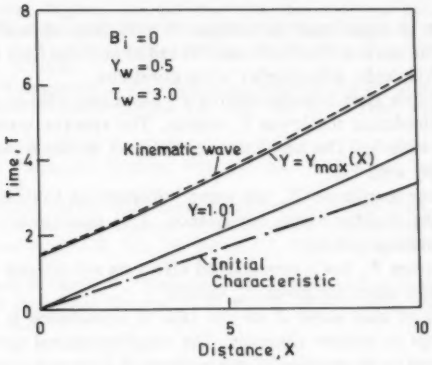

FIG. 13.—Path of Wave in XT Plane, $F_o = 0.5$

wave subsidence. The speed of the peak is lesser in narrower channels (larger B_i) corresponding to greater subsidence.

The computational results were used to compare the speed of the wave peak with that of a corresponding kinematic wave. The speed (v_w) of a kinematic wave is given by (8)

$$v_w = \frac{1}{b}\frac{dq}{dy} \quad \ldots\ldots\ldots\ldots\ldots\ldots\ldots\ldots\ldots\ldots\ldots\ldots\ldots\ldots\ldots\ldots \quad (23)$$

Nondimensionalizing Eq. 23 (with respect to v_o) for wide channels and using Manning's formula,

$$V_w = V + \frac{2}{3} Y^{2/3} \quad \ldots\ldots\ldots\ldots\ldots\ldots\ldots\ldots\ldots\ldots\ldots\ldots\ldots\ldots\ldots\ldots \quad (24)$$

The nondimensional kinematic wave speed can be calculated from Eq. 24 based

on the computational results of Y and V for the wave peak. Typical results presented in Fig. 13 shows that the speed of the kinematic wave approximates the speed of the flood wave peak very well. The concept of a kinematic wave implies that the bed slope term dominates over the other slope terms in the equation of motion (4). Therefore we might expect the flood wave to move more closely like a kinematic wave at higher F_o values and the computation clearly confirm this conclusion.

The path in the XT plane along which the depth is 1% above the initial uniform flow depth is also shown in Fig. 13. This path diverges from the initial characteristic as the 1% increase in Y denotes a larger percentage of the local wave amplitude as X increases.

Conclusions

An extensive parametric study on the propagation of a sinusoidal wave in prismatic open channels leads to the following important conclusions:

1. There can be significant subsidence in prismatic open channels. This is particularly so for narrow channels, smaller initial uniform flow Froude numbers and inflow hydrographs with smaller wave durations.
2. Initial uniform flow Froude number F_o has some influence on subsidence with greater subsidence for lower F_o values. The relative wave amplitude Y_w^* varies linearly with F_o. The nondimensional speed of the wave peak does not vary significantly with F_o.
3. Inflow wave amplitude Y_w has some influence on subsidence, with lower Y_w values giving slightly higher subsidence. This nonlinearity is found to be lesser in the discharge results.
4. Wave duration T_w has a pronounced effect on subsidence with subsidence being significantly more for lower T_w values.
5. The effect of side slope Z on the rate of subsidence is not particularly significant except in narrow channels. The nondimensional speed of the wave peak is also found to be practically independent of Z except in narrow channels. The width parameter, B_i, has a significant effect on subsidence, which is least in wide channels corresponding to $B_i = 0$. The speed of the wave peak is lesser in narrow channels corresponding to greater subsidence.
6. All computational results show that the relative wave amplitude, Y_w^*, and the relative discharge rise, Q_w^*, decrease exponentially with distance in the initial reaches. This exponential fit will hold good up to a larger distance in cases where subsidence in lesser.
7. There is a very good agreement between the speed of the wave peak and that of the corresponding kinematic wave.

Acknowledgment

The writers are thankful to the reviewers for their useful comments.

Appendix I.—References

1. Amein, M., and Chu, H. L., "Implicit Numerical Modeling of Unsteady Flows,"

Journal of the Hydraulics Division, ASCE, Vol. 101, No. HY6, Proc. Paper 11378, June, 1975, pp. 717–732.
2. Baltzar, R. A., and Lai, C., "Computer Simulation of Unsteady Flows in Waterways," *Journal of the Hydraulics Division*, ASCE, Vol. 94, No. HY4, Proc. Paper 6048, Apr., 1968, pp. 1083–1117.
3. Fletcher, A. G., and Hamilton, W. S., "Flood Routing in an Irregular Channel," *Journal of the Engineering Mechanics Division*, ASCE, Vol. 93, No. EM3, Proc. Paper 5282, June, 1967, pp. 45–62.
4. Henderson, F. M., *Open Channel Flow*, the Macmillan Publishing Co., Inc., New York, N.Y., 1966.
5. Issacson, E., Stoker, J. J., and Troesch, B. A., "Numerical Solution of Flow Problems in Rivers," *Journal of the Hydraulics Division*, ASCE, Vol. 84, No. HY5, Proc. Paper 1810, May, 1958, pp. 1–18.
6. Lakshmana Rao, N. S., and Sridharan, K., "Effect of Channel Shape on Gradually Varied Flow Profiles," *Journal of the Hydraulics Division*, ASCE, Vol. 97, No. HY1, Proc. Paper 7796, Jan., 1971, pp. 55–64.
7. Liggett, J. A., and Woolhiser, D. A., "Difference Solutions of the Shallow Water Equations," *Journal of the Engineering Mechanics Division*, ASCE, Vol. 93, No. EM2, Proc. Paper 5189, Apr., 1967, pp. 39–71.
8. Lighthill, M. J., and Whitham, "On Kinematic Waves, I," *Proceedings, Royal Society (London)*, London, England, Vol. 229, No. 1178, May, 1955, pp. 281–316.
9. Mozayeny, B., and Song, C. S., "Propagation of Flood Waves in Open Channels," *Journal of the Hydraulics Division*, ASCE, Vol. 95, No. HY3, Proc. Paper 6561, Mar., 1969, pp. 877–892.
10. Price, R. K., "Comparison of Four Numerical Methods for Flood Routing," *Journal of the Hydraulics Division*, ASCE, Vol. 100, No. HY7, Proc. Paper 10659, July, 1974, pp. 879–899.
11. Sakkas, J. G., and Strelkoff, T., "Dimensionless Solution of Dam-Break Flood Waves," *Journal of the Hydraulics Division*, Vol. 102, No. HY2, Proc. Paper 11910, Feb., 1976, pp. 171–184.
12. Stoker, J. J., *Water Waves*, Interscience Publishers, Inc., New York, N.Y., 1957.
13. Strelkoff, T., "Numerical Solution of Saint-Venant Equations," *Journal of the Hydraulics Division*, ASCE, Vol. 96, No. HY1, Proc. Paper 7043, Jan., 1970, pp. 223–253.
14. Terzidis, G., and Strelkoff, T., "Computations of Open Channel Surges and Shocks," *Journal of the Hydraulics Division*, Vol. 96, No. HY12, Proc. Paper 7780, Dec., 1970, pp. 2581–2610.

Appendix II.—Notation

The following symbols are used in this paper:

A = nondimensional cross-sectional area, a/y_o^2;
a = cross-sectional area of flow;
B_i = inverse of nondimensional bed width, y_o/b;
b = bed width of channel;
C_1 = coefficient in Eq. 19;
C_2 = coefficient in Eq. 19;
d_o = hydraulic mean depth at depth, y_o;
F_o = initial uniform flow Froude number, $v_o/\sqrt{gd_o}$;
g = acceleration due to gravity;
K = exponent in Eq. 18;
l_o = length scale, y_o/S_o;
Q = nondimensional discharge, q/q_o;
Q_w^* = nondimensional relative discharge rise (Eq. 15);
q = discharge;

q_o = discharge corresponding to initial uniform flow;
r = hydraulic radius;
r_o = hydraulic radius at depth y_o;
S_f = friction slope;
S_o = bed slope;
T = nondimensional time, t/t_o;
T_w = nondimensional wave duration, t_w/t_o;
t = time;
t_o = time scale, l_o/v_o;
t_w = wave duration;
V = nondimensional velocity, v/v_o;
V_w = nondimensional kinematic wave speed;
v = velocity of flow;
v_o = velocity of initial uniform flow;
W = nondimensional top width, w/y_o;
w = top width;
X = nondimensional distance along channel, x/l_o;
x = distance along channel;
Y = nondimensional depth of flow, y/y_o;
Y_w = nondimensional initial wave amplitude, y_w/y_o;
Y_w^* = nondimensional relative wave amplitude, (Eq. 13);
y = depth of flow;
y_o = depth of initial uniform flow;
y_w = initial wave amplitude;
Z = side slope of trapezoidal channel;
ϕ_1 = function given by Eq. 8; and
ϕ_2 = function given by Eq. 9.

Demand Forecasting in Water Supply Networks

By Patrick F. Perry[1]

Introduction

The rapid increase in energy costs in recent years has focused attention more sharply on the potential for energy savings in the operation of water distribution networks. The largest single cost element is often the cost of operating the pumping stations to meet consumer demands, in terms of quantity and pressure, distributed throughout the network. A fundamental requirement for scheduling pumps in an optimum way is a forecast of what the consumer demands are likely to be, say 24 h ahead in time. Provided this forecast is reasonably accurate, the reservoir levels can be allowed to rise or fall according to whether the actual demand is below or above forecast, enabling pump energy savings to be made by operating the pumps at constant output. For such purposes, the main requirement is for an accurate 24 h forecast of total demand. For many networks, however, there is considerable potential for energy saving by off-peak pumping for electrically driven pumping stations with variable speed drives. Such situations require an accurate forecast of the demand variation throughout the day. This more difficult problem is examined here.

This paper is concerned with formulating the hour by hour demand forecasting problem within the framework of an on-line pump scheduling scheme, and with comparing two well-known statistical forecasting methods to evaluate their effectiveness in terms of accuracy and computational feasibility. The computational results are based on data from the East Worcestershire Waterworks company in the United Kingdom (5,6,16). The first method uses Kalman filtering techniques with a temperature or rainfall variable controlling the propagation of the residual component of demand. The second method is based on the Karhunen-Loève spectral expansion and has the advantage that it uses only past load data and does not require any meteorological inputs.

Load forecasting is still considered more of an art than a science (9,14). For this reason many distribution industries, such as electricity, gas, and water supply, maintain a number of load forecasters who base their prediction on experience and insight. Basically they maintain records of past load behavior,

[1]Lect., Civ. Engrg. Dept., Imperial Coll., London SW7 2AZ, England.

Note.—Discussion open until February 1, 1982. To extend the closing date one month, a written request must be filed with the Manager of Technical and Professional Publications, ASCE. Manuscript was submitted for review for possible publication on June 3, 1980. This paper is part of the Journal of the Hydraulics Division, Proceedings of the American Society of Civil Engineers, ©ASCE, Vol. 107, No. HY9, September, 1981. ISSN 0044-796X/81/0009-1077/$01.00.

together with past weather conditions, industrial strikes, and other factors which are known to significantly affect demand. Based on this information a load prediction is made by comparing the conditions with those of a similar day some time in the past, whose characteristics they have recorded on file. The resulting forecast is frequently quite adequate.

The disadvantages with this approach lie in the fact that large amounts of data have to be stored, only one or two forecasts can be made daily, and the method is highly subjective and therefore liable to human errors and biases. Alternatively, this intuitive approach is sometimes advantageous if the complexity of the problem is such that human insight may be the best way of arriving at a forecast when conditions deviate significantly from the norm.

Over the past few years a serious attempt has been made to develop mathematical models which can be implemented in a computer for automatic load forecasting. These methods, which have been well surveyed by Matthewman and Nicholson (13) and Gupta (5) are of two main types. One method is to establish a mathematical model based on the correlation between load and weather, and the second is to base this model on the relationship between the present and past values of the load. Arguments against weather correlation models have been raised since they require weather data monitoring, which is sometimes not readily available for on-line implementation in the United Kingdom, although it is in California. Techniques using only past load data have the advantage of being much simpler to implement in the sense that data is more readily available. Also it is argued that some weather effects on the load can have relatively long time constants, of the order of 24 h, and are therefore easily identifiable and predictable in terms of the most recent past load data. On the other hand, in cases where weather effects have shorter response times, of the order of 2 h–3 h, it seems quite sensible not to reject evident correlation between them and the load pattern. The use of past and present weather would seem to be very significant in arriving at better load forecasts for lead times of 24 h or more, the argument being that past load data alone does not contain information about the present and most recent weather effects. In addition, if weather variables are incorporated into the model, then the effects of sudden changes in weather conditions can be taken into account and perhaps contingency predictions obtained for different possible weather conditions.

Possibly the widest use of short term load estimation has been in the electricity supply industry. Work on load models based on weather correlations has been done by Dryar (4), Davies (2) and Heinemann (10). The basic approach is to find a deterministic relationship between the peak load and the average daily weather effects considered significant. Load variations with time of day are not considered and there is no measure of confidence or uncertainty associated with the prediction.

The most important load correlation technique is the method of Farmer and Potton (7) who introduce a probabilistic structure into the model. Essentially, load observations over a period of about 6 weeks in the past are used to evaluate the autocorrelation function, whose eigenvalues and eigenvectors are then used to model the load using a finite Karhunen-Loève expansion. The parameters of the expansion can then be recursively updated to fit the most recent observations. This method, which has been used extensively in practical applications, has the advantage that it provides a continuous forecast and error standard

deviation. A similar approach is presented by Christiaanse (1) who models hourly load readings by a time series of functions with a 1-week period. Toyoda (17) was the first to suggest a state space load model incorporating both the effects of weather, temperature, and humidity, as well as the effects of the most recent demand observation. The method uses Kalman filtering techniques for providing continuous forecast and error standard deviation. Galiana (8) used a similar model and extensively tested the method on real data.

Load forecasting techniques have been used to a lesser extent in other industries. In the case of water supply, De Moyer, Gilman, and Goodman (3) performed some preliminary work on demand estimation using a Fourier series method with an associated accuracy determination. So that no more terms than necessary were calculated for the series, a statistical test was used to indicate the number of harmonics which significantly add to the series representation of actual demand data. For summer consumption, maximum daily temperature is used to improve the prediction accuracy. Shimron and Shamir (15) use time series analysis methods for forecasting water demands several hours in advance using recorded hourly readings. Two basic models are used—one is a "means" model, which forecasts future demands as weighted averages of selected past data, and the other is an "additive" model, which decomposes the historical data into several basic time series, extrapolates each time series separately into the future, and then adds them together to produce the forecast demands. The disadvantage with both of these methods is that the accuracies obtainable suggest that they are inappropriate for use in on-line optimal control.

The two primary aims for a good prediction method are accuracy of forecast and ease of implementation. Exact numerical accuracy depends to a large extent on the particular network and data being analyzed, and will also be closely related to the length of forecast required. Shorter prediction times result in better accuracy, but if forward predictions in excess of 24 h are required, then errors will rapidly become unacceptable unless more sophisticated techniques are used. On the other hand, emphasis must be placed on techniques which are readily implementable on-line and will not burden the available computer excessively. Methods which collect and process data on-line to update the current forecast are clearly desirable, as are methods which give a continuous record of the model's confidence in the forecast or estimate of the prediction error. The two methods outlined in this paper have been specifically designed to satisfy most of these requirements.

Role of Forecasting in an On-Line Pump Control Scheme

Forecasting plays a central role in the on-line scheduling of pumps in water supply networks. The main reason for this is that the savings to be gained by hourly "fine tuning" of pump schedules are limited by the accuracy with which hourly demands can be forecast.

To fully appreciate the necessity for accurate on-line forecasts, it is necessary to look more closely at the relationship between the on-line forecasting problem and the problem of on-line pump control. They are both computationally demanding tasks which should be combined with data acquisition and monitoring on a water supply network to enable models to be updated and schedules to be implemented.

Fig. 1 shows a schematic relationship showing the interaction between a computer system, which measures network data and carries out pump scheduling and forecasting calculations, and an actual network consisting of pipes, pumps, reservoirs, valves, etc. The basis of this interaction is that the computer must construct demand estimates based on the latest observed network parameters, such as pressures and flows, since on most water supply networks there is no direct on-line metering of consumer demands. When these forecasts have been made, an optimization calculation is carried out to determine the optimum pump schedule which is then implemented on the network. The important feature of Fig. 1 is that the optimal control calculation is based on a forecast which in turn depends on actual on-line pressure and flow measurements from the network. In other words, the mechanism for feedback control from the network is via the demand forecasting model.

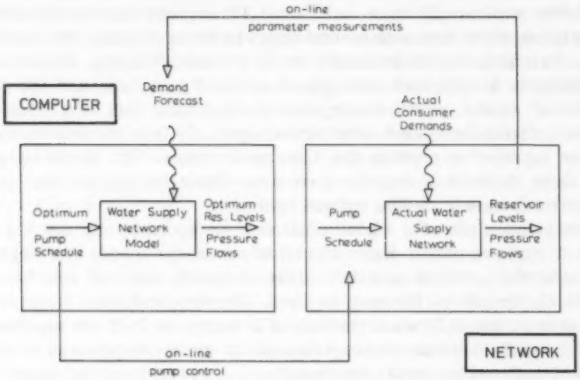

FIG. 1.—Schematic Relationship between On-Line Demand Forecasting and Optimal Control

In terms of control theory, the state variables on the network are fed back by the computer to provide a basis for deterministic optimal control of pumping. Among the state variables on the network, as will be shown in the next section, are the residual components of the water demand. Thus the pump control problem can be viewed as a state feedback problem in optimal control where there is uncertainty in both the state propagation and measurement equations. The problem of estimating the state under such circumstances can be solved using the Kalman filter approach, which is the first of the techniques considered for demand forecasting, and is clearly suitable to on-line implementation due to the advances made in the computational aspects of filtering since the 1960s.

An alternative to the feedback filtering approach is the spectral expansion procedure which relates demand forecasts to historic trends in demand, updated to take account of the most recent observations. This is the second of the two methods of forecasting considered.

This paper examines both of the forecasting methods to determine which

is most suitable for use in an on-line computerized pump scheduling scheme. Several such schemes are currently in operation, both in the United States and Europe, and in most cases forecasting is done on an ad-hoc basis or using some very simple modelling relationships. Such rudimentary forecasts are not appropriate to sophisticated computerized systems which rely on an accurate forecast to generate savings in pumping costs.

Modelling Water Demand

The water demand at any location on a water distribution network depends on the pattern of water consumption of the individual industrial, commercial, public, agricultural, and domestic users in a given area. On aggregate, these can be assumed to exhibit a cyclical trend which can be modelled as a time series with inherent uncertainty. Meteorological factors may affect demand in a systematic way, e.g., domestic consumption during the summer can be significantly affected by high temperatures. It is often difficult, however, to incorporate such factors into a model except in a most general sort of way.

Consider the total water demand $L(k)$ at time k as the sum of a periodic $y_p(k)$ and a residual $y_r(k)$ component. The periodic component over a 24-h period can be modelled as a Fourier Series

$$y_p(k) = a_o^p + \sum_{i=1}^{n_p} (a_i^p \sin i\, w_o k + b_i^p \cos i\, w_o k) \quad \ldots\ldots\ldots\ldots\ldots\ldots (1)$$

in which n_p, a_i^p and b_i^p are to be determined; and w_o = the natural frequency. The residual component can be written as an auto-regressive-moving-average (ARMA) model of the form

$$y_r(k) = \sum_{i=1}^{n} a_i^r y_r(k-i) + \sum_{j=0}^{m} b_j^r u(k-j) + \sum_{l=1}^{p} d_l w(k-l) \quad \ldots\ldots\ldots\ldots (2)$$

in which u = a meteorological parameter; w = white noise; and n, m, p, a_i^r, b_j^r, d_l are constants to be determined. The w noise has first and second order statistical properties

$$E[w(k)] = 0$$

$$E[w(k)\, w(\tau)] = \begin{matrix} 0 & k \neq \tau \\ Q & k = \tau \end{matrix} \quad \ldots\ldots\ldots\ldots\ldots\ldots\ldots\ldots\ldots\ldots (3)$$

An alternative approach to splitting the demand into a periodic and independently propagated residual component is to consider the total demand $L(k)$ as a nonstationary time series with characteristic modes represented by a series expansion of orthogonal eigenfunctions of the demand data covariance matrix. Thus for a particular day period k of N discrete intervals, the total water demand is represented by the mth sample function $q_m(k)$ of an ensemble of M days

$$q_m(k) = \sum_{i=1}^{K} b_{mi} \lambda_i^{1/2} \phi_i(k) + \gamma_m(k); \quad k = 1, 2, \ldots N; \quad m = 1, 2, \ldots M \quad \ldots (4)$$

in which the coefficients b_{mi}, λ_i, K, N, M can be estimated.

These two forms of demand model suggest different kinds of forecasting methods which can be used for accurate and computationally efficient forecasts. The former is primarily a time-series model to which a wide range of techniques which are well known and well tested can be applied. The Kalman theory (11) is one such approach which can be extended to simultaneously estimate and update time series model parameters, while generating the forecast based on the latest state observations (8). The second approach is based on spectral expansion (12), and decides on the basis of historic data what the most dominant characteristic modes of demand are. While the scope for using advanced time

TABLE 1.—Kalman Filter Prediction Model Parameters

Parameter (1)	Value (2)
(*a*) Periodic Model	
a_o^p	872
a_1^p	−151.2
a_2^p	−120.4
a_3^p	52.2
a_4^p	10.9
a_5^p	−51.1
a_6^p	16.7
b_1^p	−130.7
b_2^p	60.9
b_3^p	28.7
b_4^p	−4.7
b_5^p	13.9
b_6^p	12.3
(*b*) Residual Autoregressive Model	
a_1^r	0.1567
a_2^r	−0.0005
(*c*) Temperature Model	
b_o^r	−17.999
b_1^r	5.599
(*d*) Noise	
Q	1,239

series methods is more limited, this approach has certain desirable properties which can be useful.

In the next section, the forecasts of water demands using both of these techniques will be developed for a given set of water demand data taken from the East Worcestershire Water Company (EWWC) in the United Kingdom. This network has a most advanced computerized telecontrol scheme which has been extensively described elsewhere (5). The calculations described here have formed the basis for an on-line forecasting scheme which has been developed and implemented.

FORECASTING WATER DEMANDS

For forecasting in an on-line environment, it is easy to show (8) that, if the model is split into independent periodic and residual components, the Kalman filtering theory can be used. The demand forecast one period ahead $\hat{L}(k+1)$ is related to an estimate of the state $\hat{\underline{x}}(k)$ of a linear dynamical system driven by white noise. The state estimate is such that the error covariance matrix

$$\underline{P}(k) = E\{[\underline{x}(k) - \hat{\underline{x}}(k)][\underline{x}(k) - \hat{\underline{x}}(k)]^T | L(i);\quad i < k\} \quad \ldots\ldots\ldots\ldots (5)$$

is minimized. The very well known Kalman filter equations have been documented

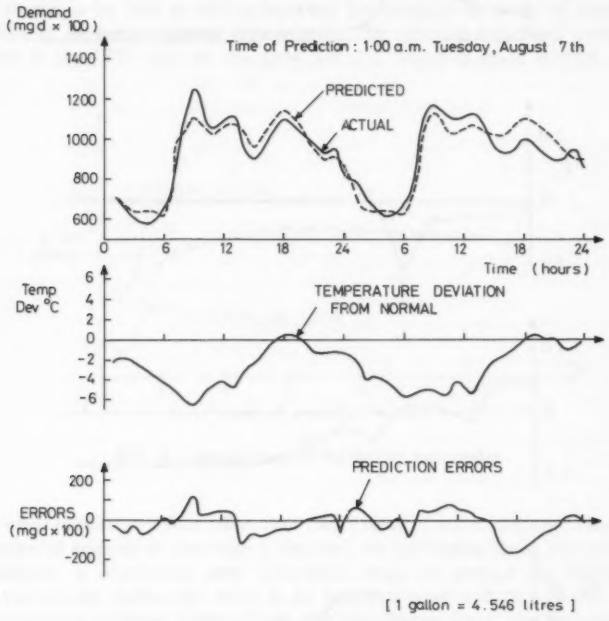

FIG. 2.—Kalman Filter Prediction

elsewhere (11). The state estimate $\hat{\underline{x}}(k)$ can be viewed essentially as a measure of the residual component of the demand. It can therefore be used as a means of updating pumping schedules to account for demand variations about the periodic base component.

Table 1 gives the numerical values for a model of six harmonics with $n = 2$, $m = p = 1$, identified using the Flectcher-Powell algorithm (8) for minimizing the least squares fit of $\hat{L}(k)$ to $\hat{L}(k)$ for the data shown in Fig. 2. The prediction accuracy over this period is shown, and the steady state error variance is of the order of 3% of peak consumption. The numerical values of the coefficients

of the noise model ensure asymptotically stable and aperiodic forecasts. Fig. 3 shows some examples of the convergence of the estimating procedure for the model parameters.

The Kalman filter prediction model as outlined here is suitable for on-line implementation because, once the model parameters have been estimated off-line

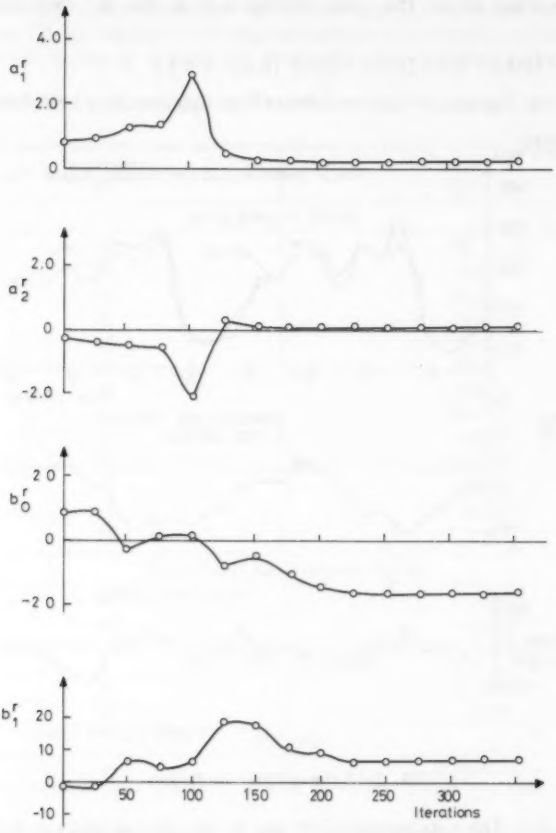

FIG. 3.—Convergence of Residual Model Parameters

from historic data, it is a relatively easy matter to update this model to take account of the latest observations in calculating the latest prediction, e.g., the off-line calculation for the model shown in Table 1 took 5 min CPU time on an IBM 370/165 computer, while the generation and updating of forecasts took only 15 sec on the same machine. Another reason for its suitability is the fact

that the optimal pump schedule can be related to the optimal demand estimate $\hat{x}(k)$ which is fed back from the network. This computation involves the solution of a matrix Riccatti equation for a linear model-quadratic cost pump schedule which can also be quite modest. Thus, the state estimate $\hat{x}(k)$ used for forecasting can also be used directly for optimal control.

By way of comparison, a spectral expansion forecast was carried out on the same data. A record of 53 days excluding weekends and Mondays was used. An exponential smoothing model with constant 0.14 was used to eliminate the base trend in the data, and the spectral expansion procedure carried out on the demands.

The accuracy of this method is particularly good for short term predictions up to a few hours ahead. Fig. 4 shows, however, that for 24 h predictions there seems to be little to choose between the methods in terms of accuracy. In terms of its computational requirements, the spectral expansion procedure requires 9 sec CPU time on the IBM 370/165 which is quite modest. Also,

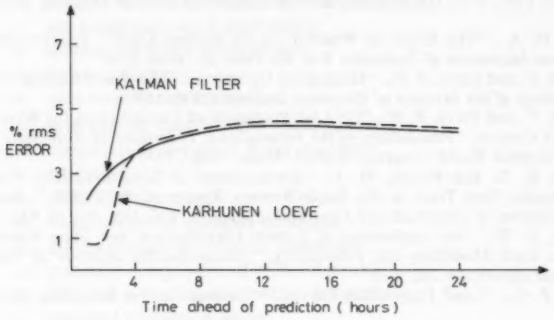

FIG. 4.—Comparison of Prediction Accuracies

it does not require any data other than past values of water demand. However, a substantial amount of storarage is required for processing these historic data. In addition, a completely new calculation must be carried out when new observations are made, and there is no simple way of updating on-line pump controls based on latest observations. For this reason alone, the Kalman filter approach is preferable for on-line use.

Conclusions

This paper has taken a preliminary look at the requirements of a forecasting system for on-line pump scheduling in a predictive environment on water supply networks. Two methods are suggested as being appropriate in terms of accuracy—the Kalman filter approach and the Karhunen-Loève spectral expansion method. The former is more attractive in terms of on-line implementation for the following reason. Part of the forecast calculation involves the estimation

of the state vector of residuals of demand. This gives the deviation of the actual demand from the periodic base component, and can therefore be used on-line for calculating the optimal pump control.

The conclusions drawn in this paper are based on actual data from an advanced telecontrolled water supply network in the United Kingdom. A forecasting scheme based on the methodology outlined in this paper has currently been successfully implemented on that network.

Appendix I.—References

1. Christiaanse, W. R., "Short Term Load Forecasting using General Exponential Smoothing," presented at the July 12–17, 1970, Institute of Electrical and Summer Power Meeting, held at Los Angeles, Calif.
2. Davies, M., "The Relation between Weather and Electricity Demand," *Proceedings of the Institution of Electrical Engineers*, Vol. 106C, 1958, pp. 27–37.
3. De Moyer, R., Gilman, H. D., and Goodman, M. Y., "Dynamic Computer Simulation and Control Methods for Water Distribution Systems," *GE Research Report No. 735D205*, Feb., 1973, GE Re-Entry and Environmental Systems Division, Philadelphia, Pa.
4. Dryar, H. A., "The Effect of Weather on the System Load," *Transactions of the American Institution of Engineers*, Vol. 63, 1944, pp. 1006–1013.
5. Fallside, F. and Perry, P. F., "Hierachical Optimisation of a Water Supply Network," *Proceedings of the Institute of Electrical Engineers*, Feb., 1974.
6. Fallside, F. and Perry, P. F., "On Line Prediction of Consumption for Water Supply Network Control," *Proceedings of the International Federation of Automatic Control*, Sixth Triennial World Congress, Boston, Mass., Aug., 1976.
7. Farmer, E. D. and Potton, M. J., "Development of Load Prediction Techniques with Results from Trials in the South-Western Region of the CEGB," *Proceedings of the Institute of Electrical and Electronic Engineers*, Vol. 115, No. 10, Oct., 1968.
8. Galiana, F. D., "An Application of System Identification and State Estimation to Electric Load Modelling and Forecasting," *Massachusetts Institute of Technology Technical Report No. 28*, 1971.
9. Gupta, P. C., "Load Forecasting Survey," Systems Control Inc., Palo Alto, Calif., 1969.
10. Heinemann, G. T., Nordman, D. A., and Plant, E. C., "The Relationship between Summer Weather and Summer Loads—A Regression Analysis," *Institute of Electrical and Electronic Engineers Transactions on Power Apparatus and Systems*, Vol. PAS-85, No. 11, Nov., 1966.
11. Kalman, R. E., "A New Approach to Linear Filtering and Prediction Problems," *Journal of Basic Engineering*, ASME, Series D, Vol. 82, 1960, pp. 35–45.
12. Matthewman, P. D., "On Power System Control," thesis presented to the University of Cambridge, at Cambridge, England, in 1969, in partial fulfillment of the requirements for the degree of Doctor of Philosophy.
13. Matthewman, P. D., and Nicholson, H., "Techniques for Load Prediction in the Electricity Supply Industry," *Proceedings of the Institute of Electrical Engineers*, Vol. 115, No. 10, Oct., 1968.
14. Nicholson, H. and Sterling, M. J. H., "Optimum Dispatch of Active and Reactive Generation by Quadratic Programming," *Institute of Electrical and Electronic Engineers Transactions on Power Apparatus and Systems*, Mar./Apr., 1973, pp. 644–654.
15. Shimron, Z. and Shamir, U., "Short Range Forecasting of Water Demands," Israel Institute of Technology, Vol. 11, No. 6, 1973, pp. 423–430.
16. Sterling, M. J. H. and Antcliffe, D. J., "A Technique for the Prediction of Water Demand from Past Consumption Data," Institution of Water Engineers, Vol. 28, No. 8, Nov., 1974, pp. 413–420.
17. Toyoda, J., Chin, M., and Inque, Y., "An Application of State Estimation to Short-Term Load Forecasting," *Institute of Electrical and Electronic Engineers Transaction PAS-89*, Parts 1 and 2, 1970.

Appendix II.—Notation

The following symbols are used in this paper:

a_o^p = Fourier series constant term;
a_i^p, b_i^p = Fourier series coefficients;
a_i^r, b_j^r = residual model coefficients;
b_{mi} = spectral expansion coefficients;
d_e = residual model noise coefficients;
E = expectation operator;
k = time period;
$\hat{L}(k)$ = water demand in period k;
$\hat{L}(k)$ = water demand forecast;
M = number of sample functions in ensemble;
m = index of sample functions;
N = number of days demand;
n_p = number of periodic terms in Fourier series;
$\underline{P}$ = state estimate error covariance;
p = number of white noise terms;
Q = noise variance;
$\underline{Q}$ = data covariance matrix;
$q_m(k)$ = mth sample function for water demand;
$u(k)$ = temperature deviation from average;
$w(k)$ = white noise;
w_0 = natural frequency;
$\underline{x}(k)$ = state vector of residual demands;
$\underline{\hat{x}}(k)$ = state estimate of residual demands;
$y_p(k)$ = periodic component of water demand;
$y_r(k)$ = residual component of water demand;
$\gamma_m(k)$ = spectral expansion error;
λ_i = ith eigenvalue of $\underline{Q}$; and
$\phi_i(k)$ = ith eigenvector of $\underline{Q}$.

SEDIMENT-CONTAMINANT TRANSPORT MODEL

By Yasuo Onishi,[1] M. ASCE

INTRODUCTION

The effects of man's activities on surface-water systems must be anticipated to prevent undesirable environmental consequences. Sediment movement is a particularly important mechanism that must be assessed because sediment is a major carrier of many hazardous materials.

Mathematical modeling is a valuable method for predicting sediment response and contaminant migration and fate. However, most available models do not account for sediment/contaminant interactions (1,10,18). The important interactions include contaminant adsorption by and desorption from sediments, and the migration (transport, deposition, scouring) of contaminated sediments (2,6, 12,13). Only when these mechanisms are considered can accurate predictions be obtained (14,19).

This paper considers the formulation and the verification of the sediment and contaminant transport model, FETRA. Because FETRA accounts for sediment/contaminant interactions (11), it provides more complete information than previous models. FETRA was applied to the James River estuary, Virginia, to simulate sediment movement and the transport of the pesticide Kepone which was discharged to the river in substantial quantities during the early 1970s (17).

MODEL DESCRIPTION

FETRA is an unsteady, two-dimensional model that utilizes the finite element computation method with the Galerkin-weighted residual technique. The following three submodels were coupled to account for the sediment/contaminant interactions: (1) A sediment transport submodel; (2) a dissolved contaminant transport submodel; and (3) a particulate contaminant transport submodel. (Particulate contaminants are those adsorbed by sediments.)

Sediment Transport Submodel.—Important sediment characteristics such as fall velocity, critical shear stresses for erosion and deposition, and adsorption capacity vary significantly with sediment sizes and types. Accordingly, sediment

[1]Staff Engr., Pacific Northwest Lab., Battelle Memorial Institute for the Dept. of Energy, P.O. Box 999, Richland, Wash.

Note.—Discussion open until February 1, 1982. To extend the closing date one month, a written request must be filed with the Manager of Technical and Professional Publications, ASCE. Manuscript was submitted for review for possible publication on June 11, 1979. This paper is part of the Journal of the Hydraulics Division, Proceedings of the American Society of Civil Engineers, ©ASCE, Vol. 107, No. HY9, September, 1981.

movements and particulate contaminant transport are modeled separately for each sediment size fraction or sediment type. (Currently, FETRA handles three sediment size fractions or sediment types.) The sediment transport submodel includes the mechanisms of: (1) Advection and diffusion/dispersion of sediments; (2) fall velocity and cohesiveness; (3) deposition on the riverbed; (4) erosion from the riverbed (bed erosion and armoring); and (5) sediment contributions from point/nonpoint sources, and subsequent mixing. Sediment mineralogy and water quality effects are implicitly included in Items 2, 3, and 4. This submodel also calculates the changes in riverbed conditions, including riverbed elevation changes due to scouring or deposition, or both, and three-dimensional distribution of sediment sizes within the bed.

The governing equation of the vertically averaged, two-dimensional sediment transport for jth sediment size fraction or sediment type was obtained from the following three-dimensional mass conservation equation (3,16):

$$\frac{\partial C_j}{\partial t} + \frac{\partial}{\partial x}(UC_j) + \frac{\partial}{\partial y}(VC_j) + \frac{\partial}{\partial z}(W - W_{sj})C_j = \frac{\partial}{\partial x}\left(\epsilon_x \frac{\partial C_j}{\partial x}\right) + \frac{\partial}{\partial y}\left(\epsilon_y \frac{\partial C_j}{\partial y}\right) + \frac{\partial}{\partial z}\left(\epsilon_z \frac{\partial C_j}{\partial z}\right) + Q_{sj} \quad \ldots\ldots\ldots\ldots (1)$$

in which C_j = concentration of sediment of jth size fraction, or type (weight of sediment per unit volume of water); Q_{sj} = source strength of jth sediment contribution; t = time; U = velocity component of longitudinal (x) direction; V = velocity component of lateral (y) direction; W = velocity component of vertical (z) direction; W_{sj} = fall velocity of sediment particle of jth size fraction or type; x, y, z = longitudinal, lateral, and vertical directions in Cartesian coordinates, respectively; and $\epsilon_x, \epsilon_y, \epsilon_z$ = diffusion coefficients of longitudinal, lateral, and vertical directions. The boundary conditions were

$$(W - W_{sj})C_j - \epsilon_z \frac{\partial C_j}{\partial z} = 0 \quad \text{at} \quad z = h \quad \ldots\ldots\ldots\ldots\ldots\ldots (2)$$

$$(1 - \gamma)W_{sj}C_j + \epsilon_z \frac{\partial C_j}{\partial z} = S_{Dj} - S_{Rj} \quad \text{at} \quad z = 0 \quad \ldots\ldots\ldots\ldots\ldots (3)$$

$$VC_j - \epsilon_y \frac{\partial C_j}{\partial y} = q_{sj} \quad \text{or} \quad C_j = C_{jo} \quad \text{at} \quad y = 0 \quad \text{and} \quad B \quad \ldots\ldots\ldots\ldots (4)$$

in which B = width of the river; C_{jo} = constant concentration of jth sediment; h = depth; S_{Dj} = sediment deposition rate per unit bed surface area for jth sediment size or type; S_{Rj} = sediment erosion rate per unit bed surface area for jth sediment size or type; γ = coefficient, i.e., probability that particle settling to the bed is re-entrained; and q_{sj} = lateral influx of jth sediment. For the model development work γ was assumed to be unity, i.e., for the same flow condition, all suspended matter settling on the riverbed as a result of fall velocity alone returns to the flow. The vertical flow velocity, W, was also assumed to be small.

Eq. 1 was vertically integrated to obtain the two-dimensional sediment-transport equations. Since velocity components and sediment concentration are generally

not uniform vertically, we use the following approach similar to the one used by Fischer (5):

$$C_j = \bar{C}_j + c_j'' \quad \ldots \quad (5)$$

$$U = \bar{U} + u'' \quad \ldots \quad (6)$$

$$V = \bar{V} + v'' \quad \ldots \quad (7)$$

$$\frac{\partial W_{sj}}{\partial z} = 0 \quad \ldots \quad (8)$$

in which $\bar{C}_j, \bar{U}, \bar{V}$ = depth averaged values of concentration of jth sediment, longitudinal velocity, and lateral velocity, respectively; and c'', u'', v'' = fluctuations from the depth averaged values of concentration of jth sediment, longitudinal velocity, and lateral velocity, respectively. Note that c'', u'', v'' are spatial deviations, not temporal deviations as are usual in turbulence analysis; all of the temporal averaging has been carried out prior to writing Eq. 1.

As in the Boussinesq diffusion coefficient concept let

$$\int_0^h u'' c_j'' dz = (\overline{u'' c_j''})\, h = -hD_x \frac{\partial \bar{C}_j}{\partial x} \quad \ldots \quad (9)$$

and $$\int_0^h v'' c_j'' dz = (\overline{v'' c_j''})\, h = -hD_y \frac{\partial \bar{C}_j}{\partial y} \quad \ldots \quad (10)$$

in which D_x and D_y = the dispersion coefficients of x and y directions.

The dispersion coefficients of x and y directions were assumed to be the same for all sediments and contaminants. Noting the equation of continuity, the kinetic water surface boundary condition, and Eqs. 2, 3, 9, and 10, the following final expression of sediment transport was obtained by substituting the aforementioned expressions into Eq. 1 and by integrating Eq. 1 over the entire river depth:

$$\frac{\partial \bar{C}_j}{\partial t} + \left(\bar{U} - \frac{K_x}{h}\frac{\partial h}{\partial x}\right)\frac{\partial \bar{C}_j}{\partial x} + \left(\bar{V} - \frac{K_y}{h}\frac{\partial h}{\partial y}\right)\frac{\partial \bar{C}_j}{\partial y}$$

$$= \frac{\partial}{\partial x}\left(K_x \frac{\partial \bar{C}}{\partial x}\right) + \frac{\partial}{\partial y}\left(K_y \frac{\partial \bar{C}}{\partial y}\right) + \frac{S_{Rj}}{h} - \frac{S_{Dj}}{h} + Q_{sj} \quad \ldots \quad (11)$$

in which $K_x = \epsilon_x + D_x \approx D_x$; and $K_y = \epsilon_y + D_y \approx D_y$. The finite element method was used to solve Eqs. 4 and 11.

To obtain the sediment concentration, sediment erosion and deposition rates, S_{Rj} and S_{Dj}, were calculated as described as follows. At each nodal point, S_{Rj} and S_{Dj} were evaluated separately for each sediment size fraction or sediment type because erosion and deposition characteristics are different for cohesive and noncohesive sediments. Both erosion and deposition of noncohesive sediments are affected by the amount of sediment the flow is capable of carrying, e.g., if the amount of sand being transported is less than the flow can carry for given hydrodynamic conditions, the flow will scour sediment from the stream bed to increase the sediment transport rate. This process occurs until the actual sediment transport rate becomes equal to the carrying capacity of the flow

or until all the available bed sediments are scoured, whichever is first. Conversely, the flow deposits sand if its actual sediment transport rate is above its capacity to carry sediment. Because of the simplicity of the formulation, DuBoy's formula (20) was used to estimate the total sediment transport capacity of flow per unit width, Q_T:

$$Q_T = \psi_D \tau_b (\tau_b - \tau_c) \quad \ldots \quad (12)$$

in which τ_b = bed shear stress; τ_c = critical shear stress defined and determined by DuBoy (20) as a function of sediment size; and ψ_D = coefficient defined and determined by DuBoy (20) as a function of sediment size. Although the DuBoy's formula is sometimes classified as a bed-load formula, it has been widely used to calculate the total sediment load because of its simplicity (20). Comparisons of computed and measured sediment loads for the Niobrara River near Cody, Neb. and the Colorado River at Taylor's Ferry, Colo., reveal that DuBoy's formula tends to overestimate a total sediment load under low flows, but provides better estimates under high flows (20).

The total sediment capacity, Q_T, per unit width at a down-current point was then compared with the actual amount of sand, Q_{TA}, being transported in the river per unit width at an up-current point. Thus

$$S_{Rj} = \frac{Q_T - Q_{TA}}{\Delta L} \quad \ldots \quad (13)$$

$$S_{Dj} = \frac{Q_{TA} - Q_T}{\Delta L} \quad \ldots \quad (14)$$

in which ΔL = distance between the up-current and down-current locations; and Q_{TA} = is obtained as a product of sand concentration and a flow rate per unit width.

For cohesive sediments, e.g., clay and silt, the following formulas developed by Partheniades (15) and Krone (8) were used:

$$S_{Rj} = M_j \left(\frac{\tau_b}{\tau_{cRj}} - 1 \right) \quad \ldots \quad (15)$$

$$S_{Dj} = W_{sj} C_j \left(1 - \frac{\tau_b}{\tau_{cDj}} \right) \quad \ldots \quad (16)$$

in which M_j = erodibility coefficient for jth sediment; τ_{cDj} = critical shear stress for sediment deposition for jth sediment; and τ_{cRj} = critical shear stress for sediment erosion for jth sediment. Values of M_j, τ_{cDj}, and τ_{cRj} must be determined by field or laboratory tests, or both (8,15,20). Similar to erosion of sand, cohesive sediment will be eroded with the rate of S_{Rj} or until all the available cohesive sediment in the bed is scoured, whichever results in a smaller amount of eroded sediment.

When the fall velocity, W_{sj} (as shown in Eq. 16), depends on sediment concentration and no aggregation occurs, the fall velocity could be assumed to be

$$W_{sj} = K_j' \bar{C}_j^{4/3} \quad \ldots \quad (17)$$

in which K'_j = an empirical constant depending on the sediment type (8).

Some studies (2,17) reveal that because of its large adsorption capacity, organic matter is a very important carrier of contaminants. Unfortunately, there have not been enough studies to quantify the rates of transport, deposition, and erosion of organic materials when these materials are transported other than by attaching to cohesive sediments. Since the mechanisms governing the erosion and deposition of organic matter are somewhat similar to those for cohesive sediments, Eqs. 15 and 16 were also used to solve the erosion and deposition rates of organic matter. The selection of the values of W_{sj}, M_j, τ_{cDj}, and τ_{cRj} in Eqs. 15 and 16 should reflect the characteristics of these materials in terms of their density, size, cohesiveness, and consolidation.

To simulate riverbed conditions as regards the bed's elevation change, sediment distribution, and armoring, FETRA divides the riverbed—except for the top layer—into a number of layers with a standard thickness. The thickness of the top layer is equal to or less than the standard thickness at any given time. Each layer consists of a combination of clean or contaminated sediments of three sizes (or types), or both, selected for sediment transport as mentioned previously. Based on the sediment erosion or deposition rate (S_{Rj} or S_{Dj}, as calculated by Eqs. 13 through 16), sediments of each size fraction (or type) will be scoured from or deposited to the bed, changing the thickness of the top layer and possibly the number of bed layers. When the top bed layer thickness reaches more than the standard thickness due to sediment deposition, a new top layer will be formed. On the other hand, when all the sediment in the top bed layer is scoured, the bed layer immediately below the original top layer becomes the new top layer. This process will continue until the actual sediment transport rate becomes equal to the carrying capacity of the flow or until the available bed sediment is completely scoured, whichever occurs first.

For the sediments of the second and third size fractions (or types), the number of bed layers eroded cannot exceed the number of layers eroded for the sediment of the first size fraction (or type). In other words, sediments of the first sediment size fraction (or type) cover and protect the sediments of the second and the third size fractions (or types) from erosion.

Contaminant distributions associated with each sediment size fraction (or type) within the riverbed were also obtained by keeping track of the amount of contaminants removed from or added to each bed layer during a simulation period due to erosion or deposition of contaminated sediment, or both, and direct adsorption/desorption between dissolved contaminants and bed sediments.

Dissolved Contaminant Transport Submodel.—Dissolved contaminants interact both with sediments in motion (suspended and bed-load sediments) and with stationary sediments in the riverbed. To account for these interactions, this submodel includes the mechanisms of: (1) Advection and diffusion/dispersion of dissolved contaminants; (2) adsorption (uptake) of dissolved contaminants by both moving and stationary sediments or desorption from the sediments into water; (3) chemical and biological degradation, or radionuclide decay of contaminants; and (4) contaminant contribution from point/nonpoint sources, and subsequent mixing. Contributions from wastewater discharges, overland runoff flow, fallout, and ground water to a river system may be treated as a part of the point/nonpoint source contributions. Effects of water quality,

e.g., pH, water temperature, and salinity, and sediment characteristics, e.g., clay minerals, can be included by changing the distribution (or partition) coefficients of contaminants.

The governing equation of dissolved contaminant transport for the three-dimensional case is

$$\frac{\partial G_w}{\partial t} + \frac{\partial}{\partial x}(UG_w) + \frac{\partial}{\partial y}(VG_w) + \frac{\partial}{\partial z}(WG_w) = \frac{\partial}{\partial x}\left(\epsilon_x \frac{\partial G_w}{\partial x}\right)$$

$$+ \frac{\partial}{\partial y}\left(\epsilon_y \frac{\partial G_w}{\partial y}\right) + \frac{\partial}{\partial z}\left(\epsilon_z \frac{\partial G_w}{\partial z}\right) - \lambda G_w - \sum_j K_j(C_j K_{dj} G_w - G_j) + Q_w \quad (18)$$

In addition to the previously defined symbols: K_{dj} = distribution (or partition) coefficient between dissolved contaminant and particulate contaminant associated with jth sediment; K_j = rate of contaminant adsorption or desorption to reach an equilibrium condition with jth sediment in motion; G_j = particulate contaminant concentration associated with jth sediment (weight of contaminant or radioactivity per unit volume of water); G_w = dissolved contaminant concentration (weight of contaminant or radioactivity per unit volume of water); Q_w = source strength of dissolved contaminant; and λ = chemical and biological degradation rates, or radionuclide decay rate of contaminant. The distribution coefficient, K_{dj}, for the jth sediment, is defined by

$$K_{dj} = \frac{\dfrac{f_{sj}}{M_j'}}{\dfrac{f_w}{V_w}} = \frac{f_{sj}}{f_w C_j} \quad \ldots\ldots\ldots\ldots\ldots\ldots\ldots\ldots\ldots\ldots \quad (19)$$

in which f_{sj} = fraction of contaminant sorbed by jth sediment; f_w = fraction of contaminant left in solution; M_j' = weight of jth sediment; V_w = volume of water; and $f_{sj}/f_w = G_j/G_w$. Eq. 19 may be rewritten as

$$G_j = K_{dj} C_j G_w \quad \ldots\ldots\ldots\ldots\ldots\ldots\ldots\ldots\ldots\ldots \quad (20)$$

Adsorption of contaminants by sediments or desorption from sediments are assumed to occur toward an equilibrium condition with the rate, K_j (unit of recriprocal of time), if the particulate and dissolved contaminant concentrations differ from their equilibrium values as expressed in Eq. 20. The boundary conditions for dissolved contaminant transport are

$$WG_w - \epsilon_z \frac{\partial G_w}{\partial z} = 0 \quad \text{at} \quad z = h \quad \ldots\ldots\ldots\ldots\ldots\ldots\ldots \quad (21)$$

$$\epsilon_z \frac{\partial G_w}{\partial z} = \sum_j \gamma_j (1 - P) D_j K_{Bj} (K_{dj} G_w - G_{Bj}) \quad \text{at} \quad z = 0 \quad \ldots\ldots\ldots \quad (22)$$

$$VG_w - \epsilon_y \frac{\partial G_w}{\partial y} = q_w \quad \text{or} \quad G_w = G_{wo} \quad \text{at} \quad y = 0 \quad \text{and} \quad B \quad \ldots\ldots\ldots \quad (23)$$

in which D_j = bed sediment diameter of jth sediment; G_{Bj} = particulate contaminant concentration associated with the jth sediment in the riverbed (weight

of contaminant or radioactivity per unit weight of sediment); K_{Bj} = rate of contaminant adsorption or desorption to reach an equilibrium condition with jth riverbed sediment; G_{wo} = constant concentration of dissolved contaminant; P = porosity of the riverbed; γ_j = density of jth sediment in the riverbed; and q_w = lateral influx of dissolved contaminant.

Eq. 22 expresses the direct adsorption or desorption between a dissolved contaminant and stationary jth sediment in the riverbed, or both. The distribution coefficients for both moving and stationary sediments were assumed to be the same as long as these sediments have the same characteristics, e.g., diameters, clay minerals, organic content. The difference in the adsorption/desorption mechanism between these two sediments is the time required to reach equilibrium. We also assumed that direct adsorption or desorption, or both, from bed sediments occurs only with sediments on the bed surface.

In order to vertically integrate Eq. 18 let

$$G_w = \bar{G}_w + G''_w \quad \ldots \quad (24)$$

$$G_j = \bar{G}_j + G''_j \quad \ldots \quad (25)$$

in which $\bar{G}_j$ = depth averaged value of particulate contaminant concentration associated with jth sediment; G''_j = fluctuation from the depth averaged value of particulate contaminant concentration; $\bar{G}_w$ = depth averaged value of dissolved contaminant concentration; and G''_w = fluctuation from the depth averaged value of dissolved contaminant concentration.

Integrating Eq. 18 over the entire river depth yields the following final transport equation of dissolved contaminants:

$$\frac{\partial \bar{G}_w}{\partial t} + \left(\bar{U} - \frac{K_x}{h}\frac{\partial h}{\partial x}\right)\frac{\partial \bar{G}_w}{\partial x} + \left(\bar{V} - \frac{K_y}{h}\frac{\partial h}{\partial y}\right)\frac{\partial \bar{G}_w}{\partial y} = \frac{\partial}{\partial x}\left(K_x \frac{\partial \bar{G}_w}{\partial x}\right)$$

$$+ \frac{\partial}{\partial y}\left(K_y \frac{\partial \bar{G}_w}{\partial y}\right) - \left[\lambda + \sum_j K_j K_{dj} \bar{C}_j + \sum_j K_{Bj}\gamma_j (1-P)\frac{D_j}{h} K_{dj}\right]\bar{G}_w$$

$$+ \sum_j K_j G_j + \sum_j K_{Bj}\gamma_j (1-P)\frac{D_j}{h} G_{Bj} + Q_w \quad \ldots \quad (26)$$

The boundary conditions for this equation are the same as those in Eq. 23.

Particulate Contaminant Transport Submodel.—The transport of sediment-attached contaminants is solved separately according to sediment size fraction (or types). This submodel also includes the mechanisms of: (1) Advection and diffusion/dispersion of particulate contaminants; (2) adsorption (uptake) of dissolved contaminants by sediment or desorption from sediment into water; (3) chemical and biological degradation, or radionuclide decay of contaminants; (4) deposition of particulate contaminants on the riverbed or erosion from the riverbed; and (5) contaminant contribution from point/nonpoint sources and subsequent mixing. Again, contributions to a river system from wastewater discharges, overland runoff flow, fallout, and ground water may be treated as a part of the point/nonpoint sources contributions. The three-dimensional distribution of the particulate contaminant within the riverbed is also computed, as mentioned earlier.

As in the transport of sediment and dissolved contaminants, the three-dimen-

sional transport equation for contaminants adsorbed by the jth sediment may be expressed as

$$\frac{\partial G_j}{\partial t} + \frac{\partial}{\partial x}(UG_j) + \frac{\partial}{\partial y}(VG_j) + \frac{\partial}{\partial z}[(W - W_{sj})G_j]$$

$$= \frac{\partial}{\partial x}\left(\epsilon_x \frac{\partial G_j}{\partial x}\right) + \frac{\partial}{\partial y}\left(\epsilon_y \frac{\partial G_j}{\partial y}\right) + \frac{\partial}{\partial z}\left(\epsilon_z \frac{\partial G_j}{\partial z}\right)$$

$$- \lambda G_j - K_j(G_j - C_j K_{dj} G_w) + Q_j \quad \ldots\ldots\ldots\ldots\ldots\ldots \quad (27)$$

in which Q_j = source strength of particulate contaminant associated with jth sediment. The boundary conditions for this case are

$$(W - W_{sj})G_j - \epsilon_z \frac{\partial G_j}{\partial z} = 0 \quad \text{at} \quad z = h \quad \ldots\ldots\ldots\ldots\ldots\ldots \quad (28)$$

$$(1 - \gamma)W_{sj}G_j + \epsilon_z \frac{\partial G_j}{\partial z} = G_j S_{Dj} - G_{Bj} S_{Rj} \quad \text{at} \quad z = 0 \quad \ldots\ldots\ldots\ldots \quad (29)$$

$$VG_j - \epsilon_y \frac{\partial G_j}{\partial y} = q_j \quad \text{or} \quad G_j = G_{jo} \quad \text{at} \quad y = 0 \quad \text{and} \quad B \quad \ldots\ldots\ldots\ldots \quad (30)$$

in which q_j = lateral influx of particulate contaminant associated with jth sediment; and G_{jo} = constant particulate contaminant concentration associated with jth sediment.

Integrating Eq. 27 over the entire depth yields the following final expression of the particulate contaminant transport equation:

$$\frac{\partial \bar{G}_j}{\partial t} + \left(\bar{U} - \frac{K_x}{h}\frac{\partial h}{\partial x}\right)\frac{\partial \bar{G}_j}{\partial x} + \left(\bar{V} - \frac{K_y}{h}\frac{\partial h}{\partial y}\right)\frac{\partial \bar{G}_j}{\partial y} = \frac{\partial}{\partial x}\left(K_x \frac{\partial \bar{G}_j}{\partial x}\right)$$

$$+ \frac{\partial}{\partial y}\left(K_y \frac{\partial \bar{G}_j}{\partial y}\right) - \left(\frac{S_{Dj}}{h} + \lambda + K_j\right)\bar{G}_j + \left(K_j K_{dj} \bar{C}_j \bar{G}_w + \frac{G_{Bj} S_{Rj}}{h} + Q_j\right) \quad (31)$$

The boundary conditions for this case are the same as those expressed in Eq. 30.

Finite Element Method.—Because of its increased solution accuracy and ready accommodation to complex boundary geometry, the finite element solution technique with the Galerkin weighted residual method (4) was used in this study to solve Eqs. 11, 26, and 31 with the boundary conditions of Eqs. 4, 23, and 30. The flow domain was divided into a series of triangular elements interconnected at nodal points. Six nodes were associated with each triangle, three at the vertices and three on the midsides. A quadratic approximation was made for the sediment and contaminant concentrations with each element. Either linear or quadratic interpolations can be used for variations of flow depth and velocity within an element. The computer program was written in FORTRAN IV language to adapt the model to CDC-7600 and VAX computers. During the following model application, the computer time required to calculate all seven substances

per computational node per time step was 0.0028 cp second on the CDC-7600 computer.

Model Application

The FETRA code was applied to simulate the migration of sediment and Kepone, a pesticide released to the James River estuary (Virginia) through Bailey Creek as shown in Fig. 1 (2,7,17). An 86-km (53-mile) estuarine reach between City Point (River Kilometer 123 or River Mile 76) and Burwell Bay (River Kilometer 37 or River Mile 23) was simulated. Tidally influenced depth and velocity distributions in the study area were obtained by the unsteady, one-dimensional code, EXPLORE (1), which gives cross-sectionally averaged velocities and flow depths. These one-dimensional results were utilized by FETRA to obtain longitudinal distributions of sediment and Kepone. Thus, results presented here are cross-sectionally averaged, longitudinal distributions that change with the tidal flow.

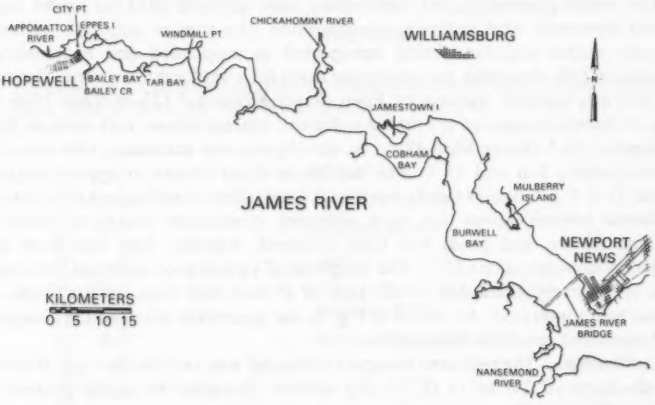

FIG. 1.—James River Estuary

Applying FETRA to the estuary also involved model calibration and verification. Since field data (2,17) indicated that a considerable amount of particulate Kepone was transported by organic materials moving independently with other sediments, sediment transport was modeled for three sediment types: (1) Cohesive sediments (clay and silt); (2) noncohesive sediments (sand); and (3) organic matter. The modeling procedure at each point in time involved first simulating the transport, deposition, and erosion of sediment. The sediment transport results were then used to simulate dissolved and particulate contaminants by accounting for the contaminant interactions with the sediments. Changes in riverbed conditions were also calculated in terms of: (1) Changes in the river bottom's elevation; (2) the distribution of cohesive sediment, noncohesive sediment, and organic matter in the bed; and (3) the distribution of particulate Kepone in the bed.

Calibration.—In the James River study, the only parameters and coefficients that were adjusted to fit the simulation results to the measured data were the dispersion coefficients, plus the erodibility coefficient and critical shear stresses used to calculate deposition and erosion rates of cohesive sediment and organic matter (Eqs. 15 and 16). The other parameters, e.g., Kepone distribution coefficients, sediment sizes, sediment fall velocities, and the like, were determined by theoretical and experimental analyses, and field measurements prior to the model simulation. Thus, the major calibration effort reproduced sediment distribution patterns similar to the measured longitudinal distribution of sediment concentrations for the 86-km (53-mile) river reach (2,11) by adjusting the longitudinal dispersion coefficient, erodibility coefficient, and critical shear stresses. The lateral dispersion coefficient was assumed to be zero because of the one-dimensional application of FETRA.

Ideally, FETRA should be calibrated with two-dimensional data. However, the use of the one-dimensional, hydrodynamic model, EXPLORE, precludes two-dimensional testing. The results mentioned in this paper are those obtained on the 31st day of the simulation.

The model parameters and coefficients were adjusted until the model reproduced measured total sediment concentration (the sum of cohesive sediment, organic matter and sand being transported as suspended and bed loads) at maximum ebb, slack tide, and maximum flood for a net freshwater river discharge of 58.3 m^3/s (2,050 cfs) at City Point (River Kilometer 123 or River Mile 76). Fig. 2 shows changes of computed sediment concentrations with time at River Kilometer 75.7 (River Mile 47.0). In this figure, the maximum ebb occurs at approximately 3 h and 15 h. The maximum flood occurs at approximately 8 h and 21 h. Fig. 3 shows tidally averaged, longitudinal distributions of computed sediment concentrations for each sediment component (cohesive sediment, organic matter, and sand) and total sediment, together with measured total sediment concentrations (2,7). The longitudinal variation of sediment concentration is relatively small due to the lack of a clear null zone (where fresh and saline water intermix). As shown in Fig. 3, the agreement between the computed and measured results is reasonable.

Verification.—The sediment transport submodel was verified for a net freshwater discharge of 247 m^3/s (8,700 cfs) without changing the model parameters and coefficients. Computed sediment concentrations were compared with measured total sediment concentrations for various tidal stages. Slack tide and tidally-averaged computer results are shown in Figs. 4 and 5 together with field data (9). These figures include computed sediment concentrations of each type of sediment (cohesive sediment, organic matter, and sand) and total sediment (the sum of the sediment components).

Computer results revealed that there are two peaks of the total sediment concentrations of approximately 100 mg/L. One occurs between River Kilometers 75 and 95 (River Miles 47 and 59), and the other around River Kilometer 55 (River Mile 34). The first peak was produced by extensive river bed scouring in the vicinity of this reach, and the second was due to the existence of a clear null zone. In Figs. 4 and 5 the computed results are compared with field data obtained in 1965 (9) and 1966. The 1966 data were supplied by M. M. Nichols, Virginia Institute of Marine Sciences (VIMS). As shown by Figs. 4 and 5, the computed and measured data agree rather closely.

To test the contaminant transport submodels, computed results for Kepone were compared with measured data at various tidal stages (2,7). Because the

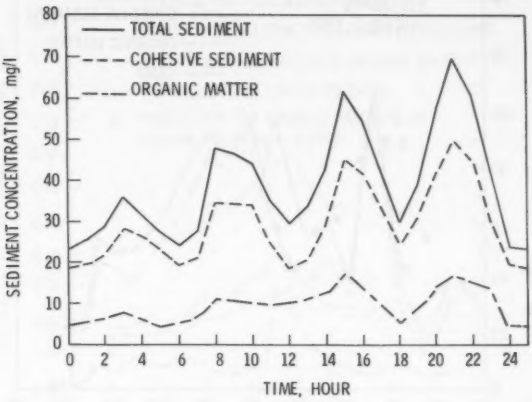

FIG. 2.—Changes of Computed Sediment Concentrations with Time at River Kilometer 75.7 (River Mile 47.0) for Net Freshwater Discharge of 58.3 m^3/s (2,050 cfs)

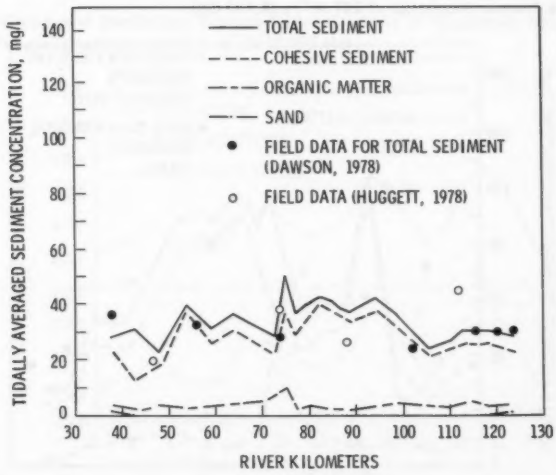

FIG. 3.—Computed Tidally Averaged Sediment Concentration of Each Sediment Type for Net Freshwater Discharge of 58.3 m^3/s (2,050 cfs)

adjustable model parameter and coefficient are all related to the sediment transport (as mentioned previously), there are no adjustable parameters and coefficients

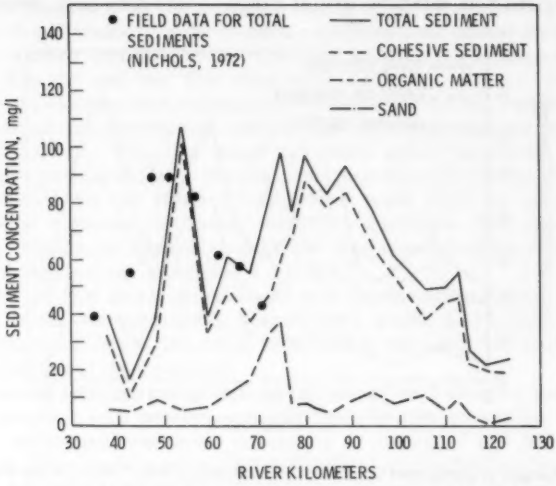

FIG. 4.—Computed Sediment Concentration of Each Sediment Type at Slack Tide for Net Freshwater Discharge of 247 m^3/s (8,700 cfs)

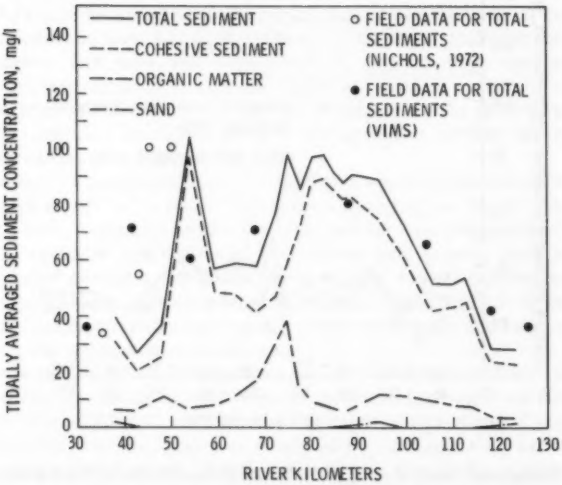

FIG. 5.—Computed Tidally Averaged Sediment Concentration of Each Sediment Type for Net Freshwater Discharge of 247 m^3/s (8,700 cfs)

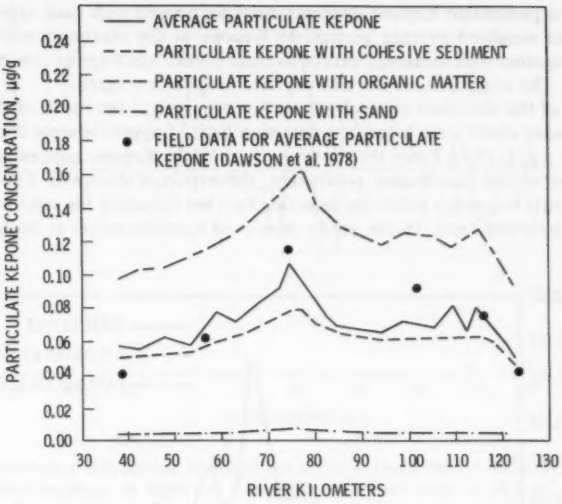

FIG. 6.—Computed Particulate Kepone Concentrations at Maximum Ebb Tide for Net Freshwater Discharge of 58.3 m^3/s (2,050 cfs)

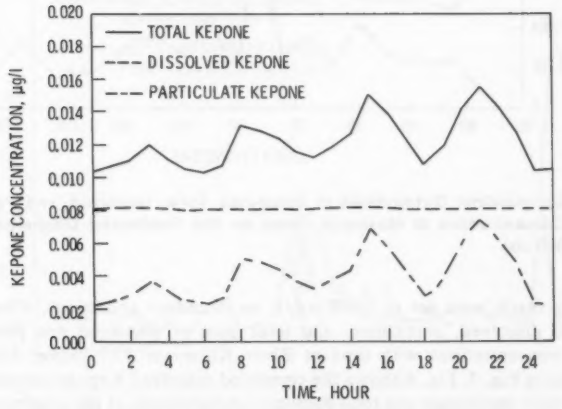

FIG. 7.—Changes of Computed Total, Dissolved, and Particulate Kepone Concentrations with Time at River Kilometer 75.7 (River Mile 47.0) for Net Freshwater Discharge of 58.3 m^3/s (2,050 cfs)

left for both the dissolved and particulate contaminant transport submodels. Thus, no calibration was performed for these contaminant transport submodels. Predicted particulate Kepone concentrations associated with each type of sediment and weighted average particulate Kepone at the maximum ebb tide are shown together with measured data of average particulate Kepone concentrations (Fig. 6). The computed results and the field data closely agree.

Most of the dissolved concentrations that occurred in the reach of the James River under study were below the detection limit of approximately 0.005 μg/L to 0.010 μg/L (2,7). From the measured particulate Kepone concentration and the value of the distribution coefficient, the expected dissolved Kepone concentration is somewhat below the detection limit but is roughly the same magnitude as the detection limit. In the study, dissolved concentrations at both ends of

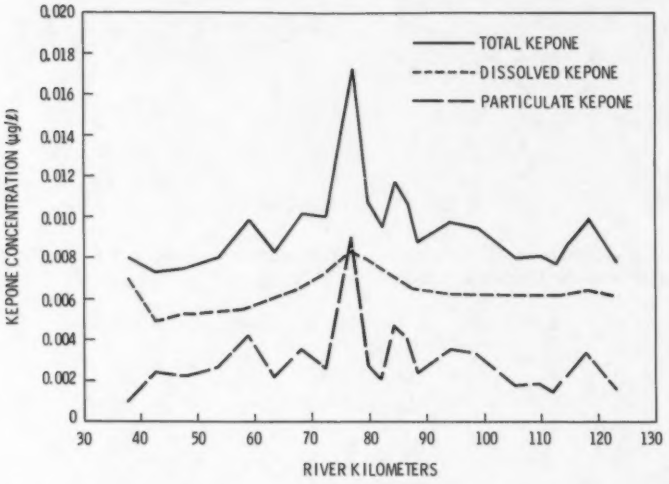

FIG. 8.—Longitudinal Distributions of Computed Total, Dissolved, and Particulate Kepone Concentrations at Maximum Flood for Net Freshwater Discharge of 58.3 m^3/s (2,050 cfs)

the study reach were set to 0.007 μg/L as boundary conditions. Changes of computed dissolved, particulate, and total (sum of dissolved and particulate) Kepone concentrations with time at River Kilometer 75.7 (River Mile 47.0) are shown in Fig. 7. Fig. 8 shows the computed dissolved Kepone concentration together with particulate and total Kepone concentrations at the maximum flood tide. This figure indicates that dissolved Kepone concentrations vary from approximately 0.0048 μg/L–0.0084 μg/L. The concentration of dissolved Kepone predicted by the FETRA code is the highest possible value found in the study area, but is still below the detection limit. Total Kepone concentrations vary from 0.007 μg/L–0.017 μg/L with peak concentration occurring at River

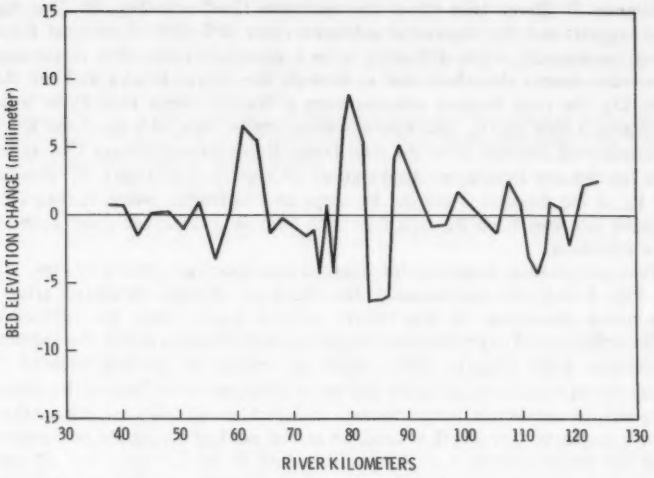

FIG. 9.—Variation of Predicted Riverbed Elevation Changes Due to Sediment Deposition or Bed Scouring, or Both, for Net Freshwater Discharge of 58.3 m^3/s (2,050 cfs)

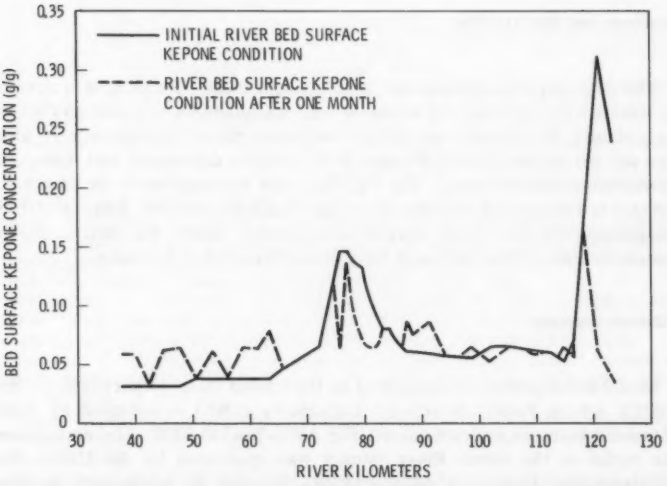

FIG. 10.—Predicted Change in Bed Surface Kepone Concentration that Occurred During One-Month Simulation for Net Freshwater Discharge of 58.3 m^3/s (2,050 cfs)

Kilometer 77 (River Mile 48) at the maximum flood tide (Fig. 8). This figure also suggests that the suspended sediments carry 12%–53% of the total Kepone being transported, while 47%–88% is in a dissolved form. The mathematical simulation results also show that at Burwell Bay (River Kilometer 37 or River Mile 23), the total Kepone concentration averaged over a tidal cycle was an estimated 0.0076 $\mu g/L$. This concentration implies that 14.0 kg of the Kepone is transported annually from the tidal James River estuary toward Cheseapeake Bay for the net freshwater discharge of 58.3 m^3/s (2,050 cfs). Of this total, 2.2 kg of the Kepone is carried by suspended sediment, while 11.8 kg of the Kepone migrates from Burwell Bay each year in a dissolved form under this flow condition.

Two computation examples for riverbed conditions are shown in Figs. 9 and 10. Fig. 9 indicates accumulated bed elevation changes predicted after the one-month simulation. In this figure, positive values along the vertical axis indicate the amount of net sediment deposition in millimeters during the one-month simulation, while negative values show the amount of riverbed scoured. The figure shows a series of scouring and deposition patterns reflecting the complex geometry of the James River estuary, in which many bays are connected by narrow channels. For this flow case, an annual net bed deposition rate averaged over the 86-km (53-mile) reach was predicted to be 1.7 mm. Fig. 10 shows the predicted change in bed-surface Kepone concentrations that occurred during the one-month simulation. Definitely, the Kepone level tended to decrease near the upper part of the estuary and to increase near the lower part (or seaward side) of the estuary with time.

Summary and Conclusions

The unsteady two-dimensional finite element model, FETRA, was developed to simulate the transport of sediment and contaminants in rivers and estuaries by including the mechanisms of sediment/contaminant interaction, e.g., absorption and desorption of contaminants; and transport, deposition, and resuspension of contaminated sediments. The FETRA code was applied to the James River estuary to simulate the transport of sediment and the pesticide, Kepone. Although additional field data were needed to rigorously verify the model, predicted concentrations agreed well with field data obtained in the estuary.

Acknowledgments

Model development was supported by the United States Department of Energy (DOE), whose Pacific Northwest Laboratory (PNL) is operated by Battelle Memorial Institute under Contract DE-AC06-76RLO 1830. The application of the model to the James River estuary was sponsored by the United States Environmental Protection Agency (EPA), through an interagency agreement between EPA and DOE. The writer wishes to express his gratitude to R. G. Baca for his assisting in the model development and to S. E. Wise for assisting in the model application.

Appendix I.—References

1. Baca, R. G., Waddel, W. W., Cole, C. R., Brandstetter, A., and Cearlock, D. B., "EXPLORE-I: A River Basin Water Quality Model," Battelle, Pacific Northwest Laboratories, Richland, Wash., 1973.
2. Dawson, G. W., "The Feasibility of Mitigating Kepone Contamination in the James River Basin," Pacific Northwest Laboratory, Richland, Wash.; submitted to the United States Environmental Protection Agency, 1978.
3. Daily, J. W., and Harleman, D. R. F., *Fluid Dynamics*, Addison Wesley Publishing Co., Inc., New York, N.Y., 1966.
4. Desai, C. S., and Abel, J. F., *Introduction to the Finite Element Method, A Numerical Method for Engineering Analysis*, Van Nostrand Reinhold Co., New York, N.Y., 1972.
5. Fischer, H. B., "The Mechanics of Dispersion in Natural Streams," *Journal of the Hydraulics Division*, ASCE, Vol. 93, No. HY6, Proc. Paper 5592, Nov., 1967, pp. 187–216.
6. Haushild, W. L., Stevens, H. H., Jr., Nelson, J. L., and Dempster, R. J., "Radionuclides in Transport in the Columbia River from Pasco to Vancouver, Washington," *Geological Survey Professional Paper 433-N*, United States Geological Survey, 1973.
7. Huggett, R., Haven, D., and Nichols, M., "Kepone-Sediment Relationships in the James River," Virginia Institute of Marine Science, Va.; submitted to the EPA Gulf Breeze Environmental Research Laboratory, Gulf Breeze, Fla., 1978.
8. Krone, R. B., "Flume Studies of the Transport of Sediment in Estuarial Shoaling Processes," Hydraulic Engineering Laboratory and Sanitary Engineering Research Laboratory, University of California at Berkeley, Berkeley, Calif., 1962.
9. Nichols, M. M., "Sediments of the James River Estuary, Virginia," *Geological Society American Member*, Vol. 133, 1972, pp. 169–212.
10. "Evaluation of Models Used for the Environmental Assessment of Radionuclide Releases," *Proceedings of a Workshop on the Evaluation of Models Used for the Environmental Assessment of Radionuclide Releases, CONF-770901*, Oak Ridge National Laboratory, Sept. 6–9, 1977.
11. Onishi, Y., and Wise, S. E., "Mathematical Modeling of Sediment and Contaminant Transport in the James River Estuary," *Proceedings of the 26th Annual Hydraulics Division Specialty Conference*, ASCE, 1978, pp. 303–310.
12. Onishi, Y., and Wise, S. E., "Finite Element Model for Sediment and Toxic Contaminant Transport in Streams," *Proceedings of the Specialty Conference on Conservation and Utilization of Water and Energy Resources*, ASCE, Aug., 1979, pp. 144–150.
13. Onishi, Y., Schreiber, D. L., and Codell, R. B., "Mathematical Simulation of Sediment and Radionuclide Transport in the Clinch River, Tennessee," *Contaminants and Sediments*, R. A. Baker, ed., Vol. 1, Chapter 18, Ann Arbor Science Publishers, Inc., Ann Arbor, Mich., 1980, pp. 393–406.
14. Onishi, Y., Serne, R. J., Arnold, E. M., Cowan, C. W., and Tompson, F. L., "Critical Review: Radionuclide Transport, Sediment Transport, and Water Quality Mathematical Modeling: and Radionuclide Adsorption/Desorption Mechanisms," *NUREG/CR-1322, PNL-2901*, Pacific Northwest Laboratory, Richland, Wash., 1980.
15. Partheniades, E., "A Study of Erosion and Deposition of Cohesive Soils in Salt Water," thesis presented to the University of California, at Berkeley, Calif., in 1962, in partial fulfillment of the requirements for the degree of Doctor of Philosophy.
16. Sayre, W. W., "Dispersion of Silt Particles in Open Channel Flow," *Journal of the Hydraulics Division*, ASCE, Vol. 92, No. HY3, Proc. Paper 6579, May, 1966, pp. 1009–1038.
17. "Kepone Mitigation Project Report," United States Environmental Protection Agency, Division of Standard and Criteria, Office of Water and Hazardous Materials, Washington, D.C., 1978.
18. "Regulatory Guide 1.EE, Methods for Estimating Aquatic Dispersion of Liquid Effluents from Routine Reactor Releases for the Purpose of Implementing Appendix I," United States Nuclear Regulatory Commission, Washington, D.C., 1976.
19. "Liquid Pathway Generic Study," *NUREG-0440*, Office of Nuclear Reactor Regulation, United States Nuclear Regulatory Commission, Washington, D.C., 1978.

20. "Sedimentation Engineering," V. A. Vanoni, ed., ASCE Task Committee for the Presentation of the Manual on Sedimentation of the Sedimentation Committee of the Hydraulics Division, ASCE, 1975.

Appendix II.—Notation

The following symbols are used in this paper:

C_j = concentration of sediment of jth type (weight of sediment per unit volume of water);
$\bar{C}_j$ = depth averaged concentration of sediment for jth type;
c_j'' = fluctuations from depth averaged concentration of sediment of jth type;
C_{jo} = constant concentration of jth sediment;
D_x, D_y = dispersion coefficients of x and y directions;
f_{sj} = fraction of contaminant sorbed by jth sediment;
f_w = fraction of contaminant left in solution;
G_{Bj} = particulate contaminant concentration associated with jth sediment in river bed (weight of contaminant or radioactivity per unit weight of sediment);
G_j = particulate contaminant concentration associated with jth sediment (weight of contaminant or radioactivity per unit volume of water);
$\bar{G}_j$ = depth averaged value of particulate contaminant concentration associated with jth sediment;
G_{jo} = constant particulate contaminant concentration associated with jth sediment;
G_w = dissolved contaminant concentration (weight of contaminant or radioactivity per unit volume of water);
$\bar{G}_w$ = depth averaged value of dissolved contaminant concentration;
G_w'' = fluctuation from depth averaged value of dissolved contaminant concentration;
G_{wo} = constant concentration of dissolved contaminant;
h = flow depth;
K_{Bj} = rate of contaminant adsorption or desorption to reach an equilibrium condition with jth riverbed sediment;
K_{dj} = distribution (or partition) coefficient between dissolved contaminant and particulate contaminant associated with jth sediment;
K_j = rate of contaminant adsorption or desorption to reach equilibrium condition with jth moving sediment;
K_j' = an empirical constant depending on sediment type;
K_x = $\epsilon_x + D_x$;
K_y = $\epsilon_y + D_y$;
M_j = erodibility coefficient for sediment of jth size fraction or type;
M_j' = weight of jth sediment;
P = porosity of river bed;
Q_{AT} = actual total sediment load per unit width;
Q_j = source strength of particulate contaminant contribution associated with jth sediment;
Q_{sj} = source strength of jth sediment contribution;

Q_T = total sediment transport capacity of flow per unit width;
Q_w = source strength of dissolved contaminant contribution;
q_j = lateral influx of particulate contaminant associated with jth sediment;
q_{sj} = lateral influx of the jth sediment;
q_w = lateral influx of dissolved contaminant;
Q_j = source strength of particulate contaminant contribution associated with jth sediment;
q_j = lateral influx of particulate contaminant associated with jth sediment;
S_{Dj} = sediment deposition rate per unit bed surface area for jth sediment;
S_{Rj} = sediment erosion rate per unit bed surface area for jth sediment;
t = time;
U = velocity component of longitudinal (x) direction;
$\bar{U}$ = depth averaged longitudinal velocity;
u'' = longitudinal velocity fluctuation from depth averaged longitudinal velocity;
V = velocity component of lateral (y) direction;
$\bar{V}$ = depth averaged lateral velocity;
v'' = lateral velocity fluctuation from depth averaged lateral velocity;
W = velocity component of vertical (z) direction;
W_{sj} = fall velocity of jth sediment;
x, y, z = longitudinal, lateral, and vertical directions in Cartesian coordinates, respectively;
γ = coefficient, i.e., probability that particle settling to bed is re-entrained;
γ_j = density of jth sediment in river bed;
ΔL = distance between up-current and down-current locations;
$\epsilon_x, \epsilon_y, \epsilon_z$ = diffusion coefficients of longitudinal, lateral, and vertical directions;
λ = chemical and biological degradation rate, or radionuclide decay rate of contaminant;
τ_b = bed shear stress;
τ_c = critical shear stress for sand defined by DuBoy;
τ_{cDj} = critical shear stress for sediment deposition for jth cohesive sediment;
τ_{cRj} = critical shear stress for sediment erosion for jth cohesive sediment; and
ψ_D = coefficient of DuBoy's formula.

DISCUSSION

Note.—This paper is part of the Journal of the Hydraulics Division, Proceedings of the American Society of Civil Engineers, ©ASCE, Vol. 107, No. HY9, September, 1981. ISSN 0044-796X/81/0009-1111/$01.00.

Discussions

Discussions may be submitted on any Proceedings paper or technical note published in any *Journal* or on any paper presented at any Specialty Conference or other meeting, the *Proceedings* of which have been published by ASCE. Discussion of a paper/technical note is open to anyone who has significant comments or questions regarding the content of the paper/technical note. Discussions are accepted for a period of 4 months following the date of publication of a paper/technical note and they should be sent to the Manager of Technical and Professional Publications, ASCE, 345 East 47th Street, New York, N.Y. 10017. The discussion period may be extended by a written request from a discusser.

The original and three copies of the Discussion should be submitted on 8-1/2-in. (220-mm) by 11-in. (280-mm) white bond paper, typed double-spaced with wide margins. The length of a Discussion is restricted to two *Journal* pages (about four typewritten double-spaced pages of manuscript including figures and tables); the editors will delete matter extraneous to the subject under discussion. If a Discussion is over two pages long it will be returned for shortening. All Discussions will be reviewed by the editors and the Division's or Council's Publications Committees. In some cases, Discussions will be returned to discussers for rewriting, or they may be encouraged to submit a paper or technical note rather than a Discussion.

Standards for Discussions are the same as those for Proceedings Papers. A Discussion is subject to rejection if it contains matter readily found elsewhere, advocates special interests, is carelessly prepared, controverts established fact, is purely speculative, introduces personalities, or is foreign to the purposes of the Society. All Discussions should be written in the third person, and the discusser should use the term "the writer" when referring to himself. The author of the original paper/technical note is referred to as "the author."

Discussions have a specific format. The title of the original paper/technical note appears at the top of the first page with a superscript that corresponds to a footnote indicating the month, year, author(s), and number of the original paper/technical note. The discusser's full name should be indicated below the title (see Discussions herein as an example) together with his ASCE membership grade (if applicable).

The discusser's title, company affiliation, and business address should appear on the first page of the manuscript, along with the *Proceedings* paper number of the original paper/technical note, the date and name of the *Journal* in which it appeared, and the original author's name.

Note that the discusser's identification footnote should follow consecutively from the original paper/technical note. If the paper/technical note under discussion contained footnote numbers 1 and 2, the first Discussion would begin with footnote 3, and subsequent Discussions would continue in sequence.

Figures supplied by the discusser should be designated by letters, starting with A. This also applies separately to tables and references. In referring to a figure, table, or reference that appeared in the original paper/technical note use the same number used in the original.

It is suggested that potential discussers request a copy of the *ASCE Authors' Guide to the Publications of ASCE* for more detailed information on preparation and submission of manuscripts.

CALCULATION OF STRONGLY CURVED OPEN CHANNEL FLOW[a]

Closure by Michael Leschziner[6] and Wolfgang Rodi[7]

The writers should like to thank Götz, Anwar, and Rodger for their interest in the paper and for their comments. Götz has pointed out that curved open channel flow with a ratio of radius-to-width <3.5 cannot exist without large separation zones. However, the measurements of Rozovskii (18) for a radius-to-width ratio of 1.0, which were taken for validation of the mathematical model in the paper, do not show any reverse-flow regions, i.e., where the longitudinal velocity is in the upstream direction. The occurrence of flow separation depends also on parameters other than the radius-to-width ratio, and the experimental flow situation of Rozovskii was chosen for the model validation precisely because separation was absent in his particular configuration.

The main comment of Anwar and Rodger is that the empirical coefficient, c_μ, in the turbulence model is not really a constant as assumed in the paper. The writers are well aware of this fact and should like to point out Refs. 42 and 43 where refined turbulence models are described that simulate the reduction of c_μ near the free surface which is necessary in order to obtain the well-known parabolic eddy-viscosity distribution in open channel flow. However, even though c_μ can vary significantly across the flow, and its average value also somewhat from one flow to another, in many cases the calculations are not very sensitive to the c_μ distribution so that the main features of a great many flows can in fact be predicted well with a constant value of $c_\mu = 0.09$. This is demonstrated in Ref. 44 where results obtained with the k-ϵ model are compared with experimental data for many different hydraulic flow situations, thus refuting the discussers' statement that the k-ϵ model cannot be applied to flow problems more general than isotropic turbulence without tuning the constants. The fixed constants of the k-ϵ model are, of course, not suitable for each and every flow, and exceptions such as strongly buoyant flows are also described in Ref. 44. This reference also concludes that simpler models like the Prandtl mixing length theory work fairly well for simple channel flow and submerged jets but require different empirical input for different problems and are not suitable whenever turbulence transport or history effects are important and when the flow is more complex than a shear layer, e.g., recirculating flows. In such cases, the additional computational effort required to solve the k and ϵ equations, which is less than 20% with a suitable numerical scheme, is certainly justified. Calculations of strongly curved open channel flow as described in the paper are not particularly sensitive to the turbulence model employed because in this case the distribution of the velocity components, on which attention was focused,

[a]October, 1979, by Michael Leschziner and Wolfgang Rodi (Proc. Paper 14927).

[6]Lect., Dept. of Mech. Engrg., The Univ. of Manchester Inst. of Sci. and Tech., P.O. Box No. 88, Manchester, England, M60 1QD.

[7]Research Engr., Univ. of Karlsruhe, Karlsruhe, W. Germany.

is governed mainly by pressure forces. Thus, a simpler turbulence model would probably have yielded similar results, including the vorticity model of Prandtl (41). The k-ϵ model was used simply because it is at present one of the most widely applicable models (44).

Anwar and Rodger have based their comment on the variation of c_μ on the evaluation of c_μ from measurements reported in Refs. 35 and 36. According to Eq. 6, evaluation of c_μ requires knowledge of the eddy viscosity ν_t, the turbulent kinetic energy k, and the dissipation rate ϵ. There is no indication in Ref. 35 that ϵ has been measured, and it is therefore not clear to the writers how the discussers have actually evaluated c_μ. This casts some doubt on the numerical values for c_μ quoted by the discussers, but the comment that c_μ is not really constant is of course still valid.

Appendix.—References

42. Hossain, M. S., "Mathematical Modelling of Turbulent Buoyant Flows" (in German), thesis presented to the University of Karlsruhe, at Karlsruhe, Germany, in 1980, in partial fulfillment of the degree of Doctor of Engineering.
43. Naot, D., and Rodi, W., "Numerical Simulation of Secondary Currents in Open Channel Flow with an Algebraic Stress Turbulence Model," Report SFB 80/T/187, University of Karlsruhe, West Germany, 1981.
44. Rodi, W., *Turbulence Models and their Application in Hydraulics—a State of the Art Review*, International Association for Hydraulic Research, Delft, the Netherlands, 1980.

Approximate Flood Routing Methods: A Review[a]

Closure by Erwin P. Weinmann[7] and Eric M. Laurenson[8]

The writers thank Ponce and Theurer, Price, and Kundzewicz for their discussion, which clarifies some of the problems dealt with in the paper and makes the paper more complete.

The terminology for the methods that neglect the inertia terms of the momentum equation warrants some further comments. In the paper, the term *approximate dynamic model* was reserved for methods based on the numerical solution of the system of Eqs. 1 and 2, but which, for reasons of computational efficiency, omitted the inertia terms.

As pointed out by Ponce and Theurer, the term *kinematic model corrected for dynamic effects*, used for the Koussis model, is not strictly correct. This term would be appropriate for a model based on the full equation of the looped rating curve, rather than on the Jones formula incorporated in the Koussis

[a]December, 1979, by Erwin P. Weinmann and Eric M. Laurenson (Proc. Paper 15057).
[7]Designing Engr., State Rivers and Water Supply Commission, Victoria, Australia.
[8]Prof. of Civ. Engrg., Monash Univ., Clayton, Victoria, Australia.

model. Expressions for a fully dynamic rating curve written in terms of the changing flow rate at one section have been proposed by Fread (28) and Simons, Li, and Simons (29). Because of its inability to model the effects of downstream disturbances and some of the approximations made in its derivation, a model based on such expressions would still be kinematic in nature, though corrected for dynamic effects, thus justifying this classification. In this context, a more appropriate terminology for the Koussis model would be *kinematic model corrected for diffusive effects*.

The question raised by Ponce and Theurer regarding the generality of the finite difference scheme proposed by Koussis has been clarified in a recent paper by Koussis (30). With regard to the two alternative expressions for the computation of the weighting coefficient θ, the writers' experience confirms the conclusion reached by Koussis that the more complicated expression is rarely warranted.

The writers appreciate the comments made by Ponce and Theurer and by Kundzewicz on upper and lower limits for reach length Δx, and welcome the opportunity to add some clarifying remarks to this section of the original paper.

As pointed out by Ponce and Theurer, a *lower limit on* Δx is equivalent to a lower limit on θ, i.e., $\theta \geq 0$. The writers agree with Kundzewicz that the answer to the question of whether $\theta = 0$ constitutes a realistic lower limit on the weighting coefficient depends on the point of view. For a *black box* model, parameter values outisde the physically realistic range are quite acceptable and, like Ponce and Theurer, the first author has successfully used negative values of θ (15). However, as θ and Δx are related through Eq. 15, or Eq. 18, it is generally possible to increase Δx, while decreasing the number of subreaches, until a positive value of θ is obtained, without significantly affecting the routing results.

The question of an *upper limit on* Δx, or an equivalent lower limit on Δt for given Δx, is of more direct importance for practical routing computations. In contrast to the theoretically based expressions recommended by Ponce and Theurer and by Kundzewicz, the writers' condition for Δx, Eq. 19, is not intended to suppress negative outflows completely, but merely as a guide to keep these within acceptable limits. The reach lengths computed from Eq. 19, therefore, should be considered as absolute maximum values. The equation also does not reflect the interdependence between Δx and Δt, which is accounted for by a separate condition. As stated in the paper, values of Δt considerably smaller than $\Delta x/\langle c \rangle = K$ may lead to negative outflows. The routing results presented in Fig. 6 of Kundzewicz' discussion appear to have been computed with a time step much smaller than his $K = 30$ min, and the negative outflows are thus not unexpected. Also, as Kundzewicz points out, the initial slope of the inflow hydrograph has an effect on the occurrence of negative ordinates. Our formula was based on experience with hydrographs having the usual S-shaped rising limb. Its slope is reflected in the time of rise T_r.

The comments by Price on a more general form of the diffusion equation are a valuable addition to the paper. Similarly to the methods based on the kinematic wave equation, the classification of the various forms of models based on the diffusion equation depends on the method used for the computation of the routing coefficients c and D. In the form defined by Eqs. 26–29, the diffusion model is indeed equivalent to the Koussis model and may, in fact,

be computationally more efficient. However, this extension is not included in the programs appended to Refs. 14 and 20.

The writers agree with Price that the concept of an equivalent channel, as introduced by Price and Kawecki (21), is a very useful one for many practical applications. There appears to be no reason why this concept could not be applied with the Koussis model as well as with other approximate routing methods.

The discussion and the references quoted by Kundzewicz draw attention to another important line of comparative investigation into different flood routing methods, based principally on linear systems theory. This approach and the approach based on numerical modelling techniques, as used by the writers, should be seen as complementary and advances with both methods should help to further rationalize flood routing computations for practical applications.

Errata.—The following corrections should be made to the original paper:

Page 1527, paragraph 3, line 8: Should read "$\langle l/c \rangle \simeq 1/\langle c \rangle$" instead of "$\langle l/c \rangle \simeq \langle l/c \rangle$."
Page 1530, paragraph 7, line 2: Should read "(7)" instead of "(6)."

APPENDIX.—REFERENCES

28. Fread, D. L., "Computation of Stage-Discharge Relationships Affected by Unsteady Flow," *Water Resources Bulletin*, Vol. 11, No. 2, 1975, pp. 213–228.
29. Simons, R. K., Li, R. M., and Simons, D. B., "On Stage-Discharge Relations of Rivers," *Proceedings*, 17th Congress of the International Association for Hydraulic Research, Aug., 1977, pp. 491–498.
30. Koussis, A. D., "Comparison of Muskingum Method Difference Schemes," *Journal of the Hydraulics Division*, ASCE, Vol. 106, No. HY5, Proc. Paper 15383, May, 1980, pp. 925–929.

STEADY-STATE ESTIMATION OF COOLING POND PERFORMANCE[a]

Closure by Gerhard H. Jirka,[4] M. ASCE and Masataka Watanabe[5]

Adams' comment regarding the applicability of simple steady-state estimation models to transient cooling pond conditions is well taken.

In general, cooling ponds experience transient effects because of two external mechanisms. The first arises from variable meteorological conditions for which the time scale is $H(\rho c_p K)^{-1}$ as mentioned by Adams. The second arises from variable power plant operation, and its time scale is the pond residence time

[a]June, 1980, by Gerhard H. Jirka and Masataka Watanabe (Proc. Paper 15449).
[4]Asst. Prof., School of Civ. and Environmental Engrg., Cornell Univ., Ithaca, N.Y.
[5]Sci., National Inst. of Environmental Studies, Tsukuba, Japan.

V/Q_o, in which V = pond volume, as mentioned by the authors. Hence, if actual transient cooling pond performance is to be modeled by the sequential application of steady-state models—with appropriately averaged or filtered input data as suggested by Adams and Koussis (6)—then, presumably, both time scales ought to be considered in the averaging or filtering procedure. In any case, the question remains whether a fully transient simulation (4) is not more straightforward, more accurate and computationally more efficient.

Bar Resistance of Gravel-Bed Stream[a]

Discussion by Arun Kumar[5] and Rema Devi[6]

A methodology is proposed for estimating resistance characteristics of inactive gravel-bed streams. It is well recognized that, at low depths of flow, lower velocities are observed than the logarithmic law predicts and friction factor increases by as much as 50% (35). However, difficulty arises in estimating it quantitatively. The authors' attempt in this direction is noteworthy.

The authors' analysis is based on two hypotheses. Observed data that do not fit into the framework of the hypotheses, are rejected, so much so that, out of 46 reaches initially chosen, only 15 have been used for further analysis. Even out of these selected reaches, some points are deleted in order to improve correlation between τ_0^* and C_B (Fig. 6). Rejecting two thirds of the data simply because of not fitting into the logic of the hypothesis casts doubt on the validity of the hypothesis itself. It is contended that field measurement of slope and grain size distribution are subject to large errors. As these parameters form part of the model, the resistance can be measured only qualitatively.

Further, the authors do not distinguish between the pool and riffle sections. The proposed analysis is based on the assumption that the flow is approximately uniform. The assumption is valid only at the riffle sections where the flow characteristics are controlled by the geometry and roughness characteristics of the sections. However, at the pool sections, inaccuracies are likely because the flow characteristics are dependent on downstream control. Therefore, the writers feel that the large amount of data not conforming to the hypothesis may be partly due to its collection within the pool sections.

The authors have used Keulgan's Eq. 2 to determine the grain resistance with roughness height as $2D_{90}$, and the bar resistance is taken dependent on the grain resistance. Hey (10) has shown that total resistance can be computed directly by taking roughness height as $3.5D_{84}$. Large roughness height is probably due to development of wake interference losses caused by large gravel in the

[a]October, 1980, by Gary Parker and Allen W. Peterson (Proc. Paper 15733).
[5]Asst. Prof. in Civ. Engrg., Delhi Coll. of Engrg., Kashmere Gate, Delhi, India.
[6]Asst. Prof. in Civ. Engrg., Indian Inst. of Tech., Hauz Khas, New Delhi, India.

bed. For the data studied, Hey (10) has shown that computed and observed discharges tally quite remarkably (standard error in discharges is only ±4.7%) both for high and low depths of flow. For the illustrative example given by the authors, the ratio of bar resistance C_B to the total resistance C at various heights H can be computed by estimating C and C_G from the Keulgan's equation corresponding to roughness height of $3.5D_{90}$ (D_{84} not being known) and $2D_{90}$, respectively.

H in meters	C_B/C
0.6	0.29
0.8	0.26
1.0	0.25
1.2	0.21

Except when $H = 0.6$ m, the C_B/C ratio compare favorably with authors analysis shown in Fig. 9 (C).

Fig. 6 represents a linear functional relationship between log C_B and log τ_G^*. The standard approach of estimating the parameters of linear regression assumes that the independent variable τ_G^* can be determined with negligible error. However, due to uncertainty in the measurement of slope and grain size distribution τ_G^* is subject to large errors. Similarly C_B is also subject to large errors. In such cases, the regression slope and its confidence limits are to be estimated using the approach given by Davis, et al. (36). The writers are of the opinion that instead of giving a point estimate of discharges at various depths, it would be better, for given depth slope and grain size distribution, if confidence limits of discharges were given. The point estimate gives a false impression that the process is highly deterministic, whereas, the real picture is exactly the opposite.

Appendix.—References

36. Bayazit, M., "Free Surface Flow in a Channel of Large Relative Roughness," *Journal of Hydraulic Research*, Vol. 14, 1976, pp. 115–125.
37. Davies, O. L., and Goldsmith, P. L., "Statistical Methods in Research and Production," Oliver and Boyd, Edinburgh, 1972.

Armored Versus Paved Gravel Beds[a]

Discussion by Paul A. Carling[3]

The authors' main definition is based on a stratigraphic distinction (Distinction 1), with reference to the vertical distribution of grain size. The stratigraphic definition, although convenient for field application, reflects ideal cases drawn from a bed-material composition spectrum controlled partly by provenance. Hence the definition may be unduly restrictive or misleading, or both, unless a consistent sampling design is advocated (7,18), and is not instructive with respect to the frequency and manner in which the protective-layer operates.

The choice of such process-related, time-dependent terms as "process of armoring," "self-stabilizing," and "formation of a stable surface layer," in many papers, suggests that a process time-based explanation of bed-material segregation would be more appropriate for engineering practice. The authors continue along such a line, arguing that (Distinction 2) armor and pavement could be defined on a basis related to the *frequency* of disruption of the layer. Unfortunately the authors do not expand on this theme. Presently, such a useful definition is qualitative and arbitrary, as there are few field data related to the frequency of disruption of protective surface layers. The authors, nevertheless, associate pavement with degraded streams and inactive beds, (22) and armor with active beds in streams that have achieved some sort of dynamic equilibrium (22), a useful concept closely tied to Distinction 2. Isolation of a design flood of specified return period (T) related to bed disruption events would be valuable in river stability problems, e.g., bed disrupted by flows > T yr flood = pavement. Beds disrupted by flows < T yr flood = armor.

It is not difficult to find an example where the stratigraphic distinction (especially if grain-size composition is strictly defined) is not in accord with a frequency based definition. The authors are clearly aware of this problem from a brief summary remark. An example of a stable cobble bed-surface wherein granules (2 mm to 4 mm) play an important role in bed stability exists (19). The description of the bed composition and implied frequency of disruption (19) is not in accord with distinctions 1 and 2.

Bagnold (15) described "a vaguely defined phenomenon called armoring" as "the continuous erosion of a granular river-bed until the residual surface solids are so large that further erosion ceases"—a process which he associated specifically with stream reaches below dams. Such a process involves the basic elements: (1) Degradation of bed height; (2) spatial concentration of coarse particles; and (3) preferential selection by a lag-action of the coarsest clasts (17). Bagnold noted that the effect did not apply particularly well to the general condition of a regular bedload supply through a natural channel. These observa-

[a]November, 1980, by D. I. Bray, and M. Church (Proc. Paper 15791).

[3]Higher Scientific Officer, Freshwater Biological Assoc., The Ferry House, Far Sawrey, Ambleside, Cumbria, United Kingdom.

tions suggest that a number of processes result in coarse gravel segregation in rivers.

The writer (16) suggests that the terms armoring and paving should be restricted to *active* processes that, at some time, have involved the hydraulic entrainment and repositioning of a fraction of the coarse bed material such that the sub-surface material is protected from entrainment. The individual terms would then be isolated with reference to the frequency of disruption of the layers. Such a definition, would preclude the hydraulic winnowing of fine surface matrix materials from around large immobile framework clasts—a process of selective entrainment of certain grain-sizes, the resultant coarse layer being a *passive* response to the process. It is suggested (16) that these latter layers be termed *censored*-layers. The terminology, being adopted from Tanner (23), encompasses the essence of the process involved, i.e., selective winnowing. Using this definition the gravel-bed surfaces described by Gessler (3), Harrison (5), and Beschta & Jackson (14) are not actively formed armor-layers but passively formed censored-layers. Given certain conditions the matrix material may be replaced in a censored layer (16,21), strengthening the structure (19), so that no granulometric distinction can be made between surface and sub-surface deposits. The coarse component at the surface will not have altered its function in the over-all bed stability, although (using the stratigraphic definitions of the authors) previously the bed would have been described as armored and laterally unarmored.

The importance of being able to identify protective surface-layers, however defined, is related, as stated by the authors, to the solution of practical problems of river bed stability within a river management framework. The stability problem revolves around the accurate prediction of material entrainment and transport. If a protective-layer controls the release of finer sub-surface materials into a transporting flow on a rising hydrograph, the progressive disruption of the bed should be detected as a flexure or discontinuity in plots of bedload grain-size against an entrainment parameter (18)—the discontinuity defining a critical threshold, T yr flood, for protective-layer disruption. It might be expected that a threshold for a compact bed surface would be greater than a threshold for individual particles (19,20). Nevertheless, the question of bed stability related to packing of almost equal size grains remains as crucial and unresolved a problem (20) as the stability of beds which develop distinct vertical grain-size segregation.

The writer would have found it useful had the authors tried to place the concepts of armor and pavement within the broader perspective of bed stability and addressed themselves to the problem of defining what critical experiments and field data are required to improve bed-stability models.

Appendix.—References

14. Beschta, R. L., and Jackson, W. L., "The Intrusion of Fine Sediments into a Stable Gravel Bed," *Journal of the Fisheries Research Board of Canada*, Vol. 36, 1980, pp. 204–210.
15. Bagnold, R. A., "An Empirical Correlation of Bedload Transport Rates in Flumes and Natural Rivers," *Proceedings*, The Royal Society of London, Series A, Vol. 372, 1980, pp. 453–473.
16. Carling, P. A., and Reader, N. A., "Structure, Composition and Bulk Properties of Upland River Gravels," *Earth Surface Processes and Landforms*.

17. Fahnestock, R. K., and Hauschild, W. L., "Flume Studies of the Transport of Pebbles and Cobbles on a Sand Bed," *Geological Society of America Bulletin*, Vol. 73, 1962, pp. 1431–1436.
18. Klingeman, P. C., and Emmett, W. W., "Field Progress in Describing Sediment Transport," *Engineering Problems in the Management of Gravel Bed Rivers*, Hey, R. D., *et al.* ed., 1980.
19. Laronne, J. B., and Carson, M. A., "Interrelationships between Bed Morphology and Bed-Material Transport for a Small, Gravel-Bed Channel," *Sedimentology*, Vol. 23, 1976, pp. 67–85.
20. Mantz, P. A., "Low Sediment Transport Rates over Flat Beds," *Journal of the Hydraulics Division*, ASCE, Vol. 106, No. HY7, Proc. Paper 15526, July, 1980, pp. 1173–1190.
21. Milhous, R. T., and Klingeman, P. C., "Sediment Transport System in a Gravel-Bottomed Stream," *Hydraulic Engineering and the Environment 21st Annual Hydraulics Division Specialty Conference*, ASCE, 1973, pp. 293–303.
22. Schumm, S. A., and Lichty, R. W., "Time, Space, and Causality in Geomorphology," *American Journal of Science*, Vol. 263, 1965, pp. 110–119.
23. Tanner, W. F., "Modification of Sediment Size Distributions," *Journal of Sedimentary Petrology*, Vol. 34, 1964, pp. 156–164.

Discussion by Robert T. Milhous,[4] M. ASCE

The authors have presented an excellent paper on the use of the terms "armored gravel bed" and "paved gravel bed." The writer agrees with the usage as proposed by the authors because: (1) The suggested usage is reasonably consistent with the usage in other areas of interest to hydraulic engineers and geomorphologists; and (2) the usage provides information about the physical processes occurring in the stream.

There is confusion over the use of "armored" and "paved"; e.g., Parker and Peterson (14) have used "paved" where the authors used "armored." In discussions the writer has had with others, it became obvious that the use of either "armored" or "paved" could be confusing if one was not quite specific as to just what was meant by each term. For this reason an alternative was proposed by Andrews (15), namely that the terms surface material and subsurface material should be used and we should not use the terms "armored" and "paved." This suggestion has, in the writer's opinion, a serious flaw in that it does not provide any insight into the physical processes involved, which is one of the major benefits obtained from the authors proposed usage. The writer suspects, one would normally prefer "paved gravel bed" to "bed with large gravel surface material and gravelly sand subsurface material" when describing a stream.

An example of the strength of the use of "armored gravel bed" and "paved gravel bed" is a reach of the Yampa River above the Little Snake River in northwestern Colorado. Most the river has an "armored gravel bed" with 5 cm–10 cm surface material except in one area where the streambed is "paved" by material in the 75 cm range. This larger material was probably transposed into the Yampa by infrequent high flood flows from the adjacent hills. In this case it is very useful to know that most of the stream is armored, but pavement also exists.

[4]Hydr. Engr., Instream Flow Group, U.S. Fish and Wildlife Service, Fort Collins, Colo.

When describing the material in the stream, the writer has used the term "armor layer" to describe the surface layer, and "bed material" to describe the material below the armor layer. In contrast, others have used "bed material" to describe a mixture of material in the armor layer and material below the armor layer. Consequently, the use, as proposed by Andrew, of surface material and subsurface material, is the preferred usage when describing the bed *material*.

The use of "armored gravel bed" and "paved gravel bed" when referring to the stream channel as a whole and "surface material" and "subsurface material" when describing the material in the stream bed would go a long way in reducing the confusion presently existing in the literature.

Appendix.—Reference

24. Parker, G., and Peterson, A. W., "Bar Resistance of Gravel-Bed Streams," *Journal of the Hydraulics Division*, ASCE, Vol. 106, No. HY10, Oct., 1980, pp. 1559–1575.

Discussion by Gary Parker,[5] M. ASCE

The distinction between armor and pavement offered by the authors represents an unfortunate case of inadvertent obfuscation in pursuit of a worthy cause. The coarse layer of immobile sediment sometimes produced by winnowing downstream of dams has traditionally been known as armor, not pavement. The precedents for this are numerous; several are Day (1), Gessler (3), Livesey (9), Little and Mayer (20), Ashida and Michiue (14), and Garde and Hasan (17). All of the above references, except Livesey, include the results of laboratory studies. The experiments are characterized by the absence of sediment infeed or recirculation, and thus can only model the phenomenon just downstream of dams traditionally called armoring.

In the context of rivers, at least, the term *pavement* seems to be of Canadian origin. Kellerhals and Bray (19) have applied the term to coarse surface layers in streams known to be periodically active. The first person to formally distinguish between the two appears to have been Bray (15), who termed a coarse surface a pavement, if surface sizes are fairly common in the substrate, and an armor, if surface sizes are rather rare in the substrate. It is implied, but more or less obvious from the above, that pavement is periodically mobilized but armor is not. Thus, Bray's original definition is exactly the opposite of the one offered now by the authors.

The authors may not have been aware that Bray's original definition has taken root in the literature. Gomez (18) specifically associates armor with immobility, and identifies pavement as a response to the most recent flood transport event. Parker (21) and Dhamotharan, Wood, Parker, and Stefan (16) have gone one step farther. They studied the formation of a coarse pavement at low shear stress, but under continuous transport of all available sizes. Both feed and recirculation configurations were used. They showed experimentally that coarse, imbricated surface pavement is so intimately tied up with bed motion

[5]Assoc. Prof., St. Anthony Falls Hydraulic Lab., Univ. of Minnesota, Minneapolis, Minn. 55414.

that it is present under such conditions. If the supply of bed load is cut off, the coarse pavement evolves into an even coarser armor. This line of thinking is consistent not only with Bray's (15) original definition, but also with the time-honored usage of the term *armor* to describe immobile surface layers downstream of dams.

Appendix.—References

25. Ashida, K., and Michiue, M., "An Investigation of River Bed Degradation Downstream of a Dam," *Proceedings*, 14th Congress, IAHR, Vol. 3, 1971, pp. C30-1–C30-9.
26. Bray, D. I., "Generalized Regime-Type Analysis of Alberta Rivers," thesis presented to the University of Alberta, at Edmonton, Alberta, Canada, in 1972, in partial fulfillment of the requirements for the degree of Doctor of Philosophy.
27. Dhamotharan, S., Wood, A., Parker, G., and Stefan, H., "Bed Load Transport in a Model Gravel Stream," *Project Report No. 190*, St. Anthony Falls Hydraulic Laboratory, University of Minnesota, Minneapolis, Minn., Dec., 1980.
28. Garde, R. J., and Hasan, S. M., "An Experimental Investigation of Degradation in Alluvial Channels," *Proceedings*, 12th Congress, IAHR, Vol. 3, 1967, pp. C5.1–C5.8.
29. Gomez, B., "Definition and Interpretation of Paved Surfaces," paper presented to BGRG at the Annual Conference of the Institute of British Geologists, 1980.
30. Kellerhals, R., and Bray, D. I., "Sampling Procedures for Coarse Fluvial Sediments," *Journal of the Hydraulics Division*, ASCE, Vol. 97, No. HY8, Aug., 1971.
31. Little, W. C., and Mayer, P. G., "Stability of Channel Beds by Armoring," *Journal of the Hydraulics Division*, ASCE, Vol. 102, No. HY11, Nov., 1976.
32. Parker, G., "Experiments on the Formation of Mobile Pavement and Static Armor," *Report*, Dept. of Civil Engineering, University of Alberta, Edmonton, Alberta, Canada, Mar., 1980.

Sand Bed Instability Due to Bed Load Motion[a]

Errata

The following corrections should be made to the original paper:

Page 2038, line 16: Should read "q_{BO}" instead of "Q_{BO}"
Page 2045, Eq. 57, right-hand side: Should read "$2\gamma_1 \kappa h_0 (F^2 \kappa h_0 \tanh \kappa h_0 - 1)$" instead of "$\gamma_1 \kappa h_0 (F^2 \tanh \kappa h_0 - 1)$"

Page 2045, Eq. 60, right-hand side: Should read "$\frac{\gamma_2}{\gamma_1}$" instead of "$\frac{\gamma_1}{\gamma_2}$"

Page 2046, Fig. 12(*a*): Should read "$\gamma_* = \gamma_2/\gamma_1$" instead of "$\gamma_* = \gamma_1/\gamma_2$"

Page 2050, line 20: Should read "$p_{d^*} = p_d \sqrt{d/(\sigma/\rho - 1)g}$" instead of "$p_{d^*} = p_d/\sqrt{d/(\sigma/\rho - 1)g}$"

---

[a]December, 1980, by Hiroji Nakagawa and Tetsuro Tsujimoto (Proc. Paper 15936).

Technical Papers

Original papers should be submitted in triplicate to the Manager of Technical and Professional Publications, ASCE, 345 East 47th Street, New York, N.Y. 10017. Authors must indicate the Technical Division or Council, Technical Committee, Subcommittee, and Task Committee (if any) to which the paper should be referred. Those who are planning to submit material will expedite the review and publication procedures by complying with the following basic requirements:

1. Titles must have a length not exceeding 50 characters and spaces.

2. The manuscript (an original ribbon copy and two duplicate copies) should be double-spaced on one side of 8-1/2-in. (220-mm) by 11-in. (280-mm) paper. Three copies of all figures and tables must be included.

3. Generally, the maximum length of a paper is 10,000 word-equivalents. As an *approximation*, each full manuscript page of text, tables or figures is the equivalent of 300 words. If a particular subject cannot be adequately presented within the 10,000-word limit, the paper should be accompanied by a rationale for the overlength. This will permit rapid review and approval by the Division or Council Publications and Executive Committees and the Society's Committee on Publications. Valuable contributions to the Society's publications are not intended to be discouraged by this procedure.

4. The author's full name, Society membership grade, and a footnote stating present employment must appear on the first page of the paper. Authors need not be Society members.

5. All mathematics must be typewritten and special symbols must be identified properly. The letter symbols used should be defined where they first appear, in figures, tables, or text, and arranged alphabetically in an appendix at the end of the paper titled Appendix.—Notation.

6. Standard definitions and symbols should be used. Reference should be made to the lists published by the American National Standards Institute and to the *Authors' Guide to the Publications of ASCE*.

7. Figures should be drawn in black ink, at a size that, with a 50% reduction, would have a published width in the *Journals* of from 3 in. (76 mm) to 4-1/2 in. (110 mm). The lettering must be legible at the reduced size. Photographs should be submitted as glossy prints. Explanations and descriptions must be placed in text rather than within the figure.

8. Tables should be typed (an original ribbon copy and two duplicates) on one side of 8-1/2-in. (220-mm) by 11-in. (280-mm) paper. An explanation of each table must appear in the text.

9. References cited in text should be arranged in alphabetical order in an appendix at the end of the paper, or preceding the Appendix.—Notation, as an Appendix.—References.

10. A list of key words and an information retrieval abstract of 175 words should be provided with each paper.

11. A summary of approximately 40 words must accompany the paper.

12. A set of conclusions must end the paper.

13. Dual units, i.e., U.S. Customary followed by SI (International System) units in parentheses, should be used throughout the paper.

14. A practical applications section should be included also, if appropriate.